Antenna Axis Offset and Intersection Determination using GPS

By

Willem Ludwig Combrinck

Submitted in partial fulfilment of the
requirements for the degree of
Master of Applied Science
in the
Department of Surveying and Geodetic Engineering
University of Cape Town
April, 1996.

DEDICATION This work is dedicated to my wife, Sandra, who had to bear the brunt of house and children for countless evenings and weekends while I hid behind the PC.

FOOD FOR THOUGHT Man may attempt to measure parts of God's creation, but may end up with unacceptable errors if he fails to remember that the final surveyor is God, who will measure man.

ACKNOWLEDGEMENTS

I would like to express my sincere gratitude to several individuals and organisations whose support made this work possible;

The director of HartRAO, Dr George Nicolson, for suggesting and allowing this work to be done. His unfaltering support and guidance ensured the success of the project.

Prof Charles Merry of UCT, the promoter of this project, for expert advice and continued support.

Dr Gerhard Soltau, IfAG, who allowed the use of several IfAG GPS receivers after their 1995 Antarctica campaign.

Prof Keith Greggor and Mr Fritz van der Merwe of the Surveying Department, University of Pretoria, who loaned me several receivers for use during the project.

Drs. Gordon MacLeod and Derck Smits for reading through countless drafts, verifying the scientific content and providing moral support.

Mr Peter E Stocker, for correcting my grammar and syntax. He greatly improved the readability of the text.

Mr Andre van der Merwe, for constructing a very good gimbal mount from a rough sketch.

Mr Dick Uytenbogaardt, who helped to install the GPS receivers in the radio telescope cone.

I, **Willem Ludwig Combrinck**, hereby declare that the work on which this thesis is based is original (except where acknowledgements indicate otherwise) and that neither the whole work nor any part of it has been, is being, or is to be submitted for another degree at this or any other University.

I empower the University to reproduce for the purpose of research either the whole or any portion of the contents in any manner whatsoever.

Signed by candidate

.....

23 July 1996

(Date)

Abstract

Modern geodesy utilises advanced space techniques such as VLBI to further the study of crustal motion as well as tidal and rotational deformations of the Earth. One of the parameters in the model used to determine the baseline length between VLBI stations, is the antenna axis offset. This offset is the distance between the secondary axis and the normal projection of the secondary axis onto the primary axis. For a non-intersecting axes antenna mounting, this offset is usually several metres in length. The accuracy of the offset value directly influences the total accuracy of the VLBI results.

This work describes how GPS is used to determine the offset and VLBI reference point. Several algorithms for calculating these parameters are investigated and evaluated. Methods are developed to minimise the size and influence of errors. An evaluation and comparison of the results to previous independent determinations of the offset, which use different techniques and instrumentation, clearly show the feasibility of using GPS. This method has the added advantage of allowing the VLBI, SLR and GPS reference frames to be co-located.

Contents

List of Figures

List of Tables

ABBREVIATIONS

AFLC	Air Force Logistics Command
AS	Anti-spoofing
CDP	Crustal Dynamics Project
CEI	Connected Element Interferometry
CEP	Celestial Ephemeris Pole
CNES	Centre National d'Etudes Spatiales
CTP	Conventional Terrestrial Pole
CTRS	Conventional Terrestrial Reference System
DAT	Data Acquisition Terminal
DEC	Declination
DOD	Department of Defence (United States of America)
DOSE	Dynamics of the Solid Earth
DOP	Dilution of precision
GPS	Global Positioning System
HA	Hour Angle
HartRAO	Hartebeesthoek Radio Astronomy Observatory
HEMTS	High Electron Mobility Transistors
IERS	International Earth Rotation Service
IfAG	Institut für Angewandte Geodäsie
IF	Intermediate Frequency
IGS	International GPS Service for Geodynamics
LLR	Lunar Laser Ranging
mas	milli-arcsecond
MASER	Microwave Amplification by Stimulated Emission of Radiation
MCS	Master Control Station
PPS	Precise Positioning Service
PR	Pseudorange
PRN	Pseudorandom noise
RF	Radio Frequency
SA	Selective availablity
SLR	Satellite Laser Ranging
SPS	Standard Positioning Service
SSB	Solar-System-Barycentric
TOA	Time of arrival
UERE	User Equivalent Range Error
VLBI	Very Long Baseline Interferometry

Chapter 1

Introduction

1.1 Background

Very Long Baseline Interferometry (VLBI) is a technique developed by astronomers to measure accurately the positions and spatial structure of astronomical radio sources utilising radio telescopes. The main components and configuration of the Hartebeesthoek Radio Astronomy Observatory (HartRAO) radio telescope are depicted in figure 1.1. The parabolic reflector has a diameter of 26 metres (m) and a

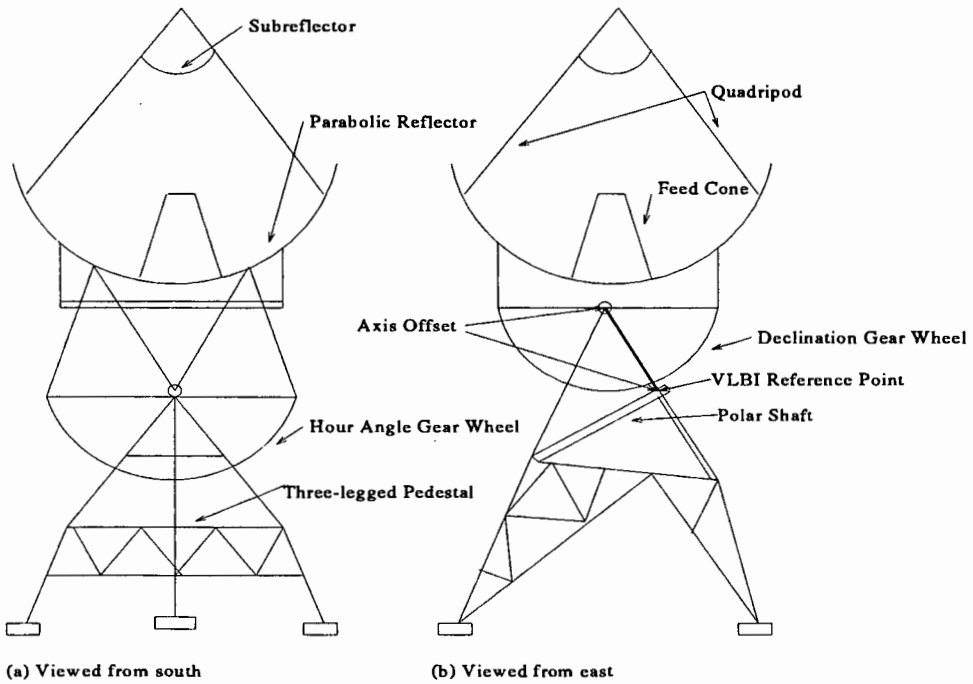

Figure 1.1: Simplified schematic of the HartRAO 26 m antenna illustrating the main structural components

prime focal distance of $\sim$ 11 m. It has an equatorial mount so that the main (polar) shaft is aligned parallel with the rotational axis of the Earth. A secondary hyperbolic reflector focuses the incoming radiowaves into feeds mounted inside a cone which is located inside the dish.

VLBI has been used since the early 70's in high precision geodynamical studies for determining the position of and baseline between stations using observations of extragalactic radio-sources (quasars). HartRAO currently supports several long term international geodetic VLBI projects.

In general, the travel time of a wavefront between the antennas at two or more sites is measured by maximising the cross-correlation function of the different signals received at the antennas. The difference in travel time (group delay) is a function of the geometry of the participating stations, the spatial distribution of the radio sources, the effects of the propagation medium and instrumental effects (Kolaczek 1989). The latter includes clock drifts and the offset of the antenna axis which is by definition the distance between the Hour Angle (HA) rotational axis and the Declination (DEC) rotational axis. The group delay is one of the parameters which allows solving for the baseline coordinates. The HartRAO antenna axis offset is the topic of this thesis.

From June to September 1993 HartRAO supported a mobile Satellite Laser Ranging system (SLR) owned and operated by the Institut für Angewandte Geodäsie (IfAG). This necessitated the construction of a very stable SLR reference pier, tied down to bedrock, which was to be used as a reference point for their project. The same reference point is to be used for this project.

The Global Positioning System (GPS) was developed by the USA Department of Defence to provide instantaneous positioning and velocity determination data for its armed forces. To ensure that four satellites are always visible to a receiver, a system was developed whereby 21+3 evenly spaced satellites placed in 12-hour orbits inclined at 55° to the equatorial plane would provide the required coverage most economically. Currently there are more than 21 operational satellites in orbit. The techniques of VLBI, GPS and SLR further the scientific understanding of Earth dynamics, earthquake mechanisms and tectonophysics.

These techniques find application (amongst others) in the following areas:

(1) Studies of the Earth's variable rotation, this includes the motion of the Earth's rotation axis with respect to the Earth as shown by polar motion and the angular position around the Earth's rotation axis describing universal time (UT1).

(2) Studies of angular momentum transfer from the atmosphere and its effect on the rotation of the Earth.

(3) Crustal dynamics - e.g. tectonic motion.

(4) Global studies of true variation of ocean levels by linking tide gauges to fundamental VLBI and SLR sites.

(5) Geophysical studies - e.g. VLBI has significantly improved our knowledge of the shape of the core-mantle boundary.

(6) Geomorphological studies - e.g. global and tectonic geomorphology.

(7) Geopotential field measurements - SLR data from LAGEOS is very important to enable measurement of long wavelength temporal components of the gravity field.

1.2 Antenna Axis Offset

The axis intersection (VLBI reference point) is, by definition, the intersection of the two axes, i.e. the HA and DEC axis of a telescope. If these axes do not intersect as in HartRAO's case, then it is the projection point of the secondary axis onto the primary axis. At HartRAO this point is situated within the HA shaft fairly close to the HA encoder. This point is supposed to be fixed and is therefore regarded as a fixed reference point. Before this point can be calculated the axis offset needs to be determined. This offset is the distance from the VLBI reference point, normal to the HA axis, to the DEC axis and is illustrated in figure 1.1. The axis offset problem can be made clear by a simple example. If one assumes a 10 metre axis offset then a tilt of the fixed axis by 10^{-4} radians (a few mm) will result in a delay error of approximately 1 mm as the axis is not exactly as it should be at a given azimuth and elevation. In a similar way a few mm non-intersection of the two axes will cause a few mm delay error.

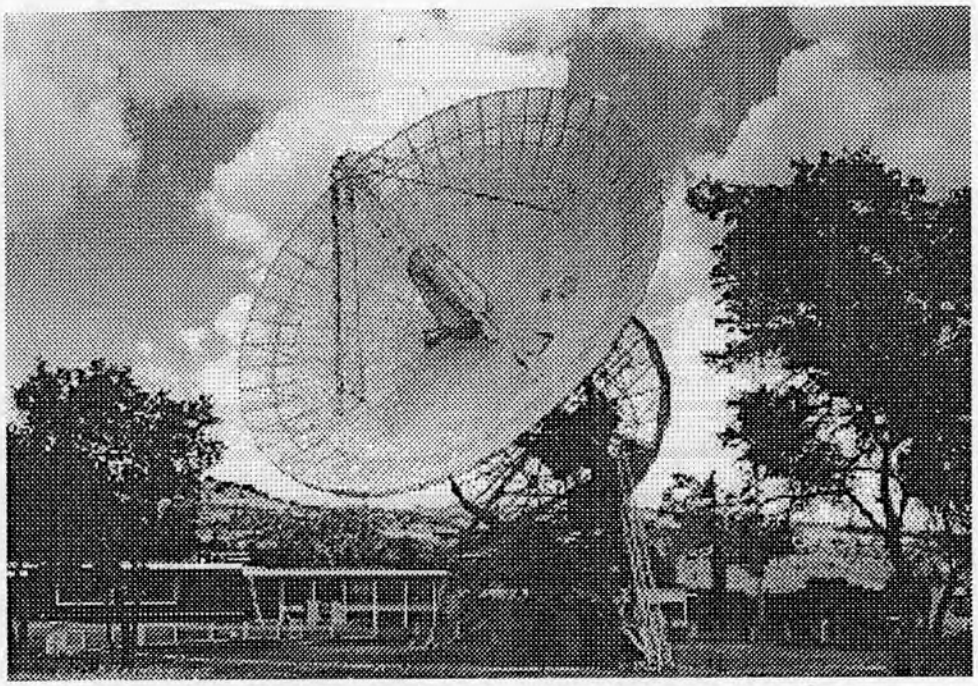

Figure 1.2: The HartRAO 26 m antenna. The HA gear wheel is clearly shown. A GPS antenna was mounted on top of the structure supporting the hyperbolic subreflector.

The axis offset has been determined by VLBI and conventional surveying instruments, but there is a difference of up to 17 mm between individual VLBI solutions and the JPL standard value of 6706 mm. A comparison of the results is made in section 7.5.

1.3 Rationale and Scientific Objective

It is important to have an independent check of the HartRAO antenna axis offset in order to verify the results of the other techniques. This will increase the reliance and validity of the model for delay terms as used for the antenna and so improve the accuracy and reliability of geodynamical results which are derived from VLBI using the HartRAO antenna. This work will also allow the three reference systems, namely VLBI, SLR and GPS to be tied to a common point, i.e. the SLR reference marker. The primary objective of this work is the determination of the axis intersection and offset of the HartRAO 26 m telescope (figure 1.2) and possible variation of these parameters due to gravitational distortion and temperature related expansion, by using GPS.

1.4 Outline and Summary

Chapter 2 introduces basic geodetic VLBI, the VLBI delay model, different antenna geometries and where the antenna axis offset fits into the model. The basics of GPS, accuracy levels of different baselines scales and the different types of observables are described in chapter 3. Chapter 4 contains the data tables and describes the methods, equipment and rationale used for sampling. Possible sources of error are described as well as preventative measures to reduce their magnitude. Chapter 5 describes three approaches to determine the antenna axis offset after data collection using GPS; analytical geometry, matrices and least-squares. The suitability of the different approaches are discussed. The software which was developed to analyse the data is briefly described in chapter 6. Approximately 6000 lines of C code were written during the course of this project. Analyses of the data and results found are described and discussed in chapter 7. Chapter 8 contains conclusions based on the results from this work. The references follow after chapter 8 and the appendix forms the last section of this work. This contains additional clarification of certain terms and a short review of the problems encountered in the literature on circle centre determination. It should not be read as a stand-alone chapter but referred to as references are made to it in the main text.

Chapter 2

Axis Offset Influence on the VLBI Delay Model

2.1 Introduction

The observed values of delay and delay rate obtained from a network of VLBI stations of a number of different radio sources, have to be processed by software specifically developed for the task. This software contains a multiparameter estimation routine which solves for the model parameters. The sophistication of the models improve in tandem to the improvement in accuracy of the VLBI instrumentation and is therefore under continuous development. In order to understand what the antenna axis offset problem is, as well as where and how it fits into the software and model that allows one to compute theoretical delays and delay rates, it is necessary to explain very briefly how a typical delay model works. The discussion is simplified in the extreme and biased towards the geodetic application of VLBI, although many principles apply similarly to astronomical VLBI.

Several software packages are in use by the Geodetic VLBI community, but the program which will be referred to specifically is Modest by Sovers & Jacobs (1994). Another program used is Calc, which is part of the Mark III geodetic analysis package (Gordon & Hughes 1994) which computes theoretical VLBI delays and rates.

In this chapter introductions are given to the historical development and basic principles of VLBI along with its basic instrumentation. The VLBI model for the observed delay is also described. The antenna axis offset is brought into context by describing its influence on the geometrical and tropospherical components of the delay model.

2.2 Geodetic VLBI

2.2.1 Historical Development

Geodetic VLBI results from microwave radio interferometry which was developed by radio astronomers for the purpose of improving their understanding of the structure and evolution of stars and galaxies [see Thompson et al. (1986) and Felli & Spencer (1989)]. It is also used in astrometry, to provide positional accuracies at the level of $\sim$ 100-300 milli-arcseconds (mas) for short (<30 km) baselines (Walter 1983) and less than 10 mas for longer ($\sim$ 10 000 km) baselines (Ma 1989) in applications such as the determination of extragalactic reference frames.

Before the development of very stable clocks, a single clock was used as a reference in a technique known as Connected Element Interferometry (CEI), a method still in use today. The radio signals were received by receivers with a common oscillator and were brought together by cables to a correlator for estimating the time or phase delays. Cross-correlation was done in real time and CEI baseline lengths were limited to tens of kilometres. During the late 1960s the development of high stability clocks such as the hydrogen MASER[1] (Vessot 1980, Reinhardt & Rueger 1980 and Sydnor 1983) led to ensured coherence and this allowed the use of an independent oscillator for each receiver. The basic principles of CEI and VLBI are essentially the same, the major differences being that in VLBI the stations operate without real time communication, and the baselines are generally more than two orders of magnitude longer. The baseline length in VLBI is constrained only by the requirement that the source be visible to both stations at the same time for a sufficient period. Signals recorded are stored on tape and correlated at a later date.

Historical reviews of Geodetic VLBI can be found in NASA Conference Publication 2115 (1980), NASA Technical Paper 2147 (1983) and Lambeck (1988). The advantages of using VLBI to make geophysical and geodetic measurements were recognised in the late 1960s (Gold 1967) and in the early 1970s Earth orientation and baseline length measurements were initiated. The Crustal Dynamics Project (CDP) of NASA was established in October 1979 and was completed in December 1991. This program utilized VLBI, SLR, Lunar Laser Ranging (LLR) and GPS. It was succeeded in 1992 by a new program termed Dynamics of the Solid Earth (DOSE) (Bosworth et al. 1993). Since their inception these programs have improved the accuracy of baseline determination from tens of centimetres to the millimetre levels which are currently being achieved (Rogers et al. 1993). The CDP VLBI data in

[1]The most stable operational frequency standard for averaging time < 1 sec.

general confirmed the NUVEL-1 plate motion model. The NUVEL-1 model was derived using considerably more data (conventional data such as transform fault orientations, spreading rates and earthquake slip vectors) than in previous models. Results and discussions of the application of CDP data can be found in Ma (1992), Ma et al. (1993), Ryan et al. (1993), Stein (1993) and McCarthy (1993).

2.2.2 Instrumentation

The basic instrumentation at a VLBI station consists of a suitable antenna, receiver, frequency standard and data acquisition terminal (DAT). The DAT is an integrated computer-controlled system which has as an input the analog intermediate frequency (IF) signal. (An IF is obtained by mixing the source frequency with a stable reference sine wave. The output from the mixer is filtered to obtain only the difference frequency.) The DAT takes the IF signal and converts selected frequency windows to video (baseband), samples and formats each video signal and records the resulting time-tagged serial data streams in parallel on magnetic tape. The first computer controlled DAT was dubbed the MK III which was developed specifically for the purpose of making geodetic measurements (NASA Technical Paper 2147 1983) and superceded previous DATs such as the MK I system used from 1972 to 1978. The MK I was a single frequency (X-band $\sim$ 3.6 cm wavelength) system with a recording bandwidth of 360 KHz. The MK II was capable of dual-frequency operation and could operate at S ($\sim$ 13 cm wavelength) and X bands with a recording bandwidth of 2 MHz. The MK II system was used at HartRAO until 1995 for astronomical VLBI, but is no longer supported by the greater VLBI community. The first MK III VLBI measurements were made in August 1979 using three stations and achieved an rms data fit of 3 cm on all three baselines (Bosworth et al. 1993).

The MK IIIA high density tape recorder was developed in 1985 and is effectively a 14-fold improvement over the MK III, allowing a higher recording rate and a reduction in the amount of tape required. Many other improvements have been made such as using high electron mobility transistors (HEMTS) in the receiver front-end to reduce system temperature. RF and IF bandwidths have been increased (Corey and Clark 1991) to 800 MHz at X-band and 240 MHz at S-band and correlators have been upgraded (Whitney 1988). HartRAO currently operates a MKIIIA tape recorder and a MK III DAT with wideband upgrade. Current limitations in accuracy are attributable more to errors in;

(1) modelling

(2) delays incurred when a radio signal passes through the atmosphere

(3) undiagnosed equipment failures

(4) the calibration system

(5) antenna deformation

than instrumentation problems (Herring et al. 1991). The antenna axis offset will change in magnitude when structural deformation is present.

2.2.3 Geometric Delay

Introductions to the principles of VLBI can be found in Ma (1978), Thompson et al. (1986) and Lambeck (1988). The time interval between the arrival of a radio wave at one end of an interferometer and its arrival at the other end is the primary observable for geodetic VLBI. This interval is termed the delay and its derivative is the delay rate observable (Ma 1978). The geometric delay can be defined (Sovers & Jacobs 1994) as that interferometer delay which would be measured by perfect instrumentation which are perfectly synchronized, if it is assumed that a perfect vacuum existed between the extragalactic source and Earth. This delay can be as large as 20 ms, changing by up to 3.1 μs per second as the Earth rotates. The geometric component of the delay is generally the largest component of the observed delay.

Basic Interferometer To be practical a two-station interferometer is considered in this example, the principles are of course applicable to any number of stations. Figure (2.1) illustrates the basic interferometric geometry. The baseline separating the antennas is D and the antennas are pointing towards the same source. Due to the distance to the source, the arriving wave front is assumed to be planar. The plane wave moves in direction $\hat{k}$. The station reference points at t_1 are denoted by station 1 = #1, station 2 = #2. At time t_2 the reference position of station 2 is #3. If station 2 had not moved this time delay would be $t_1 = (D/c)\sin\theta$. Here t_1 is the geometric delay and c the speed of light. However, station 2 has moved due to the rotation of the Earth. Baseline D is the baseline vector. The distance l is the sum of the two solid lines perpendicular to the planar wave front. The time taken for the wave front to move this distance is the actual time delay. The appropriate equations can be found in Sovers & Jacobs (1994).

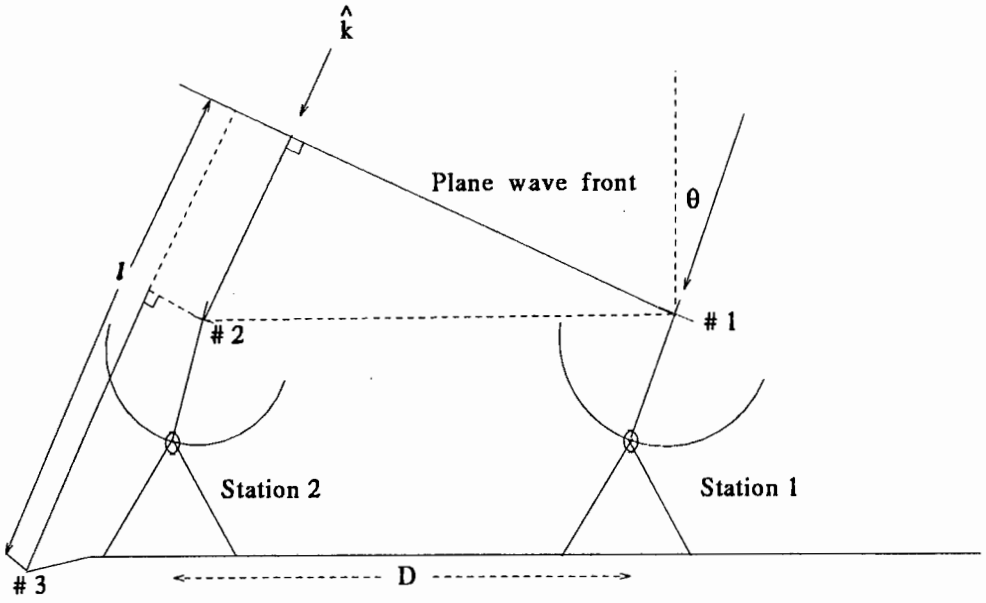

Figure 2.1: Geometry of an elementary interferometer. Adapted from Thompson et al (1986) and Sovers & Jacobs (1994).

2.3 VLBI model for the Observed Delay

A delay model is the sum of four major model components:

(1) **GEOMETRY**

Assume a station has perfect, synchronized instrumentation, with the space separating the radio telescope and the observed object being a perfect vacuum. The interferometric delay would then be the *geometric delay* and can be as large as 20 ms with changes of up to 3.1μs per second as the Earth rotates.

(2) **CLOCK**

A delay that models the behaviour of a station clock. For a 24 hr session, the HartRAO clock (Hydrogen MASER) drifts $\approx 0.19\mu$s.

(3) **TROPOSPHERE**

The delay due to the wet and dry component of the troposphere. This is approximately 2 metres in path length, i.e. $\approx$ 6.6 ns.

(4) **IONOSPHERE**

For a typical ionosphere the delay is approximately 0.1-2 ns.

Numerous coordinate transformations are required to relate the stellar reference frame used to the Earth-fixed reference frames in which the stations are located.

They will not be discussed here and can be found in Sovers & Jacobs (1994). It is however necessary to summarise the calculation of the VLBI model for the observed delay. The MODEST model is used; subcentimetre relativistic complications caused by locally varying Earth potential are not included.

Summary of Steps Required to Calculate VLBI Delay Model

(1) The proper locations of the two stations as measured in an Earth-fixed frame at the time that the wave front intersects station 1 at position #1 must be specified.

(2) The station locations must be modified for tectonic motion, solid Earth tides and other local station motion.

(3) The station locations must then be transformed to a celestial coordinate system with the origin in the centre of mass of the Earth.

(4) Transform the station locations to a frame at rest relative to the centre of mass of the Solar System, rotationally aligned with the celestial geocentric frame.

(5) Determine the time delay for the passage of the wave front from position #1 to #3 in this Solar-System-Barycentric (SSB) frame. Correct for source structure and add the delay caused by the differential gravitational retardation of the signal.

(6) Transform this SSB geometric delay back to the celestial geocentric frame moving with the Earth.

This completes the geometric portion of the delay model. To complete the model:

(7) Add the contributions due to tropospheric delays, clock offsets and the effects of the ionosphere on the signal.

Including the Antenna Axis Ofset The discussion so far indicates how a time delay model would be calculated for two points which are fixed with respect to the Earth's crust. In reality an antenna is not a true Earth-fixed point. There are delays due to instrumentation in the system and furthermore, sections of the antenna move relative to the Earth. The antenna axis offset affects the geometrical and tropospheric component of the delay model.

2.3.1 Antenna Geometry

Several antenna geometries exist and not all of them have an antenna axis offset. Four common antenna mount types are:

(1) Intersecting Azimuth-Elevation,

(2) Azimuth-Elevation with Offset,

(3) Hour Angle-Declination (Equatorial),

(4) X-Y.

The HartRAO antenna has an Hour Angle-Declination mounting, where the main axis (polar axis) is parallel to the Earth's rotation axis. A generalised antenna pointing system is shown in figure (2.2), with unit vector unit vector $\boldsymbol{s}$ pointing to the apparent source position. A symmetry axis AD is parallel to $\boldsymbol{s}$. Point A is the end view of the DEC axis which rotates in the plane perpendicular to the axis. A distance H, which is the antenna axis offset, separates the DEC axis from the second rotation axis which is the polar axis BE. All the points on the polar axis are fixed relative to the Earth, so that any point could be used for the fiducial point which terminates this end of the baseline. In practice point P, the VLBI reference point, is used. This is the intersection of the two axes, i.e. the HA and DEC axis of a telescope. If these axes do not intersect as in HartRAO's case, it is the intersection point obtained when the plane containing the secondary axis A and perpendicular to BE is projected onto the primary axis BE. At HartRAO this point is situated within the HA shaft close to the HA shaft position encoder. This point is supposed to be fixed and is therefore regarded as a fixed reference point.

The plane Q, which contains the rotation axis A, is an isophase plane for plane wave fronts as it coincides with the wave front. If l is the length of a line from P to the Q plane and is perpendicular to that plane, the wave front will reach the axis intersection point P at a time $\Delta = l/c$ after the wave passes through axis A. If τ_0 is the model delay for a wave front to pass from P on antenna N^o 1 to a point P on antenna N^o 2, the model should be changed to:

$$\tau = \tau_0 - (\Delta t_2 - \Delta t_1) = \tau_0 + (l_1 - l_2)/c. \tag{2.1}$$

The subscripts refer to antennas N^o 1 and N^o 2. Following a treatment by Sovers & Jacobs (1994) which is based on work by Wade (1970) on the effect of nonidentical

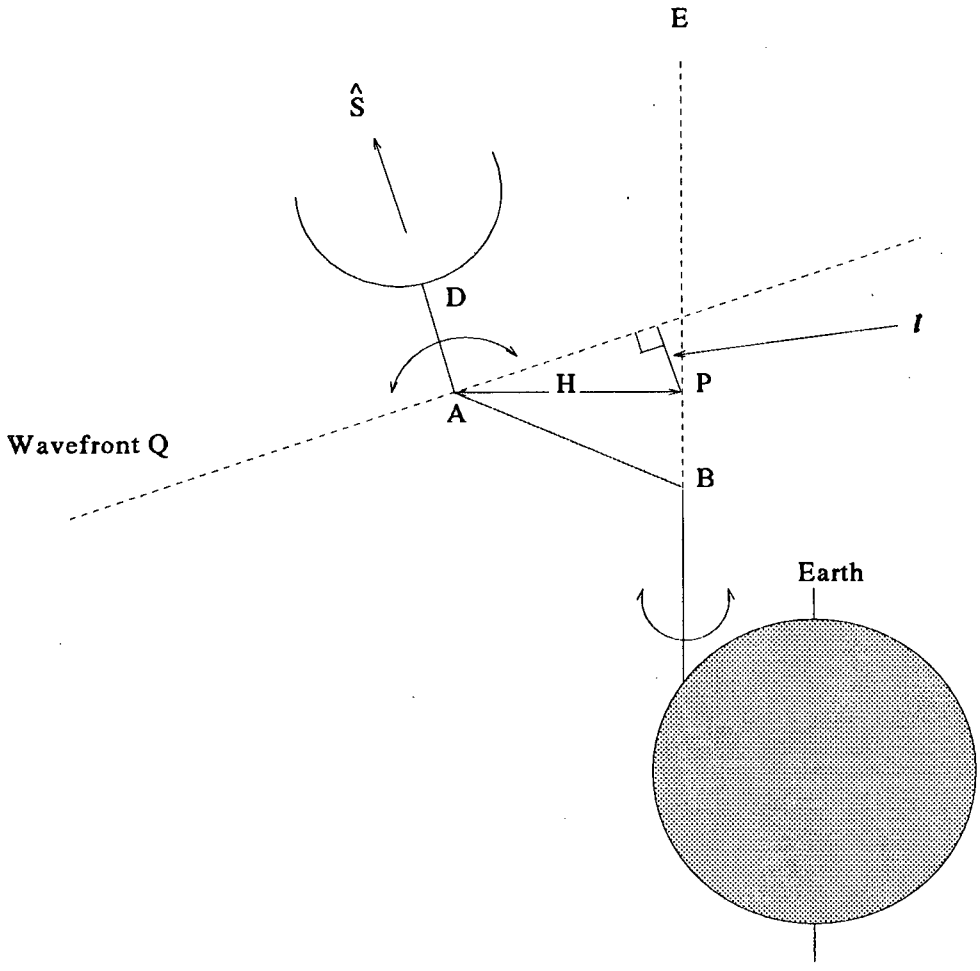

Figure 2.2: Generalized schematic representation of the geometry of a two-station VLBI network. Only one station is shown. Adapted from Sovers & Jacobs (1994).

antenna mountings of the NRAO [2] three-element interferometer, two other coplanar vectors, $\boldsymbol{I}$ along BE and positive away from Earth, and $\boldsymbol{L}$ from P to A are defined. Then one has

$$\boldsymbol{L} = \pm H \frac{\boldsymbol{I} \times [\boldsymbol{s} \times \boldsymbol{I}]}{\mid \boldsymbol{I} \times [\boldsymbol{s} \times \boldsymbol{I}] \mid} \tag{2.2}$$

Where the $\pm$ is chosen to give $\boldsymbol{L}$ the direction from P to A. When $\boldsymbol{s}$ and $\boldsymbol{L}$ are parallel or antiparallel the plus sign is used when the antenna moves closer to the source as H increases. Since

$$\boldsymbol{I} \times [\boldsymbol{s} \times \boldsymbol{I}] = \boldsymbol{s} - \boldsymbol{I}[\boldsymbol{I} \cdot \boldsymbol{s}] \tag{2.3}$$

[2]National Radio Astronomy Observatory, Green Bank, West Virginia.

then

$$l = \boldsymbol{s} \cdot \boldsymbol{L} = \pm H\sqrt{1 - [\boldsymbol{s} \cdot \boldsymbol{I}]^2} \tag{2.4}$$

For an HA-DEC mount the vector $\boldsymbol{I}$ is aligned towards the north pole in the northern hemisphere and towards the south pole in the southern hemisphere. For the HartRAO antenna one can write

$$l = \pm H \cos(S_{DEC}), \tag{2.5}$$

where S_{DEC} is the source declination.

2.3.2 Effect of the Troposphere

The neutral lower atmosphere (troposphere) affects radio propagation by refraction, absorption and scattering (Thompson et al. 1986). The troposphere's two major constituents are the dry and wet components. MODEST has the capability to model each wet and dry component as an azimuthally symmetric function of the local geodetic elevation angle.

Dry Component: The dry component consists primarily of oxygen and nitrogen. The excess path length which is caused by this dry component can be accurately estimated by measuring the barometric pressure. The excess path length does not depend on the height distribution of temperature or total density, but under conditions of hydrostatic equilibrium it depends only on the surface pressure P_0. The excess path length is 231 cm in the local zenith direction at sea level, where under standard conditions $P_0 = 1013$ mb. The dry excess path length in the zenith direction is discussed in detail by Thompson et al. (1986) and the appropriate equations are not repeated here.

Wet Component: The wet component is not easily modelled as it is not well mixed in the atmosphere and its correlation with ground-based meteorological measurements is poor. At zenith the delay contribution can reach 20 - 30 cm. Long baselines allow the use of the interferometer data to determine the delay contribution due to water vapour as part of the parameter estimation process which improves the accuracy in the determination of this parameter.

Antenna Axis Offset Altitude Correction: The secondary rotation axis of Equatorial and X-Y mounts has a vertical movement with changing dish orientation. In the case of the HartRAO antenna this is the declination axis A in Figure 2.2.

This vertical movement leads to variation in the zenith troposphere delay of 1 - 2 mm. This zenith variation is increased by the mapping function to 1 - 2 cm when the antenna is pointing towards a source at low elevation. The correction added to the zenith dry tropospheric delay in the model used by MODEST (Sovers & Jacobs 1994) is

$$\delta_\tau = -\rho z_{dry}(\frac{H}{\Delta})\psi. \tag{2.6}$$

Here ρz is the additional delay at local zenith due to the troposphere, H is the antenna axis offset, ψ is an angular factor which depends on the type of antenna mounting and Δ is the dry troposphere scale height ($\sim$ 8.6 km). For the HartRAO equatorial mount,

$$\psi = \cos\phi \cos h, \tag{2.7}$$

where h is the local HA east of the meridian and ϕ is the geodetic latitude.

2.4 Summary

The very high precision obtained in geodetic VLBI requires the use of delay models which are as accurate as possible. In order to be accurate at the subcentimetre level, parameters such as the axis offset must be known to a high degree of accuracy as it has a direct impact on the VLBI delay model by influencing the dry tropospheric and geometric delay.

Chapter 3

GPS

3.1 Introduction

The GPS program was initiated in 1973 when the United States Air Force, Army, Navy, Marine Corps and Defence Mapping Agency decided to use their combined technical resources to develop a very accurate space-based navigation system. Personnel from these agencies were assembled into the initial cadre of a GPS Joint Program Office and were later joined by a contingent of nine other NATO member nations (Parkinson & Gilbert 1983). The primary justification for the GPS program was military (Daly 1993) but the number of civilian users and applications are growing daily. GPS provides highly accurate time, velocity and positional data as well as meeting the common radio positioning requirements of a broad spectrum of users. Depending on the mode of use and the equipment used, high precision measurements can be made in geodetic applications. It is therefore utilised in geodetic programmes to supplement and strengthen the databases which are used to build models of the Earth's gravity fields, ocean tides, sea surface topography, orientation, global sea level and ocean circulation. It is especially suitable for high precision short baseline work. GPS is seen as the primary tool of geodesists due to the dramatic improvements in techniques and processing software, availability and economical access to GPS equipment, portability and the benefits of international collaboration (Blewitt 1993). This chapter briefly describes the general system, observables, system accuracy and carrier phase precision.

3.2 General System Description

The GPS system comprises three major segments; Space, Control and User segments. Operation of the Space and Control segments is managed by the USAF Space Com-

mand and the supporting command for GPS operations is the responsibility of US Air Force Logistics Command (AFLC).

3.2.1 Space Segment

The fully operational space segment was planned to have a constellation of 21 satellites, plus 3 operational spares, in six planes with four satellites per plane. Their orbits are nominally circular with an inclination of $\sim 55°$ and have a period of 12 hours. Orbital height is approximately 20 200 km. The satellites transmit a spread spectrum signal on two frequencies in the L band, known as Link 1 (L1)=1575.42 MHz and Link 2 (L2)=1227.6 MHz. The L1 signal is modulated with a precision (P) ranging code and a coarse/acquisition (C/A) ranging code, whereas the L2 signal is only modulated with the P-code. All signal components are controlled by atomic clocks which is the key to the system's accuracy. Superimposed on the codes are navigation message data, which includes satellite clock and ephemeris parameters, UTC synchronization information and satellite signal health data. At present four to eight satellites are visible with an elevation mask of 15°.

3.2.2 User Segment

User Access

Two methods are used to lower the accuracy of the system (Hoffman-Wellenhof et al. 1993).

Selective availability (SA). SA mainly affects single receiver usage and is achieved primarily by dithering the satellite clock frequency. The transmitted navigation message can also be truncated which denies the user the ability to accurately compute the coordinates of the satellites.

Anti-spoofing (AS). This feature is invoked randomly to negate potential spoofing (hostile imitation) of PPS users. This ability essentially turns off the P-code or turns on an encrypted Y-code.

Levels of Service

There are two basic levels of service provided by GPS:

Precise Positioning Service (PPS) The PPS can provide 8 metre circular error probable (CEP) positioning and 100 ns (one sigma) UTC time transfers. CEP is defined as the radius of a horizontal circle containing 50 % of all possible

position fixes. This service is only available to authorised users and is primarily intended for military users. Access to the PPS is controlled by US Department of Defence (DOD) by invoking SA and AS.

Standard Positioning Service (SPS) This service is specified to produce 100 m horizontal positioning and approximately 337 ns UTC time transfer accuracy.

Users are divided into two categories, those who have access to the PPS and the balance are by default users of the SPS. A PPS-capable GPS receiver has the built-in cryptographic logic which allows cryption/decryption processing with the PPS keys. Normally PPS-capable GPS receiver sets apply PPS encryption/decryption processing for SA and AS functions, although some GPS receivers used in geodetic survey networks operate in a limited PPS mode. With these GPS receivers PPS encryption processing is required only for real-time support of the AS function as the SA decryption functions are taken care of during post-processing.

3.2.3 Control Segment

The control segment consists of one Master Control Station (MCS) at Falcon AFS in Colorado and five monitor stations located at Hawaii, Kwajalein, Diego Garcia, Ascension and the MCS (NATO 1991). The MCS collates the tracking data from the monitor stations and calculates the satellite orbit and clock parameters. Three ground control stations which are co-located with the monitor stations at Kwajalein, Diego Garcia and Ascension upload the results as determined by the MCS.

Many other non-military monitor stations contribute to the development of refined orbits and the collection of data for geodynamic research. A ROGUE GPS receiver (SNR-8) is located at the Satellite Applications Centre of the Council for Scientific and Industrial Research at a distance of $\sim$ 2 km from the HartRAO antenna. This receiver is part of the CNES GPS network, which includes four other stations at Pamatai (Tahiti island), Kerguelen (Kerguelen islands), Kourou (French Guiana) and Grasse (southern Alps in France). The five CNES stations contribute to the International GPS Service for Geodynamics (IGS) which uses data from a global network of more than fifty stations distributed around the world. Results from the IGS are depicted in figure (3.1). The data covers a period of nearly five years, from 22nd January 1991 to the 29th September 1995. The reference frame is ITRF 1993.

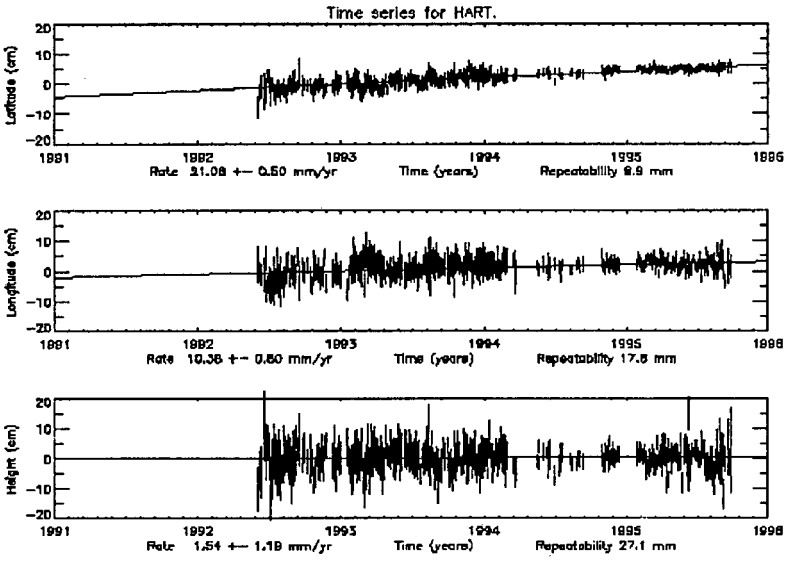

Figure 3.1: Latitude, longitude and height as a function of time of the CNES ROGUE GPS receiver located at Hartebeesthoek. Source: IGS Central Bureau, http://sideshow.jpl.nasa.gov/mbh/global/Hart.gif

3.3 GPS Observables

There are two GPS observables which are used to determine position. Lower precision applications such as navigation use *pseudo ranges*. In geodetic surveying *carrier phases* are used as it allows high precision.

3.3.1 Pseudo Range

GPS position determination is based on a concept termed *time of arrival ranging* (ARINC 1991). A simple example would be to consider the emission of a signal at some precise instant in time t_1 from a stationary transmitter. The signal arrives at a receiver some time later, say t_2. The time difference $t_2 - t_1$ allows the determination of the time of arrival (TOA) value. The range (distance) between receiver and transmitter can be found by multiplying the TOA with the signal propagation speed. When four satellites are observed simultaneously, the (x, y, z) position and receiver clock offset can be found from a single observation. In surveying terminology, this is resection by distance.

The GPS satellites transmit pseudorandom noise (PRN) sequence-modulated ra-

dio waves. The PRN codes are predefined strings of binary data which are generated from the satellite clock that serves as the time of transmission encoding for the signals. The code structure of the P and C/A codes, shift register configuration, code generation and code timing relationships are described in STANAG 4294 (1990) and will not be discussed here. The transmission of each satellite is unique even if they all transmit on the same frequency. This allows the GPS receiver to differentiate between the signals. This is accomplished by the GPS receiver generating a precise replica PRN sequence which is mixed in the receiver, slewed forward and backwards in time by a code-tracking loop until maximum correlation is achieved. The magnitude of the slewing is the observed TOA value.

The clock in the GPS receiver is not synchronized with the satellite clock, so that the TOA is not directly applicable to the simple example above. The receiver clock has a bias which is found by the data-processor of the GPS receiver set. When the observed TOA is multiplied by the signal propagation delay to find the geometric range, the receiver clock bias is included. This total range is termed a *pseudo range* (PR) measurement. The measured PRs are affected by the tropospheric and ionospheric propagation delays. The TOA therefore includes both the propagation delay and the clock offset. The general expression for the PR technique (Leick 1990) can be written as

$$[t_k + dt_k - (t^p + dt^p)]c = \rho_k^p + I_k^p + T_k^p. \tag{3.1}$$

Rewriting equation (3.1) in terms of the TOA and the speed of light c it follows that

$$P_k^p = (t_k - t^p)c = \rho_k^p + (dt^p - dt_k)c + I_k^p + T_k^p. \tag{3.2}$$

The subscript k refers to the GPS receiver, the superscript p refers to the satellite. Therefore receiver time(reception) is denoted by t_k, the satellite clock (transmit) time is t^p. Ionospheric delay is indicated by I_k^p and tropospheric delay by T_k^p. The topocentric (observer centred) distance between the satellite and GPS receiver at the times of transmission and reception is given by the equation for the true distance between two points, so that

$$\rho_k^p = \sqrt{(u^p - u_k)^2 + (v^p - v_k)^2 + (w^p - w_k)^2} \tag{3.3}$$

where the CTRS (see Appendix A.11) Cartesian coordinates of the receiver k and the satellite p is given by (u_k, v_k, w_k) and (u^p, v^p, w^p) respectively.

Position Determination using Pseudo Range

Using the PR as observable, equation (3.1) contains seven unknown parameters. The satellite clock error is negligible in this application and the ionospheric and tropospheric delays can be approximated by models. The four unknown parameters can be found from four PRs measured simultaneously to four satellites, giving the system of four ranging equations (Leick 1990, ARINC 1991):

$$P_k^1 = \sqrt{(u^1 - u_k)^2 + (v^1 - v_k)^2 + (w^1 - w_k)^2} + c\ dt_k \tag{3.4}$$

$$P_k^2 = \sqrt{(u^2 - u_k)^2 + (v^2 - v_k)^2 + (w^2 - w_k)^2} + c\ dt_k \tag{3.5}$$

$$P_k^3 = \sqrt{(u^3 - u_k)^2 + (v^3 - v_k)^2 + (w^3 - w_k)^2} + c\ dt_k \tag{3.6}$$

$$P_k^4 = \sqrt{(u^4 - u_k)^2 + (v^4 - v_k)^2 + (w^4 - w_k)^2} + c\ dt_k \tag{3.7}$$

A simplified user position determination algorithm would be:

(1) Track PRN sequences from four satellites.

(2) Multiply TOA values by the speed of light to obtain four PR measurements.

(3) Correct PR measurements for ionospheric and tropospheric delays. Add correction for difference between each satellite's clock and GPS system time, effects of relativity, etc. A 50 Hz digital data stream (navigation message) transmitted from the satellites along with their P- and C/A codes contains the necessary information, such as GPS sytem time of transmision, ephemeris and clock data for the particular satellite. Also included are the almanac data for all the satellites, coefficients for the ionospheric delay model and satellite health information to make these adjustments.

(4) Perform a position/time solution by solving the four range equations and compute the (x, y, z) position fix in terms of the WGS-84 coordinate system.

3.3.2 System Accuracy Characteristics

Two important parameters cause the GPS to show statistical accuracy distributions. Firstly, there is the error in the measured PRs and secondly, the accuracy limiting factor due to satellite geometry. These two factors are important as it leads to an understanding of the limitations of GPS and allows prediction of position and time accuracies.

User Equivalent Range Error (UERE)

The error in the determination of the PRs from each satellite is caused by errors in the the prediction of the satellite's orbit, the stability of its clock, errors in the navigation message, ionospheric and tropospheric model errors as well as correlation errors. The UERE is contained in the navigation message and in conjunction with DOP factors enables estimates of the precision in point positioning which can be achieved.

Dilution of Precision (DOP) Factors

The DOP factors are commonly used as a measure of the error contributed by the effect of the geometry of the satellite distribution on the position and time solution. Leick (1990) describes DOP factors to be *"simple functions of the diagonal elements of the covariance matrix of the adjusted parameters"*. This description becomes clear when it is realized that the Kalman filter in a GPS receiver contains a matrix of the estimates (the covariance matrix) of the PR errors. The Kalman filter characterizes noise sources resulting from errors in the ionospheric corrections, user clock drift etc, in order to minimise their error introducing effect. It is a recursive (linear combination of previous estimates and present data) mean-square estimator which in a least-squares sense, produces the minimum covariance estimate of the state vector, which includes parameters such as GPS receiver position and time. The error covariance matrix satisfies a Ricatti equation (Blinchikoff & Zverev 1976), which is relatively easy to solve using a microprocessor, which in turn facillitates implementation in a GPS receiver. The diagonal of the covariance matrix contains the variances of the position errors and the receiver clock bias error. Leick (1990) describes the derivation of the covariance matrix as

$$Q_X = (A^T A)^{-1} = \begin{bmatrix} \sigma_u^2 & \sigma_{uv} & \sigma_{uw} & \sigma_{ut} \\ \sigma_{vu} & \sigma_v^2 & \sigma_{vw} & \sigma_{vt} \\ \sigma_{wu} & \sigma_{wv} & \sigma_w^2 & \sigma_{wt} \\ \sigma_{tu} & \sigma_{tv} & \sigma_{tw} & \sigma_t^2 \end{bmatrix} \tag{3.8}$$

After transformation to the local geodetic coordinate system, the covariance submatrix is given as

$$Q_{LG} = \begin{bmatrix} \sigma_n^2 & \sigma_{ne} & \sigma_{nh} \\ \sigma_{eh} & \sigma_e^2 & \sigma_{eh} \\ \sigma_{hn} & \sigma_{he} & \sigma_h^2 \end{bmatrix} \tag{3.9}$$

where the subscripts refer to the local geodetic northing, easting and height.

A good DOP has a low number ($\sim 2-3$) whereas a bad DOP has a high number. Intuitively, the best possible DOP would be given by one satellite directly overhead and three satellites spaced evenly on the horizon. High DOPs result when the satellites are clustered together or form a line. As the satellite positions are predictable, DOP values can be calculated during the planning stages of a survey to ensure good values. To conclude this section the special types of DOPs are described briefly and their expressions given.

VDOP Vertical DOP. Describes the effect of satellite geometry on height.

$$VDOP = \sigma_h \tag{3.10}$$

HDOP Horizontal DOP. Indicates dilution of precision for horizontal positions.

$$HDOP = \sqrt{\sigma_n^2 + \sigma_e^2} \tag{3.11}$$

PDOP Position DOP. Combined vertical-horizontal position value.

$$PDOP = \sqrt{\sigma_u^2 + \sigma_v^2 + \sigma_w^2} \tag{3.12}$$

TDOP Time DOP. Time dimension effect of geometry.

$$TDOP = \sigma_t \tag{3.13}$$

GDOP Geometric DOP. A composite measure of the vertical-horizontal-time dimensions.

$$GDOP = \sqrt{\sigma_n^2 + \sigma_e^2 + \sigma_h^2 + \sigma_t^2 \cdot c^2} \tag{3.14}$$

3.3.3 Carrier Phases

Carrier phase measurements are more precise than PR measurements and are used on both short and very long baselines with high precision. Baseline repeatability of 2 mm + 2 x 10^{-9} x L (L denotes baseline length) were demonstrated by Blewitt and Lichten (1992) using data from 21 globally distributed P-code receivers.

The question "what is a carrier phase" is best answered by starting at first principles. The phase observable is the difference in phase between the transmitted carrier wave from the satellite and the receiver oscillator signal at a specified epoch t. The phase of a wave thus only has meaning when it is specified relative to another

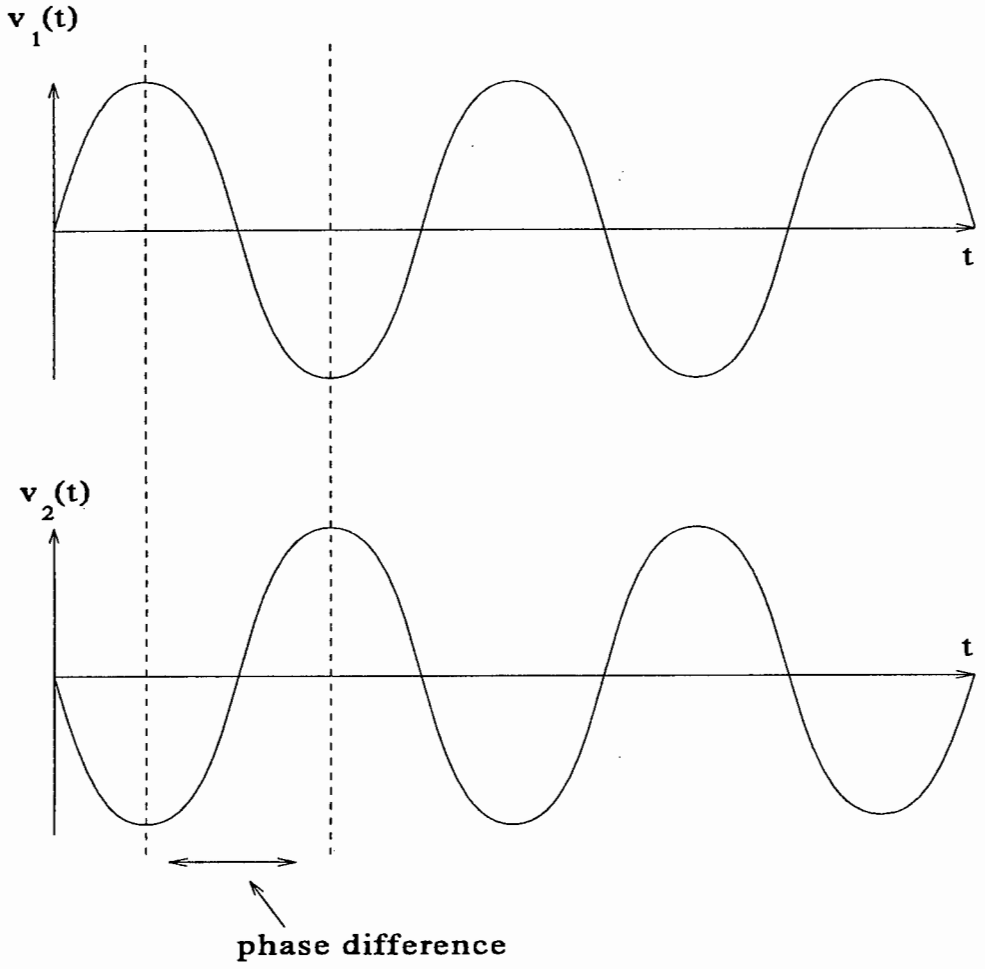

Figure 3.2: Phase relationship of two waves of the same frequency but 180° out of phase.

wave of the same frequency. One can express the initial phase mathematically as the angle ϕ in the equation

$$v(t) = V_0 \sin(2\pi f t + \phi) = V_0 \sin(2\pi t/T + \phi) \tag{3.15}$$

where one complete period T corresponds to 360° and $v(t)$ is the amplitude v of the wave as a function of time t. The phase is the argument $(2\pi t/T + \phi)$. The angular frequency ω equals $2\pi f$. Figure 3.2 depicts two waves which are 180° out of phase. The wavelength of the L1 carrier is approximately 19 cm, therefore the fraction of the carrier phase in our example would be about 9.5 cm. Once the integer number of carrier cycles is known, the accuracy of the phase measurement will be determined by how accurate this phase difference is determined. Any two sine waves of arbitrary phases but of the same frequency will add together to form a carrier of the same

frequency and a definite phase ϕ. One can thus write

$$V_1 \sin(\omega t + \phi_1) + V_2 \sin(\omega t + \phi_2) = V_0 \sin(\omega t + \phi) \tag{3.16}$$

The example of two waves 180° out of phase will therefore add to give zero. The basic phase equation can be written (Leick 1990) as:

$$\varphi_k^p(t) = \varphi^p(t) - \varphi_k(t) + N_k^p(1) + noise \tag{3.17}$$

The carrier phase observable in units of cycles for satellite p and receiver k is denoted by $\varphi_k^p(t)$. The received phase of satellite p as measured at the receiver k is denoted by $\varphi^p(t)$, whereas $\varphi_k(t)$ denotes the receiver oscillator phase. The unknown number of integer cycles at the initial epoch is denoted by the constant $N_k^p(1)$. Once signal acquisition has started the whole number of cycles are counted. The phase measurements are ambiguous and unless the absolute range difference at the initial epoch is determined, the phase measurement only provides the changes in range over the observed period. The initial integer ambiguity depends on the receiver-satellite combination at the initial epoch and remains the same over a particular observing period. This allows the initial and unknown integer ambiguity to be represented by a single bias term. A cycle slip can occur when tracking is interrupted due to blockage of the signals, weak signals or incorrect signal processing due to receiver software failure (Wellenhof et al. 1993). This cycle slip will alter the integer number of cycles, although the fractional phase measurement after reacquisition of the signal will be the same as if the tracking had not been interrupted. Several techniques have been developed to fix cycle slips, such as search techniques, discrete Kalman filtering, optimized Cholesky decomposition and in the case of dual-frequency data in code and carrier, widelaning ambiguity fixing. Fast techniques are very important for real time applications and much research is currently in progress (Frodge et al. 1993) to find better and faster ambiguity resolution methods. Brief descriptions of several techniques can be found in Leick (1990), Blomenhofer et al. (1993) and Chen (1993).

Following discussions by Hoffman-Wellenhof et al. (1993) and Leick (1990) the expressions for the double difference observable is derived. The notation follows those of Leick (1990). Atmospheric effects on the travel time τ of the carrier from the satellite is omitted for the sake of simplicity. The real travel time is a function of not only the geometric distance between the receiver and the satellite, but is also affected by the tropospheric and ionospheric delay. The troposheric time delay is caused by angular bending of the radio waves (which increases its path length) and a decrease

in the propagation velocity of the radio wave. The free thermal electrons in the ionosphere increases the apparent path length of the carrier. A complete description of the ionospheric correction model and tropospheric correction reference model is given in STANAG 4294.

Following Leick (1990) the received satellite carrier phase is related to the transmitted carrier phase by

$$\varphi^p(t) = \varphi^p_{Tr}(t - \tau) \tag{3.18}$$

where the subscript T indicates the transmitted phase. Using the Taylor series equation (3.18) can be expanded at epoch t with argument $-\tau$ so that

$$\varphi^p(t) = \varphi^p_{Tr}(t) - \dot{\varphi}^p_{Tr}(t)\tau + \frac{1}{2}\ddot{\varphi}^p_{Tr}(t)\tau^2 + \ldots. \tag{3.19}$$

The satellite and receiver clock frequencies are assumed perfect so that all frequencies are constant, therefore

$$f^p = f_k = f. \tag{3.20}$$

In reality of course, the GPS receiver uses a phase locked loop which enables it to synthesize its local oscillator frequency from a quartz crystal. Typical stability of an unovened quartz crystal is about 1 part in 10^{-6} and for an ovened crystal about 1 part in 10^{-7}. This is a factor of 10^5 or even a factor of 10^6 less stable than the stability of the satellite clock which should have a stability of about 1 part in 10^{-12} for an averaging time interval of 1000 seconds if it is a cesium or rubidium standard.

The inverse of the period $\frac{1}{T}$ and the time derivative equals the frequency so that

$$\dot{\varphi}^p = f^p = \frac{1}{T} \tag{3.21}$$

and therefore

$$\varphi^p(t) = \varphi^p_{Tr} - f\tau \tag{3.22}$$

To fully grasp the significance of equation (3.22) it is important to recognize that $f\tau$ is in fact the topocentric receiver-satellite distance divided by the wavelength of the transmitter carrier. The travel time τ is defined by

$$\tau = \rho^p_k(t)/c \tag{3.23}$$

where the receiver-satellite distance is ρ^p_k and c is the speed of light, which according to STANAG 4294 is 2.99792458×10^8m/s for WGS 84. Thus,

$$f\tau = \rho^p_k(t)/\lambda, \tag{3.24}$$

where λ is the wavelength of the transmitted carrier. Therefore $f\tau$ represents the number of wavelengths (or complete integer cycles), plus a fractional residual which will fit into the receiver-satellite distance. Substituting (3.22) into (3.17) gives

$$\varphi_k^p(t) = \varphi_{Tr}^p(t) - f\tau - \varphi_k(t) + N_k^p(1) + noise. \tag{3.25}$$

The undifferenced carrier phase observation is then found by substituting equation (3.23) into (3.25):

$$\varphi_k^p(t) = \varphi_{Tr}^p(t) - \frac{f\rho_k^p(t)}{c} - \varphi_k(t) + N_k^p(1). \tag{3.26}$$

Single difference Given two receivers k and m which are observing the same satellite p at the same preset epochs, the single difference phase observation is

$$\Delta_{km}^p = \varphi_k^p(t) - \varphi_m^p(t), \tag{3.27}$$

which is equal to

$$\Delta_{km}^p = -\frac{f}{c}[\rho_k^p(t) - \rho_m^p(t)] - [\varphi_k(t) - \varphi_m(t)] + N_{km}^p, \tag{3.28}$$

where the new integer ambiguity is

$$N_{km}^p = N_k^p - N_m^p. \tag{3.29}$$

Double difference The double difference phase observation as used in this work is obtainable when two receivers k and m observe two (or more) satellites p and q at the same time, so that

$$\Delta_{km}^{pq} = \Delta_{km}^p - \Delta_{km}^q, \tag{3.30}$$

which is equal to

$$\Delta_{km}^p = -\frac{f}{c}\{(\rho_k^p(t) - \rho_m^p(t)) - (\rho_k^q(t) - \rho_m^q(t))1\ \} + N_{km}^{pq}, \tag{3.31}$$

where

$$N_{km}^{pq} = N_{km}^p - N_{km}^q. \tag{3.32}$$

The initial receiver phase $\varphi_k(t)$ and $\varphi_m(t)$ have cancelled.

The transmitted phase $\varphi_{Tr}^p(t)$ is cancelled in the single difference observation as it was common to both phase expressions in the single difference expression. The single difference would then still be affected by receiver clock errors, but in the double difference observation this is also mostly cancelled which makes the double difference observable virtually free of satellite and receiver clock errors. More complete expressions for the derivation of the double difference phase observation can be found in Leick (1990).

3.3.4 Carrier Phase Precision

In general the vertical component has a greater standard deviation than the horizontal components. This is due to the fact that the vertical component is not as constrained and is more sensitive to errors in tropospheric delay (Blewitt 1993). Precision in the vertical component increases with a larger number of satellites being observed simultaneously as the correlation coefficient between the vertical station coordinate and zenith tropospherical delay decreases. Blewitt (1993) summarises the following precision levels as a function of network scale.

Very Local $10^{-2} - 10^{0}$ km: 0.1-1 mm in 10^{2} seconds.

Local $10^{0} - 10^{2}$ km: 1-4 mm in 10^{3} seconds.

Regional $10^{2} - 10^{3}$ km: 4-10 mm in 10^{4} seconds.

Global $10^{3} - 10^{4}$ km: 10 mm in 10^{5} seconds.

These levels are not normally acquired with standard commercial software packages. Several major software packages which have been produced for geodynamics research are capable of 10^{-8}L baseline accuracy. Examples are; BERNESE by the University of Berne, Switzerland; GIPSY/OASIS by the Jet Propulsion Laboratory and TOPAS by the Institute of Astronomical and Physical Geodesy, University of FAF, Munich. These packages are all capable of orbit improvement and contain advanced modelling features which lead to higher precision. In this work, a standard TRIMVEC-PLUS package was used.

3.4 Error Sources

The unpredictable behaviour of the time and frequency standards serving as a reference for GPS receivers is the main source of error in a measurement. By the process of differencing, the errors resulting from receiver and satellite clocks can be virtually eliminated. Differencing can be done between receivers, satellites, epochs or a combination of these. Differencing reduces the effect of the ionosphere and troposphere when receivers are close to each other, so that dual-frequency operation is not necessary for short ($\sim$ 3 km) baselines, therefore only L1 was used in this work. No improvement in accuracy would result if dual frequency data was used.

3.4.1 Single Difference

The single difference observable is the basis for the differential mode of GPS surveying receivers. This observable is not very useful when using receivers with internal crystal oscillators as noise from the oscillator dominates the measurements as described in section (3.3.3) even though the observable is largely independent of satellite frequency drift and offset. In the case of HartRAO, the MASER could have been used as an external reference for the receivers which would have made the single difference observable useful but practical problems with long cable lengths, their calibration and the calibration of distribution amplifiers made this approach impracticable.

3.4.2 Double Difference

With this observable the effect of instabilities in the receiver and satellite oscillators are largely cancelled as shown in section (3.3.3). This observable was used to determine the data points in this work. The TRIMVEC-PLUS double difference fix solution was used as it is the preferred solution for baselines < 15 km.

3.4.3 Triple Difference

This observable is the difference of two double differences for two consecutive time epochs. Triple differencing eliminates cycle ambiguities as the initial integer ambiguity cancels. In general, for baselines longer than ~ 50 km, this observable could produce the best result.

3.5 Summary

The GPS system is suitable for a multitude of Earth science and other applications. GPS allows highly accurate measurements to be made on scales ranging from very local to global using the carrier phase observable and advanced software. Several errors are reduced and eliminated by the process of differencing and for the short baselines as used in this work, single frequency receivers are adequate.

Chapter 4

Experimental Method and Data Collection

4.1 Introduction

A GPS receiver fixed to the apex of the quadripod[1] of the telescope traced arcs of two circles when the antenna was moved on its axes. Points were sampled on the two arcs, the DEC arc which is traced when the HA axis is fixed and the HA arc when the DEC axis is fixed. The ultimate aim was to use these points on the arcs to determine the circles and their centres described by the arcs in order to calculate the axis offset and the VLBI reference point. This chapter describes the methods and equipment used to sample the data. It also contains tables of the raw (uncorrected) data. Two separate data sets were obtained. Data set 1 was obtained during the period 17 - 21 February 1995 and data set 2 was obtained between 3 - 6 August 1995. The two data sets are made up of different sessions, such as GPS048, GPS050, etc. which indicate the day number when the session started. Each session is divided into a number of one hour visits to a specific point on the HA or DEC circle arcs. The rationale for the different data sets are given as well as a description of the gimbal used to mount the GPS antenna on the telescope to allow levelling of the GPS antenna in order to reduce the effect of phase centre shifts.

4.2 Basic Planning

Tables of the PDOP were generated and values below 4 were obtained for most of the time with only one high PDOP which lasted about 15 minutes per 24 hour period. Visibility tables listing satellite locations were used in conjunction with a polar plot

[1]The quadripod supports the secondary hyperbolic reflector which reflects the radio waves coming from the main dish into the cone which contains the different feeders for the receivers.

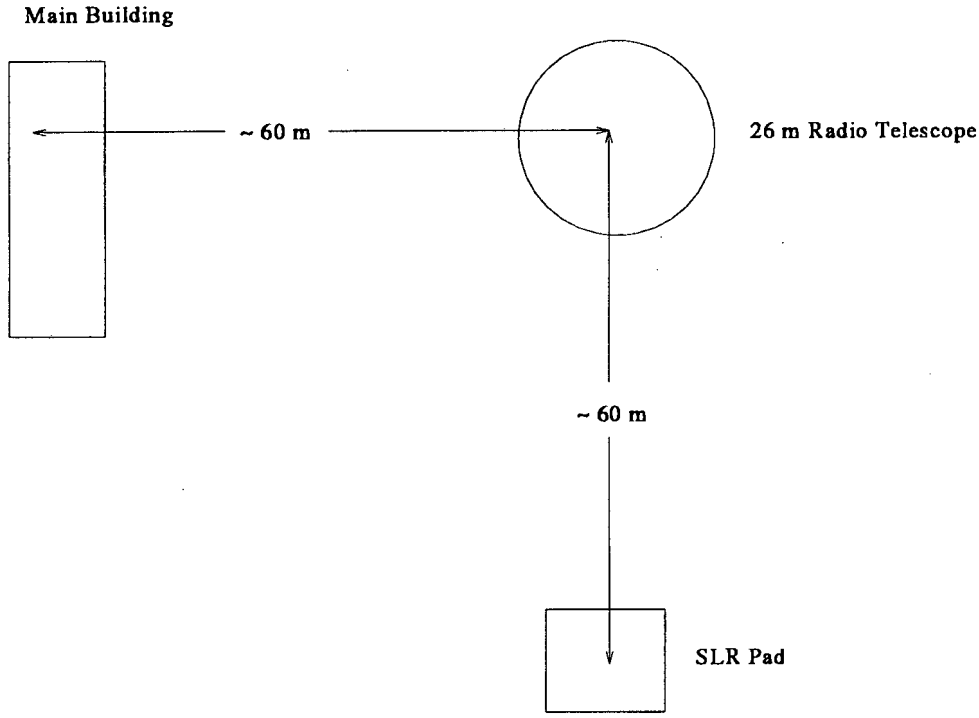

Figure 4.1: Plane representation of basic network indicating relative positions of GPS antennas mounted on radio telescope, SLR pad and main building roof.

to determine optimum geometry and best DOP. It was decided to use all available time regardless of PDOP in order to measure as many points as possible. With the full constellation of satellites available, satellite geometry and visibility were sufficient during the collection of both data sets.

4.3 Basic Network

Figure 4.1 illustrates a plane view of the general network. The vectors of the GPS receivers to the telescope intersected approximately at right angles. A GPS antenna was mounted in a suspended gimbal which was fixed to the apex of the quadripod of the main dish. The quadripod can be seen clearly in figure 1.2. A stationary GPS receiver was located on the SLR reference pier. A 3rd receiver was stationed on the cement roof of the main building for which a brass stud served as reference.

4.4 GPS Instrumentation

The receiver on the roof was a single frequency Trimble (L1) SST receiver and the other two were dual frequency Trimble SSE receivers. The antennas were Trimble Geodetic L1 for the single frequency and Trimble Geodetic L1/L2 for the dual frequency receivers respectively. Only single frequency (L1) observations were used as tropospheric and ionospheric modelling are not required for very short baselines as described in chapter 3. The antennas on the roof and SLR pad were each mounted on a tribach and set up on wooden tripods. The antennas were levelled and positioned as accurately as possible over the markers. Antenna slanted heights were measured from the reference mark to the bottom of the GPS antenna groundplane using standard rod type rulers.

4.5 Processing Methods

The software used for processing the data was Trimble Trimvec Plus. This was run in automatic batch mode after the session, antenna heights and reference coordinates had been set. The SLR reference point was used as the fixed point in the network. The software was also run interactively to inspect the data for cycle slips. No cycle slips were found on the samples inspected. In batch mode, automatic cycle slip detection and correction is performed.

A selection of the data was inspected for multipathing by dividing the one hour session of a single data point into six ten minute sessions which were then reprocessed. The repeatability of the solutions of the individual ten minute sessions were within 3-4 mm, which indicated that little or no multipathing was present. Deviations of some centimetres would occur if multipathing was a problem.

The basic processing model used was the double difference fix solution as described in section (3.3.3).

4.6 Exclusion of Roof Data

Initially it was planned to combine the data from the SLR pad and that of the roof receivers to strengthen the network and reduce errors. However, after processing the roof data it was found to be inferior to that of the data collected on the SLR pad. The rms error of each point was larger which increased the spread in the data points measured on the DEC and HA circles when the roof was used as a reference. A complete analysis of the data was done to ascertain the effect it would have on the

accuracy and errors if the data were to be combined. For the DEC and HA circles, the standard deviations of the mean zenith coordinates increased by a factor of three and two respectively. This clearly illustrated the statistical principle that a few good measurements are better than many bad ones. The value of the roof receiver data was therefore limited to that of a control point. If for instance the telescope data showed large errors, it would have been compared to the repeatability of the roof data points as the baseline lengths were about the same. Larger relative errors on the telescope would immediately have indicated observational technique errors such as an ineffective gimbal, or multipathing.

The data collected on the roof is therefore *not* included in the solutions for the axis offset and VLBI reference point.

Several factors are thought to have influenced the roof data adversely. The roof is not as stable as the SLR pad. A large metal tower situated on the roof towards the south-east of the GPS antenna as well as several lower metal posts, rails and wires on the roof could cause loss of lock to satellites as well as multipathing. The Trimble receiver was an older generation L1 only receiver and not a dual frequency SSE, perhaps the older generation hardware and software of the receiver is not quite as good as that of the later receivers.

4.7 Telescope Control

The telescope was controlled by the Mk IV Field System which is used to control the telescope during all VLBI experiments. Input files were written which contained the required information to steer the telescope to particular positions at specified times. A small sample of one of the files is included as an example.

```
"Snap file for GPS215 antenna axis offset experiment 03/08/95
"start schedule=gps215,#1
"DEC circle
"Start time 1400 UT
WX@!,+10m
XLOG=ON
"get rid of feed offset
FEED=NONE
"station 1
SOURCE=HADCUNCR,000000.0,205324.0,0
TRACK
```

```
!215150030
"station 2
SOURCE=HADCUNCR,000000.0,-255324.0,0
!215150430
TRACK
!215160530
"station 3
```

During the experiment, the Field System generates a log file which contains information such as the time the command is executed and the error (HA and DEC Delta's) which the shaft positional encoders find from that of the specified position.

```
213091948;" MARK IV Field System Version  8.29
213091948;location,hartrao ,j,-27.69,-25.89,1416.5,72326201,195,20,60,1990
213091948;horizon1,0.,10.,360.
213091948;head0,all,even,odd,odd,adaptive,no,5.0000,0
213091948;head1,175.6,13.4,3.6,175.6,12.6,-6.6,171.40,171.40
213091948;head2,182.0,14.0,-32.3,190.8,14.0,11.6,169.39,169.39
213091948;antenna,25.9,30.0,30.0,-88.0,88.0,-88.0,45.0,
213091948;equip,195,330,240,60,20,8450.0
213091948;time,-5.055,144.244,rate
213091948:"station 2
213091948:source=hadcuncr,000000.0,-255324.0,0
213091948#antcn#Initialization: No pointing model - all in PC Steer
213091948#antcn#Commanding to raw hour angle/declination
213091950#antcn#Source:  hadcuncr  ( Feed = None )
213091950#antcn# HAcommand    0.000   DECcommand -25.890
213091950:!+4m
213092350:track
213092350#antcn#Checking onsource status - extended error logging
213092350#antcn#Status:  Onsource
213092350#antcn#Source:  hadcuncr  ( Feed = None [0.000,0.000] )
213092350#antcn#Clocks:   Universal Time        MJD           LST(mean)
213092350#antcn# Mark IV  1995/213.09:23:50.40  49930.391556  07:52:39.34
213092350#antcn# Antenna  1995/213.09:23:51.47  49930.391568  07:52:40.49
213134422#antcn#Status:  Onsource
213134422#antcn#Source:  hadcuncr  ( Feed = None [0.000,0.000] )
```

```
213134422#antcn#Clocks:   Universal Time        MJD            LST(mean)
213134422#antcn# Mark IV  1995/213.13:44:22.20  49930.572479   12:13:53.94
213134422#antcn# Antenna  1995/213.13:44:22.27  49930.572480   12:13:54.09
213134422#antcn#Command: Hour Angle         Declination
213134422#antcn# Mark IV   43.000           -25.890
213134422#antcn# Antenna   43.000           -25.890
213134422#antcn#Coords:  Hour Angle         Declination
213134422#antcn# Source   02h52m00.00s      -25 53´24.0"
213134422#antcn# Beam     02h51m59.28s      -25 53´13.2"
213134422#antcn# Delta    00h00m00.72s       00 00´10.8"
```

Controlling the telescope is therefore a relatively easy task once the command language has been mastered. A project such as this can be run without attendance once the telescope and the GPS receivers have been programmed for the individual sessions starting, duration and completion time.

4.8 GPS Antenna Gimbal

Moving the telescope away from the zenith point in either axis would cause a tilt of the GPS antenna away from its horizontal position. This would cause a shift of the antenna phase centre. An ideal antenna would be insensitive to rotation and changes in inclination. The largest effect however, would be on the visibility of satellites, as the groundplane of the antenna would obscure satellite signals. In order to reduce these effects, a gimbal was designed to support the GPS antenna at the apex of the quadripod of the telescope. The gimbal (figure 4.2) has axes which rotate on ballbearings which are located at the ends of each axis. Initially it was found that movement was too free and the slightest wind caused a rocking effect which rendered the gimbal unuseable. A set of felt washers were made up and installed between the rotating sections of each axis. This acted as a sliding clutch which dampened the rocking effect considerably. Gusts do however still rock the gimbal as well as do birds when perched on the antenna. The effect of a bird can well be imagined, as its body can block some of the signals which may lead to loss of lock to a satellite. Fortunately birds were not often seen perched on the antenna, therefore this did not prove to be a major problem. It would however be prudent to include an infrared sensor and buzzer to scare off birds. The axes of the gimbal intersect at right angles and the point of intersection was designed to coincide with the antenna phase centre.

Figure 4.2: Gimballed GPS antenna mounted on the telescope quadripod.

4.9 Data Set 1

A specific telescope position is referred to by its HA coordinate in hours, minutes, seconds and by its DEC coordinate in degrees, minutes, arcseconds. All data points are referred to the SLR reference point. Data set 1 consists of data that was gathered during session GPS048, GPS050 and GPS052. The first data set was sampled in a random way so as to alleviate any systematic errors, thus there was no fixed sequence as to the points visited.

GPS048 With reference to figure 4.3, there are two arcs which the GPS antenna scribes when the telescope is moved in either axis with the other axis fixed. Firstly, an arc on a great circle is scribed when the DEC axis is moved with fixed HA axis. Secondly, an arc on a small circle is scribed when the DEC axis is fixed and the HA axis is moved. A similar distribution of data points were used for GPS052 but on different positions. To conserve space a separate figure is not included for GPS052.

The *zenith point* of the telescope is the point where the dish is horizontal and is

Table 4.1: Data set 1: Sessions GPS048 and GPS052; DEC circle data points

Data Point	X	Y	Z
1	60.686	-56.633	-2.792
2	60.988	-56.482	-3.833
3	61.215	-56.357	-4.897
4	61.388	-56.270	-5.980
5	61.481	-56.215	-7.069
6	61.515	-56.200	-8.666
7	61.315	-56.310	-10.847
8	61.111	-56.419	-11.920
9	60.845	-56.557	-12.978
10	60.511	-56.733	-14.010
11	60.1094	-56.9381	-15.0078
12	59.652	-57.177	-15.979
13	59.144	-57.447	-16.913
14	58.571	-57.743	-17.802
15	57.942	-58.077	-18.642
16	57.272	-58.422	-19.434
17	56.555	-58.800	-20.175
18	55.783	-59.202	-20.844
19	54.984	-59.624	-21.467
20	54.143	-60.063	-22.015
21	53.265	-60.522	-22.498
22	52.368	-60.991	-22.910

Table 4.2: Data set 1: Sessions GPS048 and GPS052; HA circle data points

Data Point	X	Y	Z
1	62.015	-71.083	-15.014
2	62.275	-69.641	-15.013
3	62.439	-68.201	-15.011
4	62.502	-66.743	-15.013
5	62.314	-63.844	-15.016
6	62.076	-62.404	-15.018
7	61.723	-60.993	-15.013
8	60.740	-58.250	-15.008
9	60.1094	-56.9381	-15.0078
10	58.586	-54.462	-15.006
11	57.696	-53.309	-15.008
12	56.732	-52.219	-15.009
13	54.580	-50.261	-15.010
14	53.403	-49.396	-15.007
15	52.185	-48.611	-15.012
16	49.568	-47.322	-15.005
17	48.204	-46.817	-15.003

facing straight up. This point had a fixed DEC coordinate of $-25°\ 53'\ 24''$, with an HA coordinate of 0 hours. Points were measured on the DEC arc with a spacing of $8°$ and on the HA arc with a spacing of $32'$ as this gave reasonable arc lengths and point distribution for the available telescope time.

Table 4.3: Data set 1: Sessions GPS048, GPS050, GPS052; Zenith data points

Data Point	X	Y	Z
GPS048	60.114	-56.936	-15.011
1	60.106	-56.941	-15.007
2	60.105	-56.939	-15.008
3	60.106	-56.942	-15.004
4	60.110	-56.940	-15.010
5	60.108	-56.938	-15.006
6	60.107	-56.937	-15.009
7	60.109	-56.937	-15.009
8	60.109	-56.935	-15.011
9	60.108	-56.940	-15.005
10	60.112	-56.938	-15.011
11	60.112	-56.938	-15.009
12	60.112	-56.936	-15.011
13	60.112	-56.936	-15.009
14	60.111	-56.936	-15.007
15	60.111	-56.936	-15.009
16	60.111	-56.939	-15.006
17	60.111	-56.937	-15.006
18	60.113	-56.938	-15.008
19	60.106	-56.939	-15.003
20	60.108	-56.940	-15.007
GPS052	60.106	-56.940	-15.006

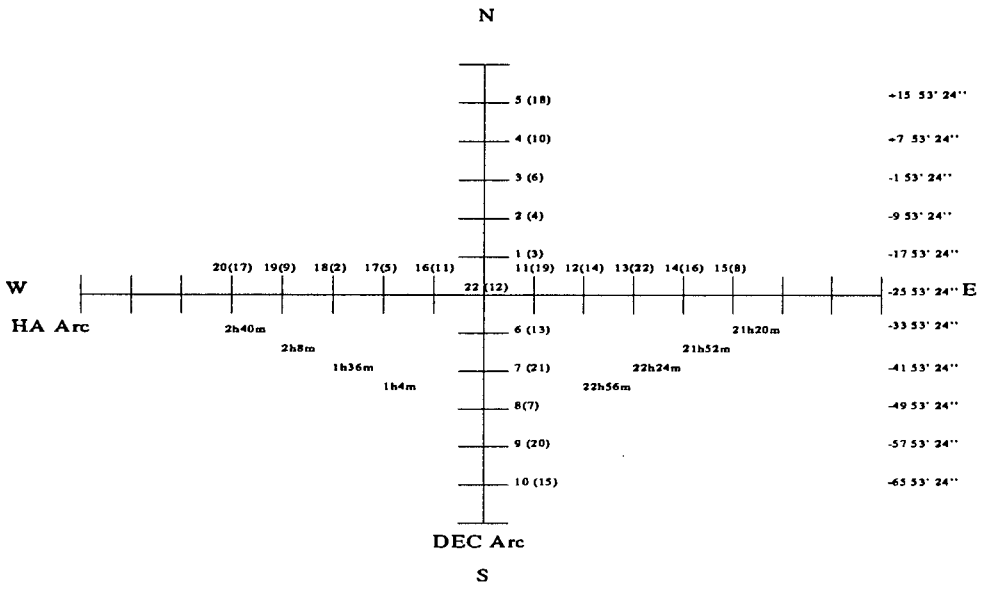

Figure 4.3: GPS048: Plane representation of HA and DEC arcs as seen from zenith. The unbracketed figures are grid points whereas the bracketed figures indicate the random sequence in which the stations were visited.

Table 4.4: Data set 1: GPS050; Zenith point statistics

Coordinate	Value (m)	σ (mm)	Δ (mm)
$\overline{X}$	60.1094	2.5	0.6
$\overline{Y}$	-56.9381	1.9	0.4
$\overline{Z}$	-15.0078	2.3	0.5

GPS050 GPS050 was a session where the telescope was kept stationary at zenith. It was hoped that this would allow the thermal signature of the telescope to be found. Unfortunately the temperature differential was small during the duration of the session. Some cloudy weather was also experienced during the daylight period, which made the data unuseable for thermal modelling, but still useful for determining the zenith point. Thermal transducers positioned on the three legs and close to the HA encoder allowed thermal monitoring. The mean values and statistics are listed in table 4.4. Considering the fact that 1-3 mm vertical movement could be due to thermal expansion, the standard deviations and standard errors are very acceptable and indicate no multipathing.

GPS052 This session was similar to GPS048 and its geometry differs in that the points measured were located on different points on the HA and DEC arcs. During this session the VLBI field system which controlled the telescope crashed so that useful data was collected up to and including point 15; the sequence was completed the following day (day 53). The data from sessions GPS048 and GPS052 were grouped into two files describing either the DEC (table 4.1) or HA (table 4.2) circle. The zenith point used for both DEC and HA tables was the average zenith point from all the sessions including GPS050 (table 4.3).

4.10 Data Set 2

As a result of experience gained during the gathering of data set 1 and the subsequent attempts at determining the offset from the data, the following ideas were incorporated into data set 2:

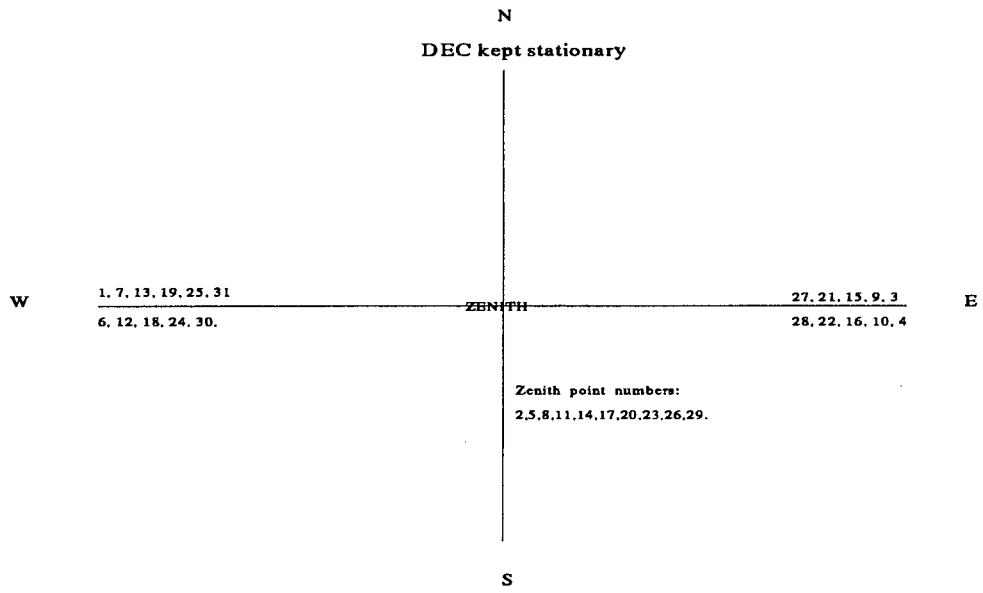

Figure 4.4: GPS213: Plane representation of HA circle containing two arcs as seen from zenith. The DEC axis was kept fixed and the HA axis moved, so that the points visited were points on the HA circle only. The zenith point numbers refer to the session numbers (see table 4.7 and table 4.5).

(1) **Thermal model** A stand alone thermal model was not feasible unless a very large number of points could be measured for many days. It was therefore decided to sequence the visits to individual points in such a way that a thermal model would be implicit in the solution of the circle centres. This was done by including a zenith point visit at every 3rd point to be measured. This is illustrated by figure 4.4. This figure precludes the inclusion of the point positions as in figure 4.3 due to space limitations on the figure, therefore the various sessions for GPS 213 and GPS 215 are tabulated with their DEC and HA positions in table 4.5. The observing sequence followed a fixed pattern, so that any given set of three points, such as 1, 2, 3 or 25, 26, 27 could be used by the centre finding software to determine the circle centre. As the temperature changed, the combination of the three points were always temperature related within the three hours, with the zenith as mid-observation. In the previous sessions such as GPS048 and GPS052, temperature differentials as large as 20° C occurred between points as a result of the random sequence of point visiting.

(2) **Distribution of points** Measuring evenly distributed points on arcs of about $\sim 90°$ were not the optimum type of distribution for solving the circle centres.

Table 4.5: Data set 2: GPS213 and GPS215; Session positions

GPS213 Sessions	HA (Hour:Minutes)	GPS215 Sessions	DEC (Deg:Min:Arcsec)
1	2:56	1	20:53:24
2	0	2	-25:53:24
3	21:04	3	-70:53:24
4	21:08	4	-69:53:24
5	0	5	-25:53:24
6	2:52	6	19:53:24
7	2:48	7	18:53:24
8	0	8	-25:53:24
9	21:12	9	-68:53:24
10	21:16	10	-67:53:24
11	0	11	-25:53:24
12	2:44	12	17:53:24
13	2:40	13	16:53:24
14	0	14	-25:53:24
15	21:20	15	-66:53:24
16	21:24	16	-65:53:24
17	0	17	-25:53:24
18	2:36	18	15:53:24
19	2:32	19	14:53:24
20	0	20	-25:53:24
21	21:28	21	-64:53:24
22	21:32	22	-63:53:24
23	0	23	-25:53:24
24	2:28	24	13:53:24
25	2:24	25	12:53:24
26	0	26	-25:53:24
27	21:36	27	-62:53:24
28	21:40	28	-61:53:24
29	0	29	-25:53:24
30	2:20	30	11:53:24
31	2:16	31	10:53:24
-	-	32	-25:53:25
-	-	33	-60:53:24
-	-	34	-59:53:24
-	-	35	-25:53:24
-	-	36	9:53:24
-	-	37	8:53:24
-	-	38	-25:53:24

Combinations of points close to the zenith point led to larger errors due to smaller angular separation. There is a restriction of $\sim 45°$ of the arc on either side of the zenith point due to GPS signal spillover from the telescope dish to the GPS antenna, so that the arc lengths could not be increased significantly. Consequently, two smaller, more dense arcs were measured on the outer edges of the arcs. This meant that for every individual solution, adequate angular separation was provided for.

Table 4.6: Temperature sequence of GPS213 (HA circle) data points

Data Point 1	Data Point 2	Data Point 3	Temp1	Temp2	Temp3	Mean	Variance
1	10	19	19.7	19.7	21.8	20.40	1.21
2	11	20	21.3	22.8	22.4	22.17	0.78
2	12	21	21.3	18.0	12.7	17.33	4.34
3	13	22	9.4	11.5	11.1	10.67	1.12
4	14	23	10.1	10.2	8.1	9.47	1.18
5	15	24	6.4	7.5	7.8	7.23	0.74
6	15	25	6.2	7.5	9.9	7.87	1.88
7	16	26	20.8	19.0	14.9	18.23	3.02
8	17	27	22.1	22.4	22.4	22.30	0.17
9	18	28	19.4	22.2	22.6	21.4	1.74

Table 4.6 shows the different sets of three data points, each of which are used to determine a circle centre point. Points 1 to 3 are the points in a set with their telescope structure temperatures temp1 to temp3. The variance indicates the relative movement in temperature during the measurement of the three consecutive points. All the useful measured arc points are used. If for some reason a specific point on the circle arc is an outlier, it is rejected, but its companions are teamed up with the next measured point on the circle arc or zenith point.

Table 4.7 contains the coordinates, times of observation and mid-observation temperatures. The first block contains the data for the circle arc towards the west, the centre block contains the zenith data and the last block contains the circle arc towards the east.

GPS215 Similar to the GPS213 session, table 4.9 contains the coordinates, times of observation and mid-observation temperatures for GPS215. The first block contains the data for the circle arc towards the north, the centre block contains the zenith data and the last block contains the circle arc towards the south.

4.11 Probable Error Sources of this Technique

Using GPS as a technique to determine points on the HA and DEC circles is not error free. Several errors were identified and appropriate steps taken to reduce their magnitude.

4.11.1 GPS Antenna Phase Centre

The antenna electrical phase centre is the reference point to which the radio signal measurement is made. This phase centre does not correspond exactly to the physical

Table 4.7: GPS213 (HA circle) data

Data Point	Session Point	X Coordinate	Y Coordinate	Z Coordinate	Day Number	Time (UTC) HH	MM	Ambient (mid-obs.) Temp. (Deg C)
1	1	61.681	-72.449	-15.009	213	08	00	19.7
2	7	61.883	-71.744	-15.011	213	14	30	21.3
3	12	61.968	-71.390	-15.002	213	19	55	9.4
4	13	62.053	-71.035	-15.002	213	21	00	10.1
5	18	62.124	-70.679	-15.005	214	02	25	6.4
6	19	62.194	-70.319	-15.004	214	03	30	6.2
7	24	62.257	-69.966	-15.013	214	08	55	20.8
8	25	62.314	-69.607	-15.015	214	10	20	22.1
9	30	62.364	-69.239	-15.008	214	15	25	19.4
10	2	60.155	-56.896	-15.015	213	09	05	19.7
11	5	60.157	-56.885	-15.015	213	12	20	22.8
12	8	60.154	-56.892	-15.012	213	15	35	18.0
13	11	60.157	-56.886	-15.007	213	18	50	11.5
14	14	60.158	-56.892	-15.009	213	22	05	10.2
15	17	60.157	-56.887	-15.007	214	01	20	7.5
16	23	60.151	-56.894	-15.010	214	08	10	19.0
17	26	60.158	-56.892	-15.014	214	11	05	22.4
18	29	60.153	-56.886	-15.009	214	14	20	22.2
19	3	48.242	-46.774	-15.009	213	10	30	21.8
20	4	48.583	-46.890	-15.009	213	11	15	22.4
21	9	48.933	-47.010	-15.003	213	16	40	12.7
22	10	49.274	-47.130	-15.003	213	17	45	11.1
23	15	49.607	-47.270	-15.004	213	23	10	8.1
24	16	49.953	-47.411	-15.008	214	00	15	7.8
25	21	50.281	-47.565	-15.007	214	05	40	9.9
26	22	50.614	-47.721	-15.008	214	06	45	14.9
27	27	50.944	-47.869	-15.013	214	12	10	22.4
28	28	51.265	-48.039	-15.013	214	13	35	22.6

antenna centre and this offset is dependent on the elevation, azimuth and intensity of the satellite signal. Two effects should therefore be taken into account, namely the antenna phase centre variation and the offset (Hoffmann-Wellenhof 1992). The antenna phase centre is not located at the same point for widely varying incident signal elevation angles, which adds to the total error in the positional computation. These could be modelled to reduce the overall error in a normal GPS application, but modelling, calibration and correction will in any event lead to a residual error. The gimbal's axis of rotation was set up to intersect the phase centre, so that movement of the telescope from data point to data point would have as little effect on the phase centre as possible. The GPS antenna keeps its orientation in all directions after installation on the gimbal.

Table 4.8: Temperature sequence of GPS215 (DEC circle) data points

Point 1	Point 2	Point 3	Temp1	Temp2	Temp3	Mean	Variance
1	14	26	21.2	19.0	14.1	18.10	3.63
2	15	27	9.4	9.4	11.2	10.00	1.04
3	16	28	8.0	8.3	7.1	7.80	0.62
4	17	29	6.0	6.2	7.6	6.60	0.87
5	18	30	4.5	5.0	7.2	5.57	1.44
6	19	31	18.3	16.6	12.6	15.83	2.93
7	20	32	19.4	20.3	20.6	20.10	0.62
8	20	33	19.4	20.3	20.9	20.20	0.76
9	21	33	13.4	10.8	20.9	15.03	5.24
10	22	34	8.7	7.9	7.5	8.03	0.61
11	23	34	7.2	7.6	7.5	7.43	0.21
12	24	35	7.9	8.0	7.0	7.63	0.55
13	25	35	8.8	13.5	7.0	9.76	3.36

4.11.2 Multipathing

A problem which gives rise to even larger errors than phase centre variations when using a conventional wide beamwidth GPS antenna is multipathing. This occurs when the satellite signal arrives at the antenna via different paths, after reflection of the incident wave by a reflecting surface. The received signals will show relative phase offsets due to different path lengths. There are several ways in which the multipathing for normal GPS surveying applications can be reduced, but if a normal wide beamwidth GPS antenna is mounted in a conventional way on the main dish, the parabolic shape of the dish and large reflective area of the cone could cause serious multipathing. It was initially thought that several centimetres of error would be present in the short baselines due to multipathing. Furthermore, the main dish is located in a valley where reflection off the slopes of the surrounding hills could add to the problem. The environment in which the measurements were to take place could require that techniques be adopted to detect the presence of multipathing. This is especially true if the elevation of the dish was such that spillover from the dish to the GPS antenna could take place. The method proposed by Fu (1992) as quoted by Raby and Daly (1993) could have been used. This method requires only single frequency carrier phase and would suit our instrumental configuration. The double difference range from a predetermined baseline is subtracted from the measured double difference carrier phase. This leaves the double difference integer ambiguity, calibration term and carrier phase noise. As the calibration terms and integers are constant, deviations from the constant mean will indicate that multipathing is present on the carrier phase measurements. This method would however be very

Table 4.9: GPS215 (DEC circle) data

Data Point	Session Point	X Coordinate	Y Coordinate	Z Coordinate	Day Number	Time (UTC) HH	MM	Ambient (mid-obs.) Temp. (Deg C)
1	1	60.641	-56.638	-2.532	215	14	00	21.2
2	6	60.719	-56.601	-2.786	215	19	25	9.4
3	7	60.816	-56.546	-3.053	215	20	30	8.0
4	12	60.887	-56.509	-3.311	216	01	55	6.0
5	13	60.950	-56.475	-3.569	216	03	00	4.5
6	18	61.029	-56.439	-3.836	216	08	25	18.3
7	19	61.091	-56.402	-4.103	216	09	30	19.4
8	24	61.150	-56.369	-4.367	216	14	55	19.4
9	25	61.210	-56.340	-4.633	216	16	00	13.4
10	30	61.259	-56.310	-4.899	216	21	25	8.7
11	31	61.308	-56.283	-5.171	216	22	30	7.2
12	36	61.345	-56.266	-5.437	217	03	55	7.9
13	37	61.388	-56.241	-5.712	217	05	00	8.8
14	2	60.155	-56.891	-15.013	215	15	05	19.0
15	5	60.156	-56.892	-15.006	215	18	20	9.4
16	8	60.156	-56.892	-15.008	215	21	35	8.3
17	11	60.157	-56.894	-15.008	216	00	50	6.2
18	14	60.155	-56.894	-15.007	216	04	05	5.0
19	17	60.155	-56.899	-15.010	216	07	40	16.6
20	20	60.156	-56.892	-15.011	216	10	55	20.3
21	26	60.159	-56.891	-15.012	216	17	05	10.8
22	29	60.155	-56.888	-15.005	216	20	20	7.9
23	32	60.150	-56.890	-15.006	216	23	35	7.6
24	35	60.150	-56.890	-15.008	217	02	50	8.0
25	38	60.157	-56.890	-15.010	217	06	05	13.5
26	3	52.185	-61.064	-23.008	215	16	10	14.1
27	4	52.410	-60.950	-22.912	215	17	15	11.2
28	9	52.639	-60.827	-22.814	215	22	40	7.1
29	10	52.863	-60.710	-22.710	215	23	45	7.6
30	15	53.080	-60.599	-22.602	216	05	10	7.2
31	16	53.312	-60.477	-22.500	216	06	15	12.6
32	21	53.527	-60.363	-22.388	216	11	40	20.6
33	22	53.753	-60.246	-22.273	216	12	45	20.9
34	33	54.394	-59.908	-21.883	217	00	40	7.5
35	34	54.611	-59.794	-21.745	217	01	45	7.0

time consuming, taking into account the number of points that were measured.

Methods to reduce multipathing such as the use of digital filtering and rf absorbent ground planes, would lead to increased complexity and cost and were not considered feasible. A large reflective backplane should reduce spillover from the dish surface to the GPS antenna and as the TRIMBLE GPS antenna has a large backplane, it was relied upon to reduce spillover. The duration of the visits to a specific point during the sessions was one hour, as this was thought to be adequate to negate the effects of possible multipathing. A few sessions were shorter as telescope time had to be shared with an astronomy program.

As was mentioned in section 4.5 a selection of the data was inspected for mul-

tipathing by investigating smaller subsets of the data of a given session, The high repeatability of the solutions of the individual subsets indicated that little or no multipathing was present.

The one hour duration of the sessions, as well as making sure that the elevation angle of the telescope was kept to the limit where no spillover from the dish could be picked up by the GPS antenna, seemed to be adequate in preventing serious multipathing.

4.11.3 Accessibility to GPS Signals

There is a considerable amount of shadowing due to the size and proximity of the main dish to the GPS antenna. The effective horizon of the GPS antenna will change with the elevation of the main dish, therefore at elevations $< 45°$ the satellite availability will be negatively affected. The telescope was never steered to elevations $< 45°$ to avoid this problem.

4.11.4 Solution Error Sources

With carrier phase measurements, the aim of data processing is to resolve the initial double difference phase ambiguities of the carrier phase (Nolan et al 1993). After determination of the ambiguities, millimetre position results are possible. The signals from the receivers are compared by a process of subtraction, and the relative position of the GPS antenna on the main dish to the GPS antenna on the SLR reference pier and main building roof is then determined by the difference signals. This differential positioning is required to remove errors common to all the receivers, such as satellite clock and ephemeris errors, selective availability as well as unmodelled ionospheric and tropospheric propagation errors. The removal of errors is due to the fact that corresponding signals from the two receivers are subtracted, so errors which are common to both receivers are cancelled out to a large degree as described in the next paragraphs.

Selective Availibility Errors Intentional dithering of the satellite frequencies, which introduce errors in the navigation time coded signals as well as intentional changes to the ephemeris parameters were compensated for by using double differencing during the processing stage.

Ionospheric Delay Errors The signal propagation delay can change by up to 6 m at night and 30 m by day. For short baselines as in this case, the ionospheric

delay is basically the same for all receivers. This is primarily due to the fact that the signal path from a given satellite as seen from the receivers is essentially the same.

Tropospheric Delay Errors This effect has a magnitude of up to 3 m and is maximum for satellites at low elevation. The extent of this effect was reduced by using a horizon mask of 15° to exclude satellites at a low elevation. The same reasoning for ionospheric delays are applicable, so that compensation is almost total for short base lines.

Ephemeris and Clock Errors Clock errors are compensated for by the double difference solution as explained in section (3.4) when the receivers in the network employ the same satellite data.

4.12 Summary

GPS can be used to measure points on an arc scribed by the movement of a radio telescope. It is necessary to visit each point for an hour in order to reduce or eliminate the effects of multipathing. Errors are compensated for by double differencing and by having short baselines so that signal propagation paths are the same to all the receivers. Baselines are not constrained by station intervisibility which allows flexibility in the network. The movement of the telescope is constrained by the requirement that the GPS antenna does not receive spillover signals from the telescope and that shadowing of the satellite signals does not lead to loss of lock. The GPS antenna needs to be gimballed to keep it level and to minimise antenna phase centre position variation. The GPS carrier phase observable is suitable for high precision short baseline and long baseline surveying. The availability of the full constellation of satellites allows maximum utilisation of observing time. The portability of the GPS receivers and antennas allow installation into fairly inaccessible locations, eg the vertex of the telescope quadripod.

Chapter 5

Offset Determination Methods

5.1 Introduction

Three separate approaches were used to determine the centres of the DEC and the HA circles; analytical geometry, matrices and least-squares. The offset could be found once these circle centres had been determined. An application of analytical geometry was developed which is more robust and accurate on this type of data distribution than the other methods to be discussed. The three approaches are discussed in some detail and comparisons made as to their suitability for solving the offset problem. The necessary notation and background required is described with the reader being referred to the appropriate appendix whenever formulations need to be derived or concepts explained in detail.

5.2 Spatial Intersection of Two Co-Planar Lines

The first attempt at finding the circle centres and axis offset used the point of closest intersection of two co-planar lines. Consider three measured points on the DEC curve, (P_1, P_2, P_3) as depicted in figure 5.1. P_9 is the centre of the circle, $d_1 = P_1P_2$, $d_2 = P_2P_3$, $d_3 = P_1P_3$, $d_4 = P_1P_6$, $d_5 = P_3P_8$, $d_6 = P_4P_9$, $d_7 = P_5P_9$. The DEC curve is the space curve traced by the GPS antenna as it was moved in declination. This discussion is also valid for data points on the HA curve. Analytical geometry is used to derive the centre and the radius. Only three points on a circle are required to define the circle (Briggs & Bryan 1910) and one can use the perpendicular bisector of the chords P_1P_2 and P_2P_3 to determine the circle centre. Using direction cosines (see Appendix A.3) and the equation for an angle between two lines (see Appendix A.4), one finds

$$\cos\theta = \frac{(x_2 - x_1)(x_3 - x_1) + (y_2 - y_1)(y_3 - y_1) + (z_2 - z_1)(z_3 - z_1)}{(d_1)(d_3)} \qquad (5.1)$$

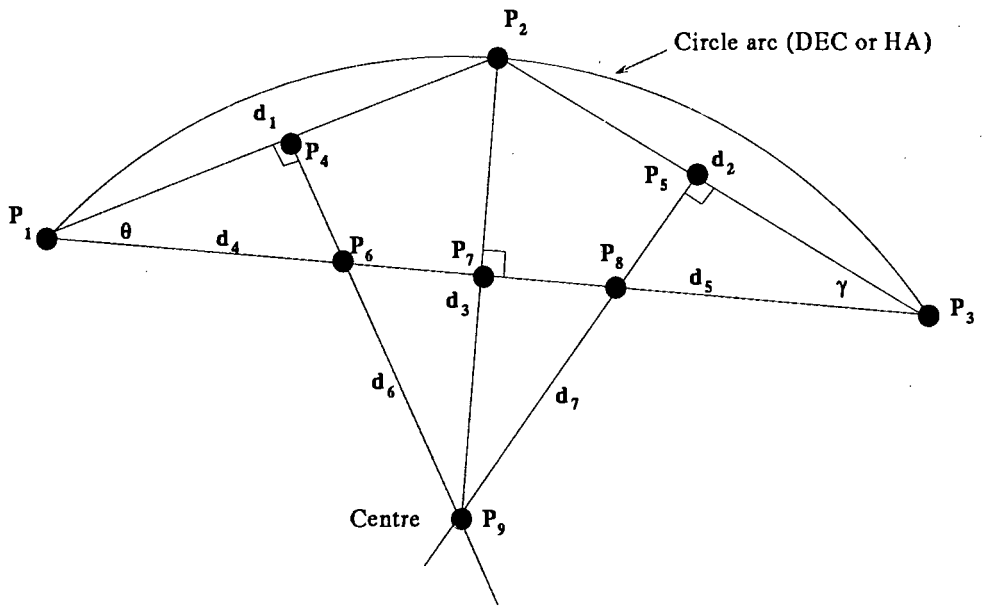

Figure 5.1: Centre of circle found by spatial intersection

and

$$\cos\gamma = \frac{(x_2 - x_3)(x_1 - x_3) + (y_2 - y_3)(y_1 - y_3) + (z_2 - z_3)(z_1 - z_3)}{(d_1)(d_3)} \tag{5.2}$$

The true length of a space line P_1P_2 is given by (Foley & van Dam 1984)

$$\sqrt{(x_2 - x_1)^2 + (y_2 - y_1)^2 + (z_2 - z_1)^2}, \tag{5.3}$$

where

$$(x_2 - x_1) : (y_2 - y_1) : (z_2 - z_1)$$

are the direction ratios of line P_1P_2. The length of lines d_1, d_2 and d_3 are found from equation (5.3) and the line lengths d_4 and d_5 would then be

$$d_4 = \frac{(d_1 \times 0.5)}{\cos\theta} \tag{5.4}$$

and

$$d_5 = \frac{(d_2 \times 0.5)}{\cos\gamma}. \tag{5.5}$$

The perpendicular bisector of chord d_1 then intersects chord d_3 in P_6 and the perpendicular bisector of chord d_2 intersects chord d_3 in P_8. The points P_4 and P_5 are found by using an equation for the mid-point of a line

$$P_i(x, y, z) = (\frac{P_o + P_x}{2}), (\frac{P_o + P_y}{2}), (\frac{P_o + P_z}{2}). \tag{5.6}$$

Using proportions, the coordinates of P_6 and P_8 are

$$x_6 = x_1 + \frac{d_4}{d_3} \times (x_3 - x_1) \tag{5.7}$$

$$y_6 = y_1 + \frac{d_4}{d_3} \times (y_3 - y_1) \tag{5.8}$$

$$z_6 = z_1 + \frac{d_4}{d_3} \times (z_3 - z_1) \tag{5.9}$$

and

$$x_8 = x_3 + \frac{d_5}{d_3} \times (x_1 - x_3) \tag{5.10}$$

$$y_8 = y_3 + \frac{d_5}{d_3} \times (y_1 - y_3) \tag{5.11}$$

$$z_8 = z_3 + \frac{d_5}{d_3} \times (z_1 - z_3) \tag{5.12}$$

The intersection of the two co-planar lines utilises the parametric representation of a line (see Appendix A.5) which is rearranged to enable extension of the line to infinity by using the fact that the two points P_4 and P_6 define the inclination of the line d_6 using their direction ratios. Similarly the two points P_5 and P_8 define the inclination of the line d_7. One can therefore use the equations

$$\left.\begin{array}{rcl} x_{d_6} & = & (x_6 - x_4) \times kv + x_4 \\ y_{d_6} & = & (y_6 - y_4) \times kv + y_4 \\ z_{d_6} & = & (z_6 - z_4) \times kv + z_4 \end{array}\right\} 0 \leq kv \tag{5.13}$$

and

$$\left.\begin{array}{rcl} x_{d_7} & = & (x_8 - x_5) \times kv + x_5 \\ y_{d_7} & = & (y_8 - y_5) \times kv + y_5 \\ z_{d_7} & = & (z_8 - z_5) \times kv + z_5 \end{array}\right\} 0 \leq kv \tag{5.14}$$

to calculate the intersection of lines d_6 and d_7. The radius is calculated by finding the distance between the intersection P_9 and point P_2. The value of kv is then incremented by a subroutine which makes use of the straight line distance between the calculated points on lines d_6 and d_7 as determined from equations (5.13) and (5.14). The closer the intersection becomes, the smaller the incremental addition to kv. This allows the intersection to be calculated to within 5×10^{-9} metres. The software has a built-in function that checks if the lines are diverging and flags intersection as soon as either the limit of 5×10^{-9} metres or divergence is reached. This was found to be sufficient for high accuracy and further improvements are not attained by reduction of this value as the accuracy is influenced by the floating point precision of the computer. Using this method, the point of closest intersection can be found for any two space lines on a path of near convergence, even if they do not lie in the same plane.

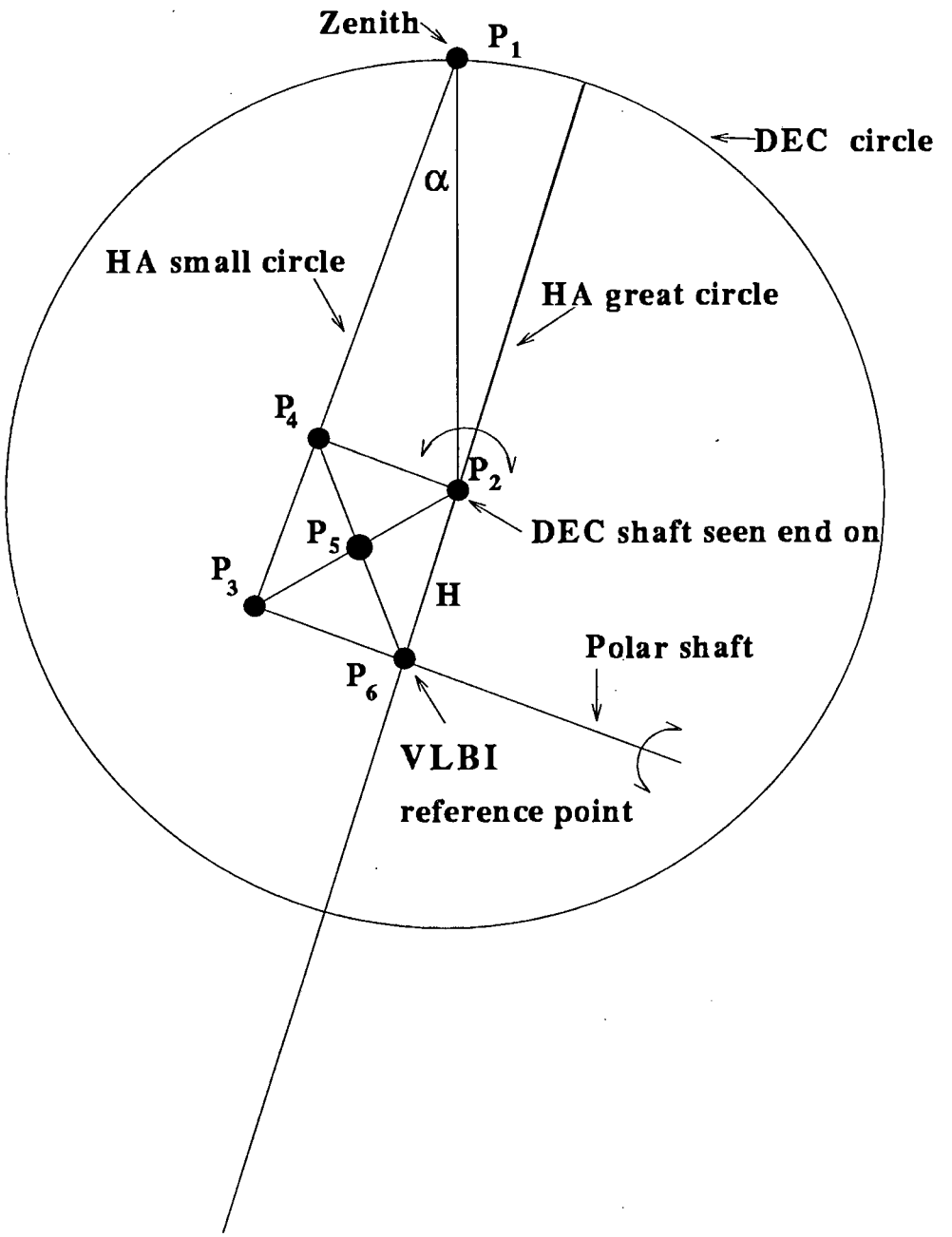

Figure 5.2: Dec and HA circle planar representation

Circle fitting figure of merit A figure of merit is generated for each centre solution, which is basically a modified least-squares error criterion,

$$FM = (R_i^2 - \overline{R}^2)^2 \tag{5.15}$$

The figure of merit is sensitive to deviations from the mean and was found very useful in evaluating individual intersections. It is used in chapter 7.

The radius and coordinates of the centre of the HA curve is determined the same way. As can be seen in figure 5.2 which depicts the DEC and HA circles where the plane of the HA circle is normal to the plane of the paper, the curve of the DEC axis is an arc of a great circle (see Appendix A.6). The telescope zenith point is P_1, P_2 is the DEC shaft seen end on, P_3 is the centre of the HA small circle, P_4 is the normal projection from P_2 onto P_1P_3, the common intersection of P_4P_6 and P_2P_3 is P_5 and P_6 is the VLBI reference point. The curve of the HA axis is a small circle, (see Appendix A.6) the centre of which is not the centre of the sphere which would be intersected by the polar shaft. Further calculations need to be made to calculate the axis offset. The equation

$$H = R_{HA} - R_{DEC} \times \cos\alpha \tag{5.16}$$

gives the offset solution for a given HA circle radius R_{HA} and DEC circle radius R_{DEC}. The cosine of the angle α is calculated using the equation for the true angle between two intersecting lines. The offset H can also be found by calculating the lines P_1P_2, P_2P_3 and P_3P_1 by following a similar approach as described in section 5.2. This is in fact done in the software as an additional check on the offset values. The coordinates of the VLBI reference point P_6 are determined by first calculating P_4 using proportions, where

$$x_4 = x_1 + \frac{d_1 \cos\alpha}{d_3} \times (x_3 - x_1), \tag{5.17}$$

$$y_4 = y_1 + \frac{d_1 \cos\alpha}{d_3} \times (y_3 - y_1), \tag{5.18}$$

$$z_4 = z_1 + \frac{d_1 \cos\alpha}{d_3} \times (z_3 - z_1). \tag{5.19}$$

Here $d_1 = P_1P_2$, $d_2 = P_2P_3$, $d_3 = P_1P_3$. Then the midpoint between P_2 and P_3 is determined using an application of equation 5.6, thus allowing the VLBI reference point to be calculated using direction ratios. The offset is calculated as the distance from P_2 to P_6 and from P_4 to P_3 as a check.

Evaluation of Method

In order to evaluate the method described in section 5.2, software (*ARCRAN*) was developed to generate an arc of given radius and resolution (see section 6.3). Any circle (or arc thereof) could thus be generated and used as test data to evaluate the method and the analysis software (*Hart3D*). The coordinates of the generated arc can be convolved with a random error of given upper and lower limits to produce a

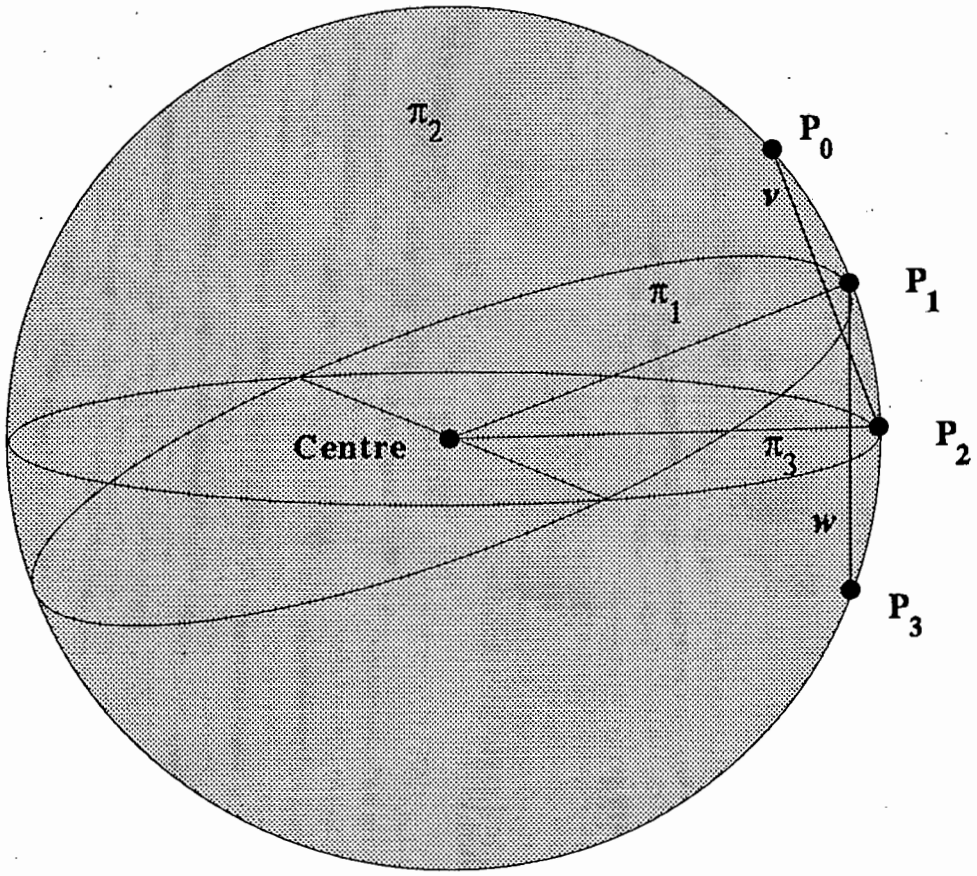

Figure 5.3: Intersection of three planes.

test data set with known radius and centre. This method was tested extensively and was found to give excellent results for data of a similar configuration to that of data set 2. The accuracy decreases with a smaller angle of intersection which indicates that the data of data set 1 close to the zenith point would result in larger errors. Using *ARCRAN* to generate an arc of about 90°, with a random error of ±5 mm on the coordinates of a circle with radius of 20 m, a radius value of 20.0012 m was determined which had a standard deviation of 7.4 mm. The standard deviations of the centre coordinates were in the range 5 to 7 mm. Repeatablity of the real data is indicated clearly by session GPS050 where the telescope was stationary.

5.3 Intersection of Three Planes

The next two sections describe how the circle centres can be found by using the intersection of three planes.

5.3.1 Analytical Geometry Approach

Using a curve which is given as a sequence of equidistant points, it is possible to determine the point of intersection if two planes π_1 and π_3 are normal to the plane of the circle. The reader should refer to figure 5.3 to follow the discussion. This method was incorporated in a program *PLANE* (see section 6.4) but is only useful with an evenly distributed (equidistant) set of points. As this requirement reduces the applications to only a special subset of the data, it is considered inferior to the method described in section 5.2. The equation of the plane π_1 can be found by expressing it in terms of the coordinates x_i, y_i, z_i, of the three points $P_i (i = 0, 1, 2)$. The general equation of a plane (Foley & van Dam 1984) is of the form

$$Ax + By + Cz + D = 0. \tag{5.20}$$

To express plane π_1 in the general form (see Appendix A.7) one can write

$$\left.\begin{array}{rcl} A_1 & = & x_2 - x_0 \\ B_1 & = & y_2 - y_0 \\ C_1 & = & z_2 - z_0 \\ D_1 & = & A_1 x_1 + B_1 y_1 + C_1 z_1 \end{array}\right\} \tag{5.21}$$

The vector $\boldsymbol{v} = [A_1, B_1, C_1]$ starts at P_0 and ends at P_2 and as P_1 is equidistant between points P_0 and P_2 plane π_1 must intersect the centre S_c of the circle at some point. Plane π_3 can then be expressed in a similar way as

$$\left.\begin{array}{rcl} A_2 & = & x_3 - x_1 \\ B_2 & = & y_3 - y_1 \\ C_2 & = & z_3 - z_1 \\ D_2 & = & A_2 x_2 + B_2 y_2 + C_2 z_2 \end{array}\right\} \tag{5.22}$$

where the vector $\boldsymbol{w} = [A_2, B_2, C_2]$ starts at P_1 and ends at P_3. The coefficients of the points (x, y, z) are the direction ratios of the normals to the planes π_1 and π_3. The coordinates of the point of intersection (X_c, Y_c, Z_c) of the three planes can be found by initially finding the line of intersection between two planes and then finding the point of intersection between this line and the 3rd plane. Given the equations (5.21) and (5.22) for planes π_1 and π_3 the direction ratios of the line of intersection are $\lambda : \mu : \nu$. The normals to the planes π_1 and π_3 are then perpendicular to the line of intersection (Gasson 1983) so that

$$A_1\lambda + B_1\mu + C_1\nu = 0 \tag{5.23}$$

and

$$A_2\lambda + B_2\mu + C_2\nu = 0 \tag{5.24}$$

If one solves in terms of λ/μ and λ/ν then

$$\lambda : \mu : \nu = (B_1C_2 - B_2C_1) : (C_1A_2 - C_2A_1) : (A_1B_2 - A_2B_1). \tag{5.25}$$

If plane π_2 is defined by the three points P_0,P_1 and P_2 or any other three points which are not co-linear, the plane can be given by equation (5.20). The line which this plane is to intersect has already been found using equation (5.25) and passes through two points, say $P_1 = (x_1, y_1, z_1)$ and $P_2 = (x_2, y_2, z_2)$. The line can then be represented by (Giloi 1978) the equation

$$\frac{x - x_1}{\cos\alpha} = \frac{y - y_1}{\cos\beta} = \frac{z - z_1}{\cos\gamma}, \tag{5.26}$$

where

$$\cos\alpha = \frac{x_2 - x_1}{d}, \cos\beta = \frac{y_2 - y_1}{d}, \cos\gamma = \frac{z_2 - z_1}{d}, \tag{5.27}$$

with

$$d = \sqrt{(x_2 - x_1)^2 + (y_2 - y_1)^2 + (z_2 - z_1)^2}. \tag{5.28}$$

Three conditions can then result(Giloi 1978, Haines 1989).

(1) The line is parallel to the plane if $A_3\cos\alpha + B_3\cos\beta + C_3\cos\gamma = 0$.

(2) The line lies in the plane if $A_3\cos\alpha + B_3\cos\beta + C_3\cos\gamma = 0$ and $A_3x_1 + B_3y_1 + C_3z_1 = 0$.

(3) If conditions (1) and (2) are not true then the point of intersection is given by

$$X_c = x_1 - t\cos\alpha \tag{5.29}$$

$$Y_c = y_1 - t\cos\beta \tag{5.30}$$

$$Z_c = z_1 - t\cos\gamma \tag{5.31}$$

where

$$t = \frac{A_3x_1 + B_3y_1 + C_3z_1 + D_3}{A_3\cos\alpha + B_3\cos\beta + C_3\cos\gamma} \tag{5.32}$$

This method works well with data which contains very small errors, but performed poorly when tested with data containing realistic size errors.

5.3.2 Matrix Approach

Another approach is to note the condition that a point p be on a plane π (Giloi 1978) is

$$p \cdot \pi = 0. \tag{5.33}$$

The intersection of three planes is therefore the point p such that $p \cdot \pi_1 = 0, p \cdot \pi_2 = 0, p \cdot \pi_3 = 0$. The three planes are written in general form and ordered as column vectors

$$\pi_1 = \begin{bmatrix} a_1 \\ b_1 \\ c_1 \\ d_1 \end{bmatrix}, \pi_2 = \begin{bmatrix} a_2 \\ b_2 \\ c_2 \\ d_2 \end{bmatrix}, \pi_3 = \begin{bmatrix} a_3 \\ b_3 \\ c_3 \\ d_3 \end{bmatrix} \tag{5.34}$$

and if M is the matrix

$$M = \begin{bmatrix} a_1 & a_2 & a_3 & 0 \\ b_1 & b_2 & b_3 & 0 \\ c_1 & c_2 & c_3 & 0 \\ d_1 & d_2 & d_3 & 1 \end{bmatrix} \tag{5.35}$$

the point of intersection can be found by inverting matrix M (5.35) and using the bottom row of M^{-1} as the coordinates of the intersection. This method is particularly suitable for programming. Program *MATFIT* (see section 6.5) was developed which uses this approach. Similarly to the above method, poor performance precluded the use of this method on real data.

5.4 Function Fitting Using Least-Squares

Least-squares is a topic well discussed in the literature (Draper & Smith 1966, Meyer 1992) therefore only relevant background material will be discussed. It is included in this work because it is a very important statistical tool, although it was found to be unsuitable to determine the DEC and HA circle centres. It did however find application in modelling the spherical function, using the centre coordinates and radius found with the method described in section 5.2. This allowed parameters for gravitational distortion to be modelled in the spherical function. This is discussed in greater detail in section 7.4.6.

5.4.1 Estimating the Parameters of a Nonlinear System

The curve traced by the measured points on the HA and DEC circles can be described by a set of points x_i, y_i, z_i on the surface of a sphere with radius s_r and centre coordinates $s_c \equiv (x_c, y_c, z_c)$ where in explicit form

$$(x_i - x_c)^2 + (y_i - y_c)^2 + (z_i - z_c)^2 = s_r^2 \tag{5.36}$$

is a nonlinear function. Mathematical models which are linear in the parameters[1] are of the type

$$y = \beta_0 + \beta_1 z_1 + \beta_2 z_2 + \cdots + \beta_p z_p + \epsilon \tag{5.37}$$

where the basic independent variables $x_1, x_2 \cdots, x_k$ are represented by z_i and y is the dependent variable and $\beta_0, \beta_1 \cdots, \beta_p$ are the unknown parameters with ϵ being the increment by which any individual y may fall of the regression line.

5.4.2 Nonlinear Estimation

Nonlinear estimation is extensively discussed in the literature (Draper & Smith 1966, Dennis et al 1981, Ratkowsky 1989, Meyer 1992). Most of the approaches to nonlinear problems try to solve for the best estimate $\hat{y}$, by using some method such as Taylor expansion, such that the nonlinear function is approximated by the linear term in the Taylor series (Meyer 1992). Once this has been done, linear least-squares can be used to determine $\hat{y}$. If one assumes that the errors in real data approaches the idealised assumption of independent, identically distributed normal errors, then the least-squares criterion is fairly robust.

If however, one departs in a major way from the standard assumptions, this would lead to large errors in the estimates. This would be the case if for example there is a prominent outlier, a seriously skew distribution or the postulated model is the wrong one. If one considers a linear regression model such as equation (5.37) and accepts the approximate validity of an assumed independent and identically distributed error, then the parameters β_p have normal distributions, are unbiased and have the minimum possible variance (*Gauss-Markov theorem*).

5.4.3 Differences Between Linear and Nonlinear Models

Linear regression models differ from nonlinear ones in that the least-squares minimum variance estimators of nonlinear regression models are not unbiased or normally distributed (Draper & Smith 1966, Ratkowsky 1989). In general, a smaller sample size increases the extent of the nonlinearity. As the sample size approaches infinity, the minimum variance estimators achieve the property of being normally distributed and unbiased. Nonlinear models whose estimators come close to being normally distributed and unbiased have been termed *close-to-linear models* (Ratkowsky 1983), whereas those who do not are termed *far-from-linear*. When a model cannot

[1] When a model is said to be linear or nonlinear, reference is made to linearity or nonlinearity in the parameters.

be transformed into the linear form it is said to be *intrinsically nonlinear.* If it can be converted into a form linear in the parameters it is termed *intrinsically linear* (Draper & Smith 1966). Equation (5.36) can be linearised to the first order in a Taylor's expansion (see Appendix A.10) and is close-to-linear. This linearisation leads to a set of n simultaneous equations which can be solved using the classical Gauss method or any modified version of it. Usually an initial starting value for the parameters to be solved is given as first approximation and the final solution is found by an iterative procedure.

Searching Parameter Space For nonlinear functions χ^2 is considered to be a continuous function of the n parameters which describe a hypersurface in n-dimensional space. This space must be searched for the minimum value of χ^2. There is a disadvantage in the analytical methods of expanding the fitting function (Bevington 1969) in that for points outside the region where the χ^2 hypersurface is approximately hyperbolic, they are not reliable in approaching the minimum with any degree of accuracy. Several other methods have been developed to search parameter space;

(1) parabolic extrapolation

(2) gradient search

(3) steepest descent

(4) grid search

(5) direct search methods

(6) ravine stepping

(7) grid search for independent parameters

(8) linear minimisation in orthogonal directions

(9) method of conjugate directions

(10) variable metric

Implementations of most of these methods are found in Press et al (1989).

5.4.4 Nonlinear Modelling

In this work, an adaptive nonlinear least-squares algorithm was used as developed by Dennis et al. (1981) and as implemented in the program NLREG (Sherrod 1991). The algorithm maintains a secant approximation S to the second-order part of the least-squares Gauss-Newton Hessian and adaptively decides when this approximation is to be used. Basically, the minimisation technique utilised is to alter each parameter value slightly and then divide the difference between successive sums of squared residuals by the amount the parameter was changed. This allows the partial derivative to be calculated with respect to the parameter and determines the change of the parameter value for the next iteration. The purpose of Press et al (1981) was to develop a more reliable algorithm than the Gauss-Newton and Levenberg-Marquardt methods and is essentially a combination of these. The algorithm was also intended to be more efficient than the secant or variable metric algorithms (such as the Davidon-Fletcher-Powell method)[2] intended for general function minimisation. For examples of algorithms using the secant method, see Conte and de Boor (1972). Algorithms using the Levenberg-Marquardt and Gauss-Newton methods can be found in Press et al (1989).

The implementation by Sherrod (1991) allows multivariate, linear, polynomial, exponential, logistic and general nonlinear regression. Complex analyses are possible as function models can be specified with conditional statements (*if, else*) and allows arrays, variables and looping (*for, do, while*). A syntax similar to the *C* programming language is used, which allows easy access to the regression functions and options. The basics of the method are described in more detail in Appendix A.14.

5.4.5 Limitations of Least-Squares as Applied to Space Curves

During attempts to use leasts-squares to fit the function of a sphere to the data, an acceptable fit could not be found. Even constraining several or all of the parameters produced poor results. Several problems arise when using least-squares to fit a circle or a space curve to data. The problems experienced are directly related to the criterion used for minimisation; several of these problems are described in Chan (1965), Kåsa (1976), Angel & Barber (1977), Anderson (1981), Berman & Culpin (1986), Gates (1993) and Gates (1994). A short review of the problems encountered with least-squares as described in the above literature is given in Appendix A.13.

It is generally apparent that for data on an arc which is less than a semicircle,

[2]Also known as DFP or Fletcher-Powell method.

estimation by least-squares is unsatisfactory. Convergence is made difficult as the error range is of the same order of magnitude for a large range of radii. Angel and Barber (1977) predict that any estimation method will experience difficulties for data where $T < [0, \pi]$. T is the polar angle in radians (see Appendix A.13). Asymptotic biases of the circle centre and radius estimates are found using different circular models and different least-squares criterion. Least-squares estimators and maximum likelihood estimators both fail to be consistent methods, especially when the distribution of the points on the circle is not over the total circumference.

5.5 Summary

Three approaches to find circle centres were discussed; analytical geometry, matrices and least-squares. Using the method of spatial intersection of two co-planar lines proved to be most suitable for the distribution and type of data in this study. The data sampling could be optimised for this method. This method requires only three data points (which could have an uneven distribution) for a single solution and is very robust. The methods using the intersection of three planes only performs well on data which contain very small errors. Least-squares is not a suitable method for determining the circle centre of data describing less than a semi-circle.

Chapter 6

Software Description

6.1 Introduction

The software required to solve for the circle centres, offset and VLBI reference point, as well as many smaller peripheral programs was written in the C language on a DOS platform. The different programs and their implementations are described and to preserve space, no code is included.

6.2 Hart3D

6.2.1 Introduction

This program utilises the concept of circle centre determination by finding the intersection of two co-planar lines as described in section (5.2). A graphical interface allows the user to view the data and access all the software functions. The data can be points in either 2-dimensional (2D) or 3-dimensional (3D) space. The interface is divided into two areas, a command and a display area. Ammeraal (1988) provided many of the 3D graphics subroutines which were freely improved to obtain higher precision. Giloi (1978), Foley & van Dam (1984), and Bielig-Schulz & Schulz (1990) were used as a basic introduction to 2D and 3D geometrical transformations used in computer graphics.

6.2.2 Axis Convention

All mathematical calculations use the traditional right-handed axes when defining points. A right-handed system of axes is used as is the convention in vector algebra. This can easily be visualized if one imagines a counterclockwise rotation of the positive x-axis through an angle of 90° about the z-axis when looking from the

positive z axis towards the origin. Counterclockwise rotation will transform the x-axis into the y-axis. The points as measured are defined relative to three mutually perpendicular planes of reference. The origin is the intersection of the three planes. Three mutually perpendicular lines of intersection ox, oy, oz, are produced by this intersection, where o is the origin.

6.2.3 Transformations

Translation

The translation of a specified data point is achieved by adding positive or negative constants to each of the coordinates of the point. If the initial coordinates are x_i, y_i, z_i then the translated point can be written as

$$\begin{aligned} x_t &= x_i + \Delta x, \\ y_t &= y_i + \Delta y, \\ z_t &= z_i + \Delta z. \end{aligned} \tag{6.1}$$

The subscript t indicates the translated coordinate and the Δ denotes the added constant. *Hart3D* also makes provision for translation by using any directed line segment AB as a shift vector. The user gives as input the start and end points of a vector and the program finds the Δx, Δy and Δz from

$$\begin{aligned} \Delta x &= x_B - x_A \\ \Delta y &= y_B - y_A \\ \Delta z &= z_B - z_A \end{aligned} \tag{6.2}$$

Scaling

Scaling an object changes its dimensions without changing their proportions. The scaling factors S_x, S_y and S_z are the real numbers by which all dimensions are multiplied. If the scaling factors are less than 1, the object is compressed, if larger than 1, the object is stretched. In the case where $S_x = S_y = S_z$ the object is homogeneously compressed or stretched. Before the scaling operation can be performed, the *fixed point* must be specified. Either the centre of the object, the origin of the coordinate system or a specified vertex (object point) can be specified as the fixed point. The fixed point remains unchanged after the scaling has been performed. If the origin o of the coordinate system is used, then for any given data point $P(x, y, z)$ a new point $P_n(x_n, y_n, z_n)$ is assigned by:

$$\begin{aligned} x_n &= S_x \cdot x, \\ y_n &= S_y \cdot y, \\ z_n &= S_z \cdot z. \end{aligned} \tag{6.3}$$

This equation can be generalised to any other fixed point instead of o, so that for a given fixed point $F(x_F, y_F, z_F)$ one uses $x - x_F$ in the place of x, $x_n - x_F$ instead of x_n which leads to:

$$\begin{aligned} x_n - x_F &= S_x \cdot (x - x_F), \\ y_n - y_F &= S_y \cdot (y - y_F), \\ z_n - z_F &= S_z \cdot (z - z_F). \end{aligned} \tag{6.4}$$

Rewriting equation (6.4) for computer efficiency,

$$\begin{aligned} x_n &= S_x \cdot x + C_1, \\ y_n &= S_y \cdot y + C_2, \\ z_n &= S_z \cdot z + C_3, \end{aligned} \tag{6.5}$$

where the constants C_1,C_2 and C_3 are computed only once before the scaling process by

$$\begin{aligned} C_1 &= x_F - S_x \cdot x_F, \\ C_2 &= y_F - S_y \cdot y_F, \\ C_3 &= z_F - S_z \cdot z_F. \end{aligned} \tag{6.6}$$

Rotation

Rotation is done by computation of the rotation matrix (Foley & van Dam 1984)

$$R = \begin{bmatrix} r_{11} & r_{12} & r_{13} & 0 \\ r_{21} & r_{22} & r_{23} & 0 \\ r_{31} & r_{32} & r_{33} & 0 \\ r_{41} & r_{42} & r_{43} & 0 \end{bmatrix}. \tag{6.7}$$

In 3D, a rotation of α degrees about the x-axis is:

$$Rx(\alpha) = \begin{bmatrix} 1 & 0 & 0 & 0 \\ 0 & \cos\alpha & \sin\alpha & 0 \\ 0 & -\sin\alpha & \cos\alpha & 0 \\ 0 & 0 & 0 & 1 \end{bmatrix}. \tag{6.8}$$

The y-axis rotation matrix is:

$$Ry(\alpha) = \begin{bmatrix} \cos\alpha & 0 & -\sin\alpha & 0 \\ 0 & 1 & 0 & 0 \\ \sin\alpha & 0 & \cos\alpha & 0 \\ 0 & 0 & 0 & 1 \end{bmatrix}. \tag{6.9}$$

The z-axis rotation matrix is:

$$Rz(\alpha) = \begin{bmatrix} \cos\alpha & sin\alpha & 0 & 0 \\ -\sin\alpha & \cos\alpha & 0 & 0 \\ 0 & 0 & 1 & 0 \\ 0 & 0 & 0 & 1 \end{bmatrix}. \tag{6.10}$$

Applications

The transformations of translation, scaling and rotation can be done using the 4×4 matrix as described. If one uses homogeneous coordinates, rotation and scaling can be done by multiplying a point with the matrix (Giloi 1978):

$$RS = \begin{bmatrix} r_{11} \cdot S_x & r_{12} \cdot S_y & r_{13} \cdot S_z & 0 \\ r_{21} \cdot S_x & r_{22} \cdot S_y & r_{23} \cdot S_z & 0 \\ r_{31} \cdot S_x & r_{32} \cdot S_y & r_{33} \cdot S_z & 0 \\ r_{41} & r_{42} & r_{43} & 0 \end{bmatrix}. \tag{6.11}$$

Translation can be done by multiplying a point with the matrix

$$T(\Delta x, \Delta y, \Delta z) = \begin{bmatrix} 1 & 0 & 0 & 0 \\ 0 & 1 & 0 & 0 \\ 0 & 0 & 1 & 0 \\ \Delta x & \Delta y & \Delta z & 1 \end{bmatrix}. \tag{6.12}$$

A matrix can be constructed to allow simultaneous rotation, scaling and translation. Taking the above matrices into account one can write

$$RS \cdot T = RST = \begin{bmatrix} r_{11} \cdot S_x & r_{12} \cdot S_y & r_{13} \cdot S_z & 0 \\ r_{21} \cdot S_x & r_{22} \cdot S_y & r_{23} \cdot S_z & 0 \\ r_{31} \cdot S_x & r_{32} \cdot S_y & r_{33} \cdot S_z & 0 \\ \Delta x & \Delta y & \Delta z & 1 \end{bmatrix}. \tag{6.13}$$

By multiplying a point $p = [x, y, z, 1]$ with the matrix RST one obtains the transformed image of p, so that $p_{RST} = p \cdot RST$.

6.2.4 Commands

The command section allows the user to access the data, display and perform transformations, e.g. rotation on the data. It also allows changing the observers viewpoint so that the 3D data can be viewed from different angles. Refer to figure (6.1) which illustrates the command and display areas. The DEC and HA (in xy plane) arcs of data set 1 are shown. Any apparent deviation from an arc on a circle is pixel orientated.

F1-Reset B/S/W/AvgZ=A The F1 function key resets optional software runtime settings to default. Batchmode/Solution counter/Wait prompt/Average zenith, are reset to default values.

F2-Save File The currently loaded data is saved to the currently open file by default, or optionally to a filename of users choice.

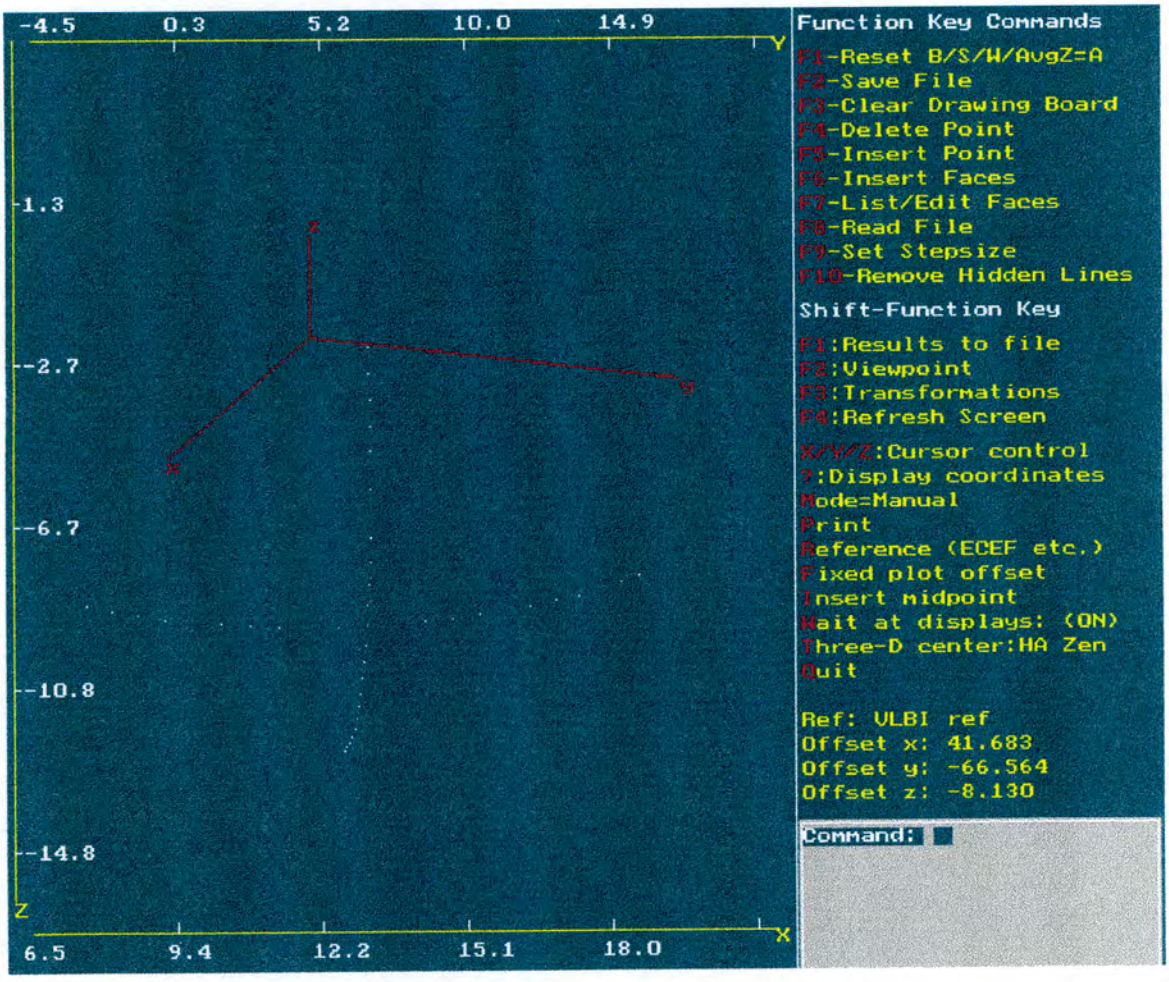

Figure 6.1: *Hart3D* Software graphics interface

F3-Clear Drawing Board Clears current display area.

F4-Delete Point An object point consists of a point number, x, y and z coordinates. These are deleted from the data point list.

F5-Insert Point A selected point is inserted into the list.

F6-Insert Faces Solid objects are bounded by flat faces and the boundaries of the faces are made from line segments. For instance, specifying a face between two points results in a line segment, specifying a face between three points results in a polygon.

F7-List/Edit Faces An objects vertices (object data points) are listed as they are connected to form a face. The face can be deleted.

F8-Read File Used to read in a file. The file must have the format (n, x, y, z).

F9-Set Stepsize The grid stepping size can be set to some value other than default, before the cursor is used to move around in 3D within the display area.

F10-Remove Hidden Lines Removes hidden lines.

Shift-F1:Results to file Statistical parameters and solution coordinates of circle centres, axis offset etc. can be written to a selected file.

Shift-F2:Viewpoint An object point, or set of points eg. the points which lie on the DEC or HA circle arcs, are located in 3D space and must be projected onto an image plane in this space. The display screen is 2D, so only a projection can be used to display the data points. The *viewpoint* is the position of the observer's eye and the viewing direction and distance can be changed by changing the spherical coordinates of the viewpoint. In this type of projection (*central projection*) the image plane is perpendicular to the optical axis (Giloi 1978).

Shift-F3:Transformations Rotation, scaling, translation, reflection and perspective is done using a 4x4 matrix as described in section 6.2.3. Allowance is made for the transformation of a subset of the data points.

Shift-F4:Refresh Screen The screen is refreshed and memory cleared.

X/Y/Z:Cursor control The cursor can be moved in the image plane in either of the 3 projected dimensions. A new point can be inserted at any location. Step size is set with function key F9.

? The coordinates are displayed for a given point. If a fixed offset was used, relative and absolute coordinates are shown.

Mode=Manual (Mode=Batch) In manual mode the centre of the circle is found by stepping from the outside of the arc towards the inside. The number of solutions can be set. If for instance an arc of a circle consists of fifty data points and number 25 is selected as zenith, the number of solutions can be set to say five, then five solutions will be found using 3 points per solution. The solutions will be found from the points (1,25,50), (2,25,49), (3,25,48), (4,25,47), (5,25,46). If batchmode has been selected, a batchfile is expected with the sequence of points to be used per solution. A typical application would be to use data collected in a temperature sequence as explained in section (4.10). Each set of three points for every individual solution is then determined by the batchfile.

Print Prints screen to dot matrix printer.

Reference (ECEF etc.) This function makes provision for selecting any predefined point as the origin. The ECEF origin would not allow visual representation of the data as the distance to the Earth's centre and that of the radii of the DEC and HA axis cannot be drawn on the same scale without losing resolution of the data points. Therefore, the data can conveniently be normalized to the SLR reference point, zenith point, offset point, or any other predefined point.

Fixed plot offset Data which is read in after a reference point has been selected is normalized to the new reference. All calculations are done using the original values, the offset values are for visualisation purposes only. The points on the DEC and HA circle arcs are referred to the SLR as reference. If the VLBI reference point is selected as reference with the above function, the display resolution will improve, but all solutions will still be relative to the SLR.

Insert midpoint Create and insert a new data point between two other selected points. This new data point will occupy the centre position between the two selected points.

Wait at displays: (ON) If this function is turned on, every display window will require a key to be pressed before calculations continue. If off, only final results are displayed with a key prompt.

Three-D centre:HA Zen This function computes the circle centres, finds the antenna axis offset and the VLBI reference point. Either the HA zenith point can be used when determining the offset, or the average of the DEC circle and HA circle averages as determined from data set 2, corrected for pointing. A simple sequence is followed in the determinations. Firstly, the DEC circle centre is found, then the HA circle centre, then the axis offset and lastly the VLBI reference point. The method is described in more detail in section (5.2).

Quit Exit the program.

6.2.5 Program Execution

One can use *Hart3D* to find either just the centre of a circle or go through a sequence of steps to determine the offset. Very little operator intervention is required as most of the steps are automatic. Standard deviations using Bessel's correction are displayed as well as standard errors of the mean for all radius, centre and offset parameters. All values and statistics are displayed in continuously updated windows as the program calculates the intersections. There is an option to write each individual parameter to file for plotting or other purposes. The statistical methods employed are described in Meyer (1992) and are discussed in chapter 7.

6.3 Arcran

Arcran was developed to test the circle centre finding methods discussed in chapter 5. An arc or circle can be generated with a given radius, density of points on the circle and whether or not random error convolution should be done on the point coordinates and angular distribution. The distribution of the errors are determined by a random number generator. The upper and lower limits of the errors can be set, eg $\pm$ 5 mm. A file is created which is in the proper readable format for the circle centre programs.

6.4 Plane

Plane determines the centre of a circle using the analytical geometry method of finding the intersection of three planes as described in section (5.3.1). A set of 4 equidistant points are required for one unique centre determination. The real data

was not all equidistant so that this could only use a subset of the data. This method is very sensitive to deviations from a true circle.

6.5 Matfit

Matfit determines the centre of a circle using the matrix method of finding the intersection of three planes as described in section (5.3.2). Three non co-linear points are required to define each plane. This method was very sensitive to deviations from a true circle.

6.6 Other Software

Other utility type programs were developed as the project progressed. Amongst others, a tensioned cubic spline fitting program was developed[1], which was used on data set 1 to try and improve the solutions when using points with small angular separation (those close to the zenith). The results are described in section 7.3.2.

[1]This was suggested by Prof Keith McGreggor of the University of Pretoria

Chapter 7

Results and Discussion

7.1 Introduction

In this chapter, the solutions for the DEC and HA circles as found using the programs are tabled and discussed. Results of the determination of the offset and VLBI reference point is given. The sources of error and the steps taken to minimise them are described. The effect of temperature on the antenna structure is investigated as far as it influences the HA and DEC circle centres. Possible deformation of the structure due to the force of gravity is modelled using least-squares. The same technique is also used to determine if there are deviations from a true circle by fitting an ellipse to the data. Several independent methods have been used to determine the HartRAO antenna axis offset prior to this work. These are briefly described and their results given. The results of the method developed using GPS as described has the distinct advantage of producing the necessary data to tie together the VLBI, SLR and GPS reference frames. The results of this work are compared to the other independent offset determinations.

7.2 Errors

7.2.1 Error Conventions

In this section the basic statistical methods used are described. The errors from rounding off numbers are least if one always rounds off numbers ending in 5 to the nearest even or odd number. The convention adopted here is to round off numbers ending in 5 to the nearest *even* number. Individual GPS measurements are quoted to 3 decimal places, with no error, as the error produced by the GPS processing software is optimistic by a factor of at least ten, which makes the *Trimble* error meaningless for statistical purposes. Mean values are quoted to four significant figures, i.e. to

0.1 mm, which is justifiable by the fact that the average is more precise than the individual measurements. The values quoted in the tables are truncated to fit the table as the full double precision values are utilised in all computations to avoid rounding off errors; rounding off is only done once all computations are completed and is used on *final* solutions. The standard deviations quoted are determined using

$$s = \sqrt{\frac{\sum(x_i - \overline{x})^2}{n-1}}, \tag{7.1}$$

where s^2 is an unbiased estimator of the parent population variance σ^2, with σ given by

$$\sigma = \sqrt{\frac{\sum(x_i - \overline{x})^2}{n}}. \tag{7.2}$$

In most cases there is no significant difference between s and σ when n is large. In this work the character σ as used in the tables refers to s in equation (7.1), therefore all standard deviations are conservative estimates as n is small in all the solutions. All independent measurements and solutions are deemed to have a best guess or estimator

$$\overline{x} = \frac{\sum x_i}{n}. \tag{7.3}$$

The standard error of the mean is found using

$$\Delta\overline{x} = \sqrt{\frac{s^2}{n}}. \tag{7.4}$$

Running mean In this work, the *running mean* is used in all the tables which describe the solutions per intersection. Therefore, considering table 7.1 as an example; where $n = 1$, there is only one independent solution, the sigmas are 0. When $n = 2$, the mean of X, $\overline{X}$ is the mean of intersections 1 and 2 and the sigma is on the running mean of intersections 1 and 2. Whenever an overline is written to indicate "the mean of", the running mean is implied. The figure of merit "FM", is also on the running mean. Any other parameter, for instance the angle $\angle P1P2$ indicates the angle for that particular intersection determination. In Table 7.7, the individual offset solution H and the running mean $\overline{H}$ is listed for comparison purposes.

7.2.2 DEC and HA Circle Errors

The measured points on the DEC and HA circles x_i, y_i, z_i where $i = 1, \ldots, N$ are given by

$$\left.\begin{array}{rcl} x_i &=& x_{i0} + \epsilon_i, \\ y_i &=& y_{i0} + \zeta_i, \\ z_i &=& z_{i0} + \eta_i. \end{array}\right\} \tag{7.5}$$

where $(\varepsilon_i, \zeta_i, \eta_i)$ is an error component consisting of several independent errors. Amongst these errors are ΔT, an error resulting from contraction and expansion of the antenna metal structure, and ΔP, an error resulting from the inability of the antenna to return to an exact point specified, i.e. a pointing error. Added to these error components is ΔU, a combination of many errors, which includes errors of the GPS observables such as tropospheric and ionospheric effects, multipathing, as well as antenna phase centre variation. It also includes the possible movement of the gimballed GPS antenna caused by high winds and perching birds. The error due to the gimbal swinging should be very small, as both rotation axes intersected the centre of the GPS antenna which is close to the phase centre. Errors due to wind loading on the antenna structure and gravitational loading are also contained within ΔU. Including these errors one can write equation (7.5) as

$$\left.\begin{array}{rcl} x_i &=& x_{i0} + x\Delta T_i + x\Delta P_i + x\Delta U_i, \\ y_i &=& y_{i0} + y\Delta T_i + y\Delta P_i + y\Delta U_i, \\ z_i &=& z_{i0} + z\Delta T_i + z\Delta P_i + z\Delta U_i. \end{array}\right\} \tag{7.6}$$

The errors may be dependent or independent. For instance the error ΔP resulting from driving the antenna in HA is largely dependent on the position from which the antenna is driving and the distance which it is driven (G. Nicolson personal communication). It is only dependent in HA drive, the DEC drive seems to be independent. The HA circle pointing will have no statistical compensation as with the DEC pointing, where on average, the total error component should be algebraically less than that of the sum of the separate contributions of the individual components due to the Gaussian error distribution. The error ΔP will however also have a smaller random component due to peculiarities of the gears, drive, etc.

All the other sources of error such as ambient temperature variation, wind loading, troposphere and ionosphere are regarded as being mostly random. The error ΔT was minimised by observing points in a thermal sequence as discussed in section 4.10 and is discussed further in section 7.4.5. The pointing error ΔP was reduced by a process of averaging and translation as described in section 7.4.1. The remaining error component, ΔU, was minimised by double difference processing, gimballing the antenna and one hour long visits to a specific station. An attempt to model some gravitational deformation using least-squares (see section 7.4.6) was made to ascertain the magnitude of this component.

7.3 Offset Determined from Data Set 1

7.3.1 Zenith Position

The zenith position used for data set 1 was the average value as found during session GPS050. The telescope was parked with the brakes locked so that the GPS receiver was at a fixed point, apart from movement due to thermal expansion.

7.3.2 HA and DEC Circle Centre Determinations

The coordinates in the centre determinations are all relative to the VLBI reference point as found from data set 2. This does not influence or affect the offset determinations in any way. It does increase the resolution of the tables. When using data set 2, the SLR reference point is used as the reference position. The tables containing the HA and DEC circle solutions list, from left to right, the intersection solution number n, the data points used in the intersection, the running mean centre coordinates $(\overline{X}, \overline{Y}, \overline{Z})$ and the standard deviations of these running averages. This is followed by the running mean radius value $(\overline{R})$, the angle in degrees between data point P1 and P2 ($\angle P1P2$), as well as between P2 and P3 ($\angle P2P3$). The meanings of these points are described in section 5.2. The far right-hand column contains FM, the figure of merit of the particular solution. The FM is described in section 5.2.

DEC circle Using *Hart3D* the DEC circle parameters were determined using all the DEC circle points (Table 7.1). It is very clear that large errors are introduced when points with small angular separation are used. These errors have a tendency to increase the value of the radius of the circle. Using the points 1, 11 and 22 give the best result, whereas using the points 10, 11 and 13 lead to an inferior result. This is clearly indicated by the figure of merit (FM) for the solutions.

Comparison of final values with first intersections Risking the pre-emption of the later discussions in this chapter, if one compares the first intersection with the final values as determined later using curve fits, it is clear that the points with large angular separation give the best result. The mean radius as determined using intersections 1 and 2 of the DEC circle is 15.7518 m, which compares very well with the final value of 15.7514 m of Table 7.3. Similarly for the HA circle as determined in Table 7.4, the first value of the mean radius is 20.8657 m, whereas the final value in Table 7.5 is 20.8656 m.

Table 7.1: DEC Circle centre solution: Data set 1

n	Inter-section	$\overline{X}$ (m)	$\overline{Y}$ (m)	$\overline{Z}$ (m)	$\sigma\overline{X}$ (m)	$\sigma\overline{Y}$ (m)	$\sigma\overline{Z}$ (m)	$\overline{R}$ (m)	$\sigma\overline{R}$ (m)	∠P1P2 (Deg)	∠P2P3 (Deg)	FM
1	1,11,22	5.8744	3.0598	0.0041	0.0000	0.0000	0.0000	15.7487	0.0000	45	43	0.000
2	2,11,21	5.8754	3.0530	0.0063	0.0013	0.0095	0.0033	15.7518	0.0043	41	39	0.009
3	3,11,20	5.8729	3.0531	0.0061	0.0043	0.0067	0.0023	15.7536	0.0043	37	35	0.012
4	4,11,19	5.8679	3.0475	0.0096	0.0106	0.0124	0.0073	15.7615	0.0161	33	31	0.194
5	5,11,18	5.8686	3.0534	0.0094	0.0093	0.0170	0.0063	15.7583	0.0156	29	27	0.195
6	6,11,17	5.8534	3.0463	0.0187	0.0381	0.0232	0.0234	15.7775	0.0489	23	23	2.000
7	7,11,16	5.8407	3.0361	0.0300	0.0484	0.0341	0.0366	15.7968	0.0678	15	19	3.954
8	8,11,15	5.8454	3.0178	0.0356	0.0468	0.0608	0.0374	15.8032	0.0654	11	15	3.748
9	9,11,14	5.8103	2.9837	0.0626	0.1142	0.1169	0.0882	15.8573	0.1734	7	11	27.433
10	10,11,13	5.7553	2.8461	0.1234	0.2046	0.4490	0.2094	15.9880	0.4445	3	7	192.190

Table 7.2: DEC Circle centre solution: Data set 1-Tensioned cubic spline fit

n	Inter-section	$\overline{X}$ (m)	$\overline{Y}$ (m)	$\overline{Z}$ (m)	$\sigma\overline{X}$ (m)	$\sigma\overline{Y}$ (m)	$\sigma\overline{Z}$ (m)	$\overline{R}$ (m)	$\sigma\overline{R}$ (m)	∠P1P2 (Deg)	∠P2P3 (Deg)	FM
1	1,50,100	5.8705	3.0546	0.0070	0.0000	0.0000	0.0000	15.7532	0.0000	47	41	0.0000
2	2,50,99	5.8714	3.0523	0.0077	0.0012	0.0032	0.0009	15.7538	0.0008	46	40	0.0003
3	3,50,98	5.8719	3.0501	0.0084	0.0012	0.0044	0.0013	15.7545	0.0014	45	39	0.0013
4	4,50,97	5.8720	3.0480	0.0091	0.0010	0.0054	0.0018	15.7557	0.0025	44	39	0.0048
5	5,50,96	5.8717	3.0464	0.0098	0.0010	0.0059	0.0021	15.7568	0.0033	43	38	0.0091
6	6,50,95	5.8716	3.0455	0.0101	0.0010	0.0057	0.0020	15.7574	0.0033	42	37	0.0094
7	7,50,94	5.8714	3.0452	0.0100	0.0009	0.0053	0.0018	15.7577	0.0031	41	36	0.0084
8	8,50,93	5.8711	3.0453	0.0099	0.0012	0.0049	0.0017	15.7578	0.0029	40	35	0.0075
9	9,50,92	5.8705	3.0454	0.0098	0.0022	0.0046	0.0016	15.7583	0.0030	40	35	0.0082
10	10,50,91	5.8695	3.0453	0.0099	0.0036	0.0043	0.0015	15.7591	0.0037	39	34	0.0129
11	11,50,90	5.8685	3.0450	0.0101	0.0048	0.0042	0.0016	15.7601	0.0049	38	33	0.0225
12	12,50,89	5.8674	3.0442	0.0105	0.0059	0.0048	0.0020	15.7615	0.0066	37	32	0.0407
13	13,50,88	5.8662	3.0430	0.0111	0.0072	0.0062	0.0030	15.7632	0.0089	36	31	0.0741
14	14,50,87	5.8648	3.0416	0.0120	0.0087	0.0081	0.0043	15.7653	0.0116	36	31	0.1254
15	15,50,86	5.8634	3.0401	0.0129	0.0099	0.0095	0.0055	15.7674	0.0138	35	30	0.1776

Taking the above into account, it is clear that only a subset of the circle data can be used in this way. In an attempt to utilise all the data, a tensioned cubic spline was fitted to the data. Only the outer sections corresponding to arcs of about 13 degrees were used to determine the circle centre. The arcs used in data set 2 also subtended an angle of about 13 degrees. This type of spline can reduce or avoid unwanted oscillations due to its inherent convexity preserving interpolation technique (Bu-qing & Ding-yuan 1989). The results are given in Table 7.2. For comparative purposes, a Bézier curve was fitted. The Bézier curve uses endpoint interpolation (Farin 1988) which ensures that the curve passes through the two points with the greatest angular separation. The results are given in Table 7.3. It is readily apparent from the values of the standard deviations (σ), which is generally the best estimate of truly random errors, that the Bézier curve approaches the theoretical circle better and as a result is more suitable to the circle centre finding algorithm than the tensioned cubic spline.

Table 7.3: DEC Circle centre solution: Data set 1-Bézier curve

n	Inter-section	$\overline{X}$ (m)	$\overline{Y}$ (m)	$\overline{Z}$ (m)	$\sigma\overline{X}$ (m)	$\sigma\overline{Y}$ (m)	$\sigma\overline{Z}$ (m)	$\overline{R}$ (m)	$\sigma\overline{R}$ (m)	∠P1P2 (Deg)	∠P2P3 (Deg)	FM
1	1,48,96	5.8739	3.0494	0.0079	0.0000	0.0000	0.0000	15.7422	0.0000	43.3	38.3	0.0000
2	2,48,95	5.8735	3.0491	0.0079	0.0004	0.0003	0.0000	15.7426	0.0005	42.5	37.5	0.0001
3	3,48,94	5.8731	3.0490	0.0079	0.0008	0.0003	0.0000	15.7430	0.0008	41.7	36.7	0.0004
4	4,48,93	5.8724	3.0490	0.0080	0.0014	0.0002	0.0000	15.7435	0.0012	40.9	35.9	0.0010
5	5,48,92	5.8717	3.0489	0.0080	0.0020	0.0002	0.0001	15.7441	0.0017	40.1	35.1	0.0023
6	6,48,91	5.8709	3.0488	0.0082	0.0027	0.0004	0.0003	15.7449	0.0024	39.3	34.3	0.0051
7	7,48,90	5.8699	3.0484	0.0084	0.0035	0.0010	0.0008	15.7459	0.0035	38.5	33.5	0.0107
8	8,48,89	5.8689	3.0479	0.0089	0.0044	0.0018	0.0014	15.7472	0.0047	37.6	32.7	0.0198
9	9,48,88	5.8678	3.0472	0.0094	0.0051	0.0026	0.0021	15.7485	0.0060	36.8	31.9	0.0322
10	10,48,87	5.8668	3.0465	0.0100	0.0058	0.0033	0.0027	15.7499	0.0071	36.0	31.1	0.0454
11	11,48,86	5.8659	3.0459	0.0106	0.0062	0.0036	0.0033	15.7511	0.0078	35.2	30.3	0.0558
12	12,48,85	5.8652	3.0457	0.0111	0.0064	0.0036	0.0036	15.7520	0.0081	34.4	29.5	0.0597
13	13,48,84	5.8648	3.0458	0.0114	0.0063	0.0035	0.0036	15.7524	0.0078	33.6	28.7	0.0569
14	14,48,83	5.8648	3.0465	0.0115	0.0060	0.0040	0.0034	15.7522	0.0076	32.8	27.9	0.0534
15	15,48,82	5.8651	3.0475	0.0111	0.0059	0.0055	0.0036	15.7514	0.0079	31.9	27.1	0.0588

Table 7.4: HA Circle centre solution: Data set 1

n	Inter-section	$\overline{X}$ (m)	$\overline{Y}$ (m)	$\overline{Z}$ (m)	$\sigma\overline{X}$ (m)	$\sigma\overline{Y}$ (m)	$\sigma\overline{Z}$ (m)	$\overline{R}$ (m)	$\sigma\overline{R}$ (m)	∠P1P2 (Deg)	∠P2P3 (Deg)	FM
1	1,9,17	-0.0509	-0.0568	-6.8720	0.0000	0.0000	0.0000	20.8657	0.0000	40.0	43.9	0.0000
2	2,9,16	-0.0495	-0.0542	-6.8721	0.0020	0.0037	0.0002	20.8632	0.0035	35.9	40.0	0.0108
3	3,9,15	-0.0600	-0.0579	-6.8762	0.0182	0.0069	0.0069	20.8743	0.0192	31.9	31.9	0.4324
4	4,9,14	-0.0582	-0.0602	-6.8752	0.0153	0.0073	0.0060	20.8737	0.0157	27.9	27.9	0.3258
5	5,9,13	-0.0564	-0.0605	-6.8826	0.0139	0.0063	0.0173	20.8722	0.0140	20.0	23.9	0.2757
6	6,9,12	-0.0728	-0.0716	-6.8932	0.0420	0.0277	0.0302	20.8919	0.0498	15.9	15.8	3.6273
7	7,9,11	-0.0568	-0.0633	-6.8882	0.0571	0.0334	0.0306	20.8739	0.0658	12.0	12.0	6.4874
8	8,9,10	0.0306	-0.0118	-6.8000	0.2529	0.1489	0.2509	20.7741	0.2889	4.1	8.3	122.7438

HA circle Following the same steps to determine the circle centre using the HA data as used for the DEC data, the dependency of data distribution on the Bézier curve is clearly seen. The HA data has several gaps and are not as uniformly distributed as the DEC data. These gaps will affect the curve mostly in the regions of the gaps, although it does affect the whole curve. Using the GPS data the circle parameters found are summarised in Table 7.4. The results using the tensioned cubic spline fit are summarised in Table 7.5 and that of the Bézier fit in Table 7.6. It is obvious from the FM that the spline fit is a more suitable fit for the HA data.

7.3.3 Offset Determinations

Using the Bézier curve as fitted to the DEC arc and the tensioned cubic spline as fitted to the HA arc the offset was determined; the results are presented in Table 7.7. The standard error of the mean (Δ) is not very significant in this table as the error distribution is not Gaussian, neither are the fitted points independent. They are included for comparison purposes to the solutions of data set 2. The standard deviation shows a large spread in the solutions and although the value 6.6953 $\pm$0.0054 m is a very reasonable offset value compared to the previously found values as men-

Table 7.5: HA Circle centre solution: Data set 1-Tensioned cubic spline fit

n	Inter-section	$\overline{X}$ (m)	$\overline{Y}$ (m)	$\overline{Z}$ (m)	$\sigma\overline{X}$ (m)	$\sigma\overline{Y}$ (m)	$\sigma\overline{Z}$ (m)	$\overline{R}$ (m)	$\sigma\overline{R}$ (m)	∠P1P2 (Deg)	∠P2P3 (Deg)	FM
1	1,50,100	-0.0483	-0.0553	-6.8731	0.0000	0.0000	0.0000	20.8634	0.0000	39.4	43.9	0.0000
2	2,50,99	-0.0474	-0.0543	-6.8731	0.0011	0.0014	0.0000	20.8622	0.0017	38.7	43.4	0.0025
3	3,50,98	-0.0467	-0.0533	-6.8731	0.0014	0.0019	0.0000	20.8611	0.0022	38.1	42.7	0.0057
4	4,50,97	-0.0462	-0.0525	-6.8732	0.0015	0.0022	0.0000	20.8603	0.0024	37.4	42.2	0.0076
5	5,50,96	-0.0460	-0.0519	-6.8732	0.0014	0.0024	0.0000	20.8598	0.0023	36.7	41.7	0.0078
6	6,50,95	-0.0459	-0.0515	-6.8732	0.0013	0.0023	0.0000	20.8595	0.0022	36.0	41.1	0.0072
7	7,50,94	-0.0457	-0.0512	-6.8732	0.0012	0.0022	0.0001	20.8593	0.0021	35.4	40.5	0.0069
8	8,50,93	-0.0446	-0.0509	-6.8735	0.0033	0.0023	0.0007	20.8581	0.0038	34.7	39.2	0.0222
9	9,50,92	-0.0429	-0.0504	-6.8740	0.0060	0.0025	0.0016	20.8564	0.0063	34.1	37.9	0.0620
10	10,50,91	-0.0415	-0.0501	-6.8747	0.0071	0.0025	0.0027	20.8550	0.0073	33.4	36.5	0.0846
11	11,50,90	-0.0414	-0.0502	-6.8756	0.0068	0.0024	0.0038	20.8550	0.0069	32.7	35.2	0.0770
12	12,50,89	-0.0430	-0.0508	-6.8764	0.0084	0.0030	0.0047	20.8566	0.0087	32.0	33.8	0.1231
13	13,50,88	-0.0455	-0.0517	-6.8771	0.0122	0.0044	0.0052	20.8593	0.0128	31.3	32.5	0.2651
14	14,50,87	-0.0478	-0.0527	-6.8776	0.0145	0.0055	0.0053	20.8618	0.0154	30.7	31.8	0.3854
15	15,50,86	-0.0496	-0.0536	-6.8779	0.0156	0.0064	0.0052	20.8638	0.0167	30.0	31.1	0.4572
16	16,50,85	-0.0508	-0.0545	-6.8779	0.0158	0.0071	0.0050	20.8653	0.0172	29.3	30.5	0.4851
17	17,50,84	-0.0515	-0.0553	-6.8779	0.0155	0.0077	0.0048	20.8663	0.0171	28.7	29.8	0.4833
18	18,50,83	-0.0517	-0.0560	-6.8777	0.0151	0.0080	0.0047	20.8668	0.0168	28.0	29.2	0.4645
19	19,50,82	-0.0515	-0.0564	-6.8776	0.0147	0.0080	0.0047	20.8668	0.0163	27.4	28.5	0.4400
20	20,50,81	-0.0503	-0.0561	-6.8775	0.0152	0.0079	0.0045	20.8656	0.0167	26.3	27.9	0.4617

Table 7.6: HA Circle centre solution: Data set 1-Bézier curve

n	Inter-section	$\overline{X}$ (m)	$\overline{Y}$ (m)	$\overline{Z}$ (m)	$\sigma\overline{X}$ (m)	$\sigma\overline{Y}$ (m)	$\sigma\overline{Z}$ (m)	$\overline{R}$ (m)	$\sigma\overline{R}$ (m)	∠P1P2 (Deg)	∠P2P3 (Deg)	FM
1	1,50,99	-0.0993	-0.1031	-6.8783	0.0000	0.0000	0.0000	20.8882	0.0000	36.5	38.5	0.0000
2	2,50,98	-0.0922	-0.1024	-6.8789	0.0099	0.0009	0.0007	20.8817	0.0092	36.0	37.6	0.0745
3	3,50,97	-0.0862	-0.1019	-6.8794	0.0126	0.0010	0.0011	20.8761	0.0116	35.4	36.7	0.1582
4	4,50,96	-0.0819	-0.1018	-6.8801	0.0134	0.0009	0.0015	20.8723	0.0122	34.8	35.7	0.1954
5	5,50,95	-0.0800	-0.1022	-6.8807	0.0123	0.0011	0.0020	20.8708	0.0110	34.3	34.7	0.1716
6	6,50,94	-0.0809	-0.1032	-6.8814	0.0112	0.0026	0.0024	20.8720	0.0103	33.7	33.7	0.1566
7	7,50,93	-0.0846	-0.1048	-6.8821	0.0142	0.0049	0.0028	20.8761	0.0142	33.1	32.7	0.3045
8	8,50,92	-0.0908	-0.1070	-6.8827	0.0219	0.0077	0.0031	20.8825	0.0226	32.5	31.8	0.7813
9	9,50,91	-0.0987	-0.1096	-6.8833	0.0313	0.0106	0.0034	20.8908	0.0324	31.8	30.9	1.6369
10	10,50,90	-0.1074	-0.1123	-6.8837	0.0404	0.0132	0.0035	20.8997	0.0417	31.2	30.2	2.7442
11	11,50,89	-0.1161	-0.1148	-6.8841	0.0479	0.0150	0.0035	20.9085	0.0491	30.6	29.4	3.8524
12	12,50,88	-0.1239	-0.1167	-6.8844	0.0530	0.0158	0.0035	20.9163	0.0540	30.0	28.8	4.6967
13	13,50,87	-0.1302	-0.1177	-6.8846	0.0557	0.0155	0.0035	20.9224	0.0562	29.3	28.2	5.1115
14	14,50,86	-0.1347	-0.1177	-6.8849	0.0561	0.0149	0.0034	20.9263	0.0559	28.6	27.7	5.1002
15	15,50,85	-0.1373	-0.1164	-6.8851	0.0550	0.0152	0.0035	20.9280	0.0543	27.8	27.1	4.8290
16	16,50,84	-0.1382	-0.1140	-6.8857	0.0532	0.0175	0.0036	20.9276	0.0525	26.9	26.6	4.5312
17	17,50,83	-0.1376	-0.1108	-6.8860	0.0516	0.0215	0.0041	20.9256	0.0515	26.0	26.0	4.3813
18	18,50,82	-0.1359	-0.1072	-6.8867	0.0506	0.0258	0.0048	20.9224	0.0517	25.1	25.5	4.4378
19	19,50,81	-0.1336	-0.1037	-6.8875	0.0502	0.0294	0.0059	20.9187	0.0529	24.1	24.8	4.6445
20	20,50,80	-0.1309	-0.1007	-6.8885	0.0503	0.0315	0.0074	20.9149	0.0541	23.1	24.2	4.8818

tioned at the end of this chapter, the sigma value of 17.4 mm is quite large. The experiment was therefore redesigned as described in section 4.10. From simulations using *ARCRAN* it was clear that it would be very difficult to obtain a much smaller spread of the offset values. The standard deviation value should however be reduced if possible. The standard error of the mean value should also be reduced and should be based on independent GPS measurements and solutions of the offset; not extrapolated points from some curve fit. Both these goals were achieved using data set 2.

Table 7.7: Offset solution: Data set 1

n	H (m)	$\overline{H}$ (m)	$\sigma\overline{H}$ (m)	$\Delta\overline{H}$ (m)
1	6.6916	6.6916	0.0000	0.0000
2	6.6892	6.6904	0.0017	0.0000
3	6.6872	6.6893	0.0022	0.0000
4	6.6861	6.6885	0.0024	0.0000
5	6.6860	6.6880	0.0023	0.0000
6	6.6864	6.6877	0.0022	0.0000
7	6.6859	6.6875	0.0021	0.0000
8	6.6789	6.6864	0.0036	0.0000
9	6.6722	6.6848	0.0058	0.0002
10	6.6736	6.6837	0.0065	0.0003
11	6.6863	6.6839	0.0062	0.0003
12	6.7073	6.6859	0.0089	0.0008
13	6.7238	6.6888	0.0135	0.0020
14	6.7257	6.6914	0.0163	0.0032
15	6.7227	6.6935	0.0177	0.0041
16	6.7175	6.6950	0.0181	0.0046
17	6.7113	6.6960	0.0179	0.0048
18	6.7045	6.6965	0.0175	0.0049
19	6.6956	6.6964	0.0170	0.0049
20	6.6732	6.6953	0.0174	0.0054

7.4 Offset Determined from Data Set 2

7.4.1 Zenith Position

The zenith point is the only point which is common to both DEC and HA circles. This point is crucial for the determination of the offset as explained in section 5.2. The pointing error ΔP only influences the determination of the zenith point, as it is assumed to be a fixed point to which the antenna is returned to. On any other points of the HA and DEC circles, the antenna pointing is of smaller consequence, as we are then only interested in the GPS measured position. Pointing errors could however cause such a point to be out of the plane of the circle, if for instance the movement of the polar shaft is not stable due to bearing movement. The magnitude of this error should be negligible and was not apparent in the data.

The uncorrected measured points for the zenith position as determined during GPS213 are listed in table 4.7 as points 10 to 18. The observations of GPS213 and GPS215 were sequenced in such a way as to allow a thermal model to be implicit in the solution. The thermal model is described in detail in section 4.10. Plots (see figure 7.1) of the uncorrected HA circle zenith points clearly shows a separation of the measured points into two groups, with maximum extension in the y coordinate. This grouping is due to hysteresis in the movement of the antenna. When the antenna drives from west to east the y coordinate is less than it should be. The antenna slightly overshoots and then moves back a bit more than the initial overshoot. The converse is true when driving from east to west, then the y coordinate is more than

it should be.

Table 7.8 lists the observations in the sequence in which they were observed. The differential of the coordinates of the points to that of the statistical are included. The ΔHA values are in millidegrees as determined by the antenna shaft encoder, where negative is towards the west and positive towards the east with zenith as centre. Observation 20 is shown to complete the sequence of the table, but was an observation of only 40 minutes duration. (This observation is not used in the solutions and was rejected on the grounds of being an outlier.) The drive towards observation 23, data point 16, was in both axes simultaneously. The anomaly in the sequence which determines the placing of a point in a group as seen for data point 16, is probably explained by this action. Point 16 should have been in group 2 if the east-west, west-east sequence was held throughout.

Pointing error correction The coordinates of the zenith were found by correcting for pointing error by a process of averaging and translation. Careful attention was paid to propagation of errors (see Appendix A.9). Table 7.9 summarises the values and results and is divided into the two zenith groups. The arithmetic average of groups 1 and 2 were found, which allowed one to find the centre of the vector connecting the two average points. Groups 1 and 2 were then translated to the centre of the vector with the value of the differential between the centre of the vector and the value of each group. The centre coordinates were found using

$$\left.\begin{array}{rcl} (\overline{x}_2 - \overline{x}_1)/2 + \overline{x}_1 & = & X_c, \\ (\overline{y}_2 - \overline{y}_1)/2 + \overline{y}_1 & = & Y_c, \\ (\overline{z}_2 - \overline{z}_1)/2 + \overline{z}_1 & = & Z_c. \end{array}\right\} \tag{7.7}$$

Subscripts 1 and 2 refers to groups 1 and 2 and subscript c refers to the vector centre coordinate. The effect of the pointing error correction is shown in figure 7.1. The uncorrected Y coordinate in graphs (a) and (c) shows a spread around the average of more than ± 4 mm. After pointing corrections, the spread decreased to less than ± 3 mm and the grouping of the y coordinates was much more centred. Table 7.10 contains the average of all the coordinates, which is the centre coordinates of the vector between groups 1 and 2, denoted as group 0, the split group is again indicated as 1 and 2. After this pointing correction, the standard deviation (σ) and standard deviation of the mean (Δ) of the offset value was reduced from 19.6 mm to 18.4 mm and from ±3.1 mm to ±2.7mm respectively.

Adjusting centre coordinates A further adjustment was necessary. The DEC circle has defined a zenith point which required no pointing correction and the HA

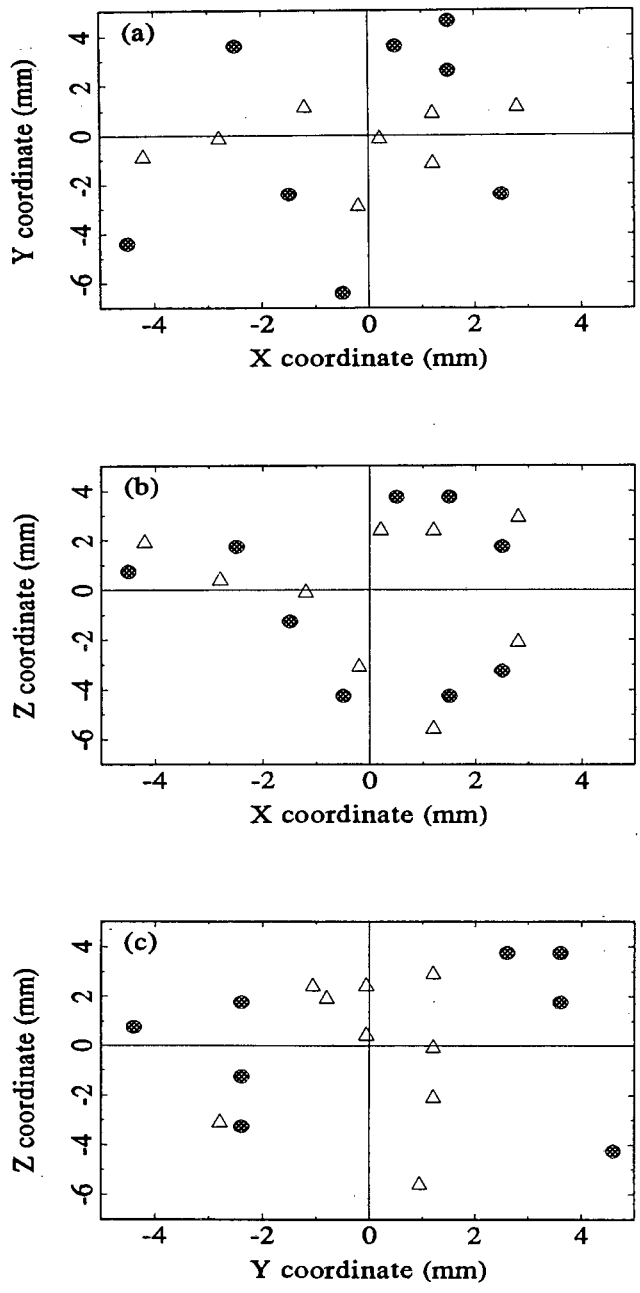

Figure 7.1: Graphs of coordinates, both corrected and uncorrected for pointing errors are shown. The triangles denote corrected coordinate and the filled circles the uncorrected coordinate. (a) Y vs X. (b) Z vs X. (c) Z vs Y. Coordinates have been normalised to the mean value.

Table 7.8: Uncorrected HA circle zenith points: GPS213

Observation number	Point number	Antenna moving	X (m)	Y (m)	Z (m)	ΔHA (mdeg)
2	10	from west	60.155	-56.896	-15.015	-
5	11	from east	60.157	-56.885	-15.015	4
8	12	from west	60.154	-56.892	-15.012	-4
11	13	from east	60.156	-56.886	-15.007	4
14	14	from west	60.158	-56.892	-15.009	-4
17	15	from east	60.157	-56.887	-15.007	4
20	-	from west	62.191	-70.318	-15.006	-5
23	16	from east	60.151	-56.894	-15.010	4
26	17	from west	60.158	-56.892	-15.014	-4
29	18	from east	60.153	-56.886	-15.009	3
			$\bar{x}(m)$	$\bar{y}(m)$	$\bar{z}(m)$	
			60.1554	−56.8900	−15.0108	
			$\Delta\bar{x}(mm)$	$\Delta\bar{y}(mm)$	$\Delta\bar{z}(mm)$	
			±0.0008	±0.0013	±0.0011	
			$\sigma_x(mm)$	$\sigma_y(mm)$	$\sigma_z(mm)$	
			0.0024	0.0040	0.0032	

Table 7.9: Zenith coordinates arranged into groups and corrections: GPS213

Group	Observation number	Point number	Antenna moving	X (m)	Y (m)	Z (m)	Δ X (mm)	Δ Y (mm)	Δ Z (mm)
1	2	10	from west	60.155	-56.896	-15.015	0.3	3.6	1.2
1	8	12	from west	60.154	-56.892	-15.012	0.3	3.6	1.2
1	14	14	from west	60.158	-56.892	-15.009	0.3	3.6	1.2
1	23	16	from east	60.151	-56.894	-15.010	0.3	3.6	1.2
1	26	17	from west	60.158	-56.892	-15.014	0.3	3.6	1.2
2	5	11	from east	60.157	-56.885	-15.015	-0.3	-3.6	-1.3
2	11	13	from east	60.156	-56.886	-15.007	-0.3	-3.6	-1.3
2	17	15	from east	60.157	-56.887	-15.007	-0.3	-3.6	-1.3
2	20	-	from west	62.191	-70.318	-15.006	-0.3	-3.6	-1.3
2	29	18	from east	60.153	-56.886	-15.009	-0.3	-3.6	-1.3

circle defined a zenith point after pointing correction. There is a small difference between these two zenith points as they are independent determinations. The offset calculation however requires that the zenith point be common to both circles. This meant that the circle centre values had to be translated with the differential between the average of the two zenith points and the individual zenith points, a similar process as used for the pointing correction. The adjustment values found were small, 0.185 mm, 1.150 mm and -1.025 mm. The necessary adjustments are made when *Average zenith* is selected from the software. This brought a further reduction in the standard deviation and standard deviation of the error of the offset value, i.e. to 16.7 mm and ±2.3 mm respectively.

Table 7.10: Summary of zenith group coordinates means and statistics: GPS213

Group	Coordinate	Mean (m)	σ (mm)	Δ (mm)
0	X_c	60.1555	4.6	1.5
0	Y_c	-56.8896	2.7	0.9
0	Z_c	-15.0108	5.2	1.7
1	$\overline{X}$	60.15520	2.9	1.3
1	$\overline{Y}$	-56.8932	1.8	0.8
1	$\overline{Z}$	-15.0120	2.5	1.1
2	$\overline{X}$	60.1558	1.9	0.9
2	$\overline{Y}$	-56.8860	0.9	0.4
2	$\overline{Z}$	-15.0095	3.8	1.9

Table 7.11: DEC Circle centre solution: Data set 2

n	Inter-section	$\overline{X}$ (m)	$\overline{Y}$ (m)	$\overline{Z}$ (m)	$\sigma\overline{X}$ (m)	$\sigma\overline{Y}$ (m)	$\sigma\overline{Z}$ (m)	$\overline{R}$ (m)	$\sigma\overline{R}$ (m)	∠P1P2 (Deg)	∠P2P3 (Deg)	FM
1	1,14,26	47.6116	-63.4609	-8.1388	0.0000	0.0000	0.0000	15.7401	0.0000	46.7	44.9	0.0000
2	2,15,27	47.6188	-63.4619	-8.1423	0.0100	0.0014	0.0049	15.7320	0.0114	45.7	44.0	0.0646
3	3,16,28	47.6141	-63.4617	-8.1363	0.0106	0.0010	0.0110	15.7381	0.0132	44.6	42.9	0.1159
4	4,17,29	47.6142	-63.4588	-8.1351	0.0087	0.0058	0.0092	15.7372	0.0109	43.7	41.9	0.0892
5	5,18,30	47.6180	-63.4563	-8.1366	0.0112	0.0075	0.0086	15.7321	0.0148	42.8	41.0	0.1736
6	6,19,31	47.6142	-63.4569	-8.1349	0.0135	0.0068	0.0086	15.7356	0.0157	41.7	39.9	0.2052
7	7,20,32	47.6143	-63.4570	-8.1351	0.0124	0.0062	0.0079	15.7358	0.0144	40.7	39.0	0.1760
8	8,20,33	47.6127	-63.4578	-8.1350	0.0124	0.0062	0.0073	15.7377	0.0143	39.7	37.9	0.1796
9	9,21,33	47.6123	-63.4583	-8.1350	0.0116	0.0060	0.0068	15.7387	0.0138	38.7	37.9	0.1685
10	10,22,34	47.6126	-63.4588	-8.1344	0.0110	0.0059	0.0067	15.7389	0.0130	37.7	35.0	0.1519
11	11,23,34	47.6109	-63.4602	-8.1328	0.0119	0.0072	0.0083	15.7411	0.0143	36.6	34.9	0.1845
12	12,24,35	47.6108	-63.4611	-8.1328	0.0113	0.0075	0.0079	15.7412	0.0136	35.7	33.9	0.1692
13	13,25,35	47.6116	-63.4595	-8.1334	0.0112	0.0091	0.0078	15.7398	0.0139	34.7	34.0	0.1767

7.4.2 HA and DEC Circle Centre Determinations

DEC circle The values found for the DEC circle centre are listed in Table 7.11. The standard deviations of the average values of the coordinates of the centre and the radius are significantly better than those found using data set 1. The FM values of data set 2 are all, with the exception of one, below 0.2 whereas data set 1 only has half of the intersections with an FM value below 0.2. This indicates a marked

Table 7.12: HA Circle centre solution: Data set 2

n	Inter-section	$\overline{X}$ (m)	$\overline{Y}$ (m)	$\overline{Z}$ (m)	$\sigma\overline{X}$ (m)	$\sigma\overline{Y}$ (m)	$\sigma\overline{Z}$ (m)	$\overline{R}$ (m)	$\sigma\overline{R}$ (m)	∠P1P2 (Deg)	∠P2P3 (Deg)	FM
1	1,10,19	41.6939	-66.5560	-14.9967	0.0000	0.0000	0.0000	20.8376	0.0000	44.0	44.0	0.0000
2	2,11,20	41.6939	-66.5590	-14.9945	0.0000	0.0042	0.0030	20.8405	0.0041	42.0	43.0	0.0147
3	2,12,21	41.6876	-66.5617	-14.9950	0.0108	0.0055	0.0023	20.8472	0.0118	42.0	41.9	0.1627
4	3,13,22	41.6855	-66.5619	-14.9924	0.0098	0.0045	0.0055	20.8492	0.0105	41.0	41.0	0.1440
5	4,14,23	41.6879	-66.5617	-14.9914	0.0101	0.0039	0.0053	20.8476	0.0097	40.0	40.0	0.1332
6	5,15,24	41.6841	-66.5620	-14.9928	0.0130	0.0035	0.0059	20.8511	0.0123	38.9	38.9	0.2201
7	6,15,25	41.6839	-66.5620	-14.9932	0.0119	0.0032	0.0054	20.8513	0.0112	38.0	38.0	0.1889
8	7,16,26	41.6814	-66.5636	-14.9962	0.0131	0.0054	0.0099	20.8537	0.0124	36.9	36.9	0.2353
9	8,17,27	41.6796	-66.5637	-14.9987	0.0134	0.0051	0.0119	20.8557	0.0131	36.0	35.9	0.2654
10	9,18,28	41.6774	-66.56487	-15.0000	0.0143	0.0058	0.0119	20.8578	0.0140	34.9	34.9	0.3077

Table 7.13: Offset solution: Data set 2

n	H (m)	$\overline{H}$ (m)	$\sigma\overline{H}$ (m)	$\Delta\overline{H}$ (m)
1	6.6733	6.6733	0.0000	0.0000
2	6.6797	6.6765	0.0045	0.0000
3	6.6965	6.6832	0.0119	0.0001
4	6.6882	6.6844	0.0101	0.0002
5	6.6768	6.6829	0.0093	0.0002
6	6.7071	6.6869	0.0129	0.0007
7	6.6887	6.6872	0.0118	0.0007
8	6.7111	6.6902	0.0138	0.0011
9	6.7178	6.6932	0.0159	0.0018
10	6.7165	6.6956	0.0167	0.0023

degree of success due to changing the experimental method. When comparing the values of data set 2 against the values as found using the tensioned cubic spline and Bézier curve it matches the final FM value of the spline very closely but the real data is worse when compared to the smooth Bézier curve. It is clear that data set 2 provides the better overall solution.

HA circle Table 7.12 summarises the final values found for the HA circle. Similar to the DEC solutions, the sigmas of the final average values of the coordinates of the centre and the radius are significantly better than those found using just data set 1. The FM values of data set 2 are better than those of the GPS data and the two curve fits. This also indicates success due to changing the experimental method. When comparing the curve fits against data set 2, the standard deviations of data set 2 are better except in the Z coordinate where it is better using the two curve fits. Overall data set 2 provides the more accurate solution.

7.4.3 Offset Determinations

The offset solutions are given in Table 7.13. Each solution n has a value H and an accompanying running mean, $\overline{H}$. The two right hand columns are the standard deviation (σ) and standard error of the mean (Δ) respectively. Solution 10 is the best estimate with a final value of 6.6956 $\pm$ 0.0023 m and having a standard deviation of 16.7 mm. This is surprisingly close to the value determined with data set 1, except the standard deviation and especially the standard error of the mean is smaller. Moreover, the errors from independent solutions using independent points and not extrapolated points due to a curve fit. The errors are thus statistically meaningful.

Table 7.14: VLBI reference point: Data set 2

Coordinate	Value (m)	σ (mm)	Δ (mm)
x	41.6800	15.8	2.0
y	-66.5641	7.5	0.5
z	-8.1310	3.9	0.1

7.4.4 VLBI Reference Point

The VLBI reference point is the intersection of the two axes as described in section 5.2 and in this work is referenced to the SLR reference point. Using *Hart3D* and data set 2 the final results obtained are listed in Table 7.14. This determination using GPS allows the three reference frames, GPS, SLR and VLBI, to be tied to a single point. This is made possible by the visit to the SLR site by a mobile satellite ranger of IfAG during 1993, together with their occupation of the SLR reference point with a GPS receiver during the 1995 Antarctica campaign. The relative coordinates of the SLR, VLBI reference point and CNES ROGUE receiver which is part of the IGS network, has already been determined in the ITRF93 and ITRF94 coordinate system (personal communication G Soltau).

The International Earth Rotation Service (IERS) coordinates (epoch 1993) for the VLBI reference point and SLR reference points are listed in Table 7.15 and Table 7.16 respectively. The relative distance and difference in coordinates $(\Delta X, \Delta Y, \Delta Z)$ from the VLBI to SLR using these values are shown in Table 7.17. This table also includes the relative VLBI to SLR reference point coordinates as determined in this work with GPS. The comparison neglects possible small differences in the VLBI and the SLR scale. No attempt was made to convert WGS84 relative coordinates (as determined in this work) to ITRF93 or ITRF94 relative coordinates using transformation parameters.

It is apparent that the relative distance between the VLBI and SLR pad reference points agree reasonably well between ITRF93 and the distance determined using GPS. The ITRF94 coordinates seem to be moving away somewhat. The definitive relative coordinates should be those determined by the local GPS tie. It is suggested that this local tie be used as a constraint in the terrestrial reference frame.

The movement in the values of the IERS are due to stochastic components in the ITRF models. There is presently much discussion between myself, IfAG and the IERS Central Bureau on the differences in the values. One has to keep in mind

Table 7.15: VLBI reference point: IERS; Epoch 1993

ITRF	VLBI X (m)	VLBI Y (m)	VLBI Z (m)
1993	5085442.774	2668263.382	-2768697.118
1994	5085442.783	2668263.415	-2768697.103

Table 7.16: SLR reference point: IERS; Epoch 1993

ITRF	SLR X (m)	SLR Y (m)	SLR Z (m)
1993	5085401.140	2668329.979	-2768688.949
1994	5085401.131	2668330.035	-2768688.916

that the coordinates for the SLR reference point are derived from independent global networks.

7.4.5 Thermal Modelling

The coordinates and temperature as a function of zenith point number are depicted in figure 7.2. There is a fair amount of spread in the points so no attempt is made to fit a curve through the data. It is however apparent, especially in the X and Z coordinates, that the magnitude of the coordinate value changes with change in antenna structure temperature. The apparent anti-correlation is a result of the sign convention of the coordinates. In the Z coordinate one can see structural movement of $\pm$ 4 mm which is approximately correlated with the temperature differential of 15° C. As part of this $\pm$ 4 mm is measurement error, the structural expansion is approximately what would be expected considering the coefficient of expansion of

Table 7.17: Comparison of relative coordinates between the VLBI and SLR reference points as determined by VLBI, SLR and GPS (data set 2)

Solution	Δ X (m)	Δ Y (m)	Δ Z (m)	Distance (m)
ITRF 1993	41.634	-66.597	-8.169	78.964
ITRF 1994	41.652	-66.620	-8.187	78.995
GPS WGS84	41.680	-66.564	-8.131	78.956

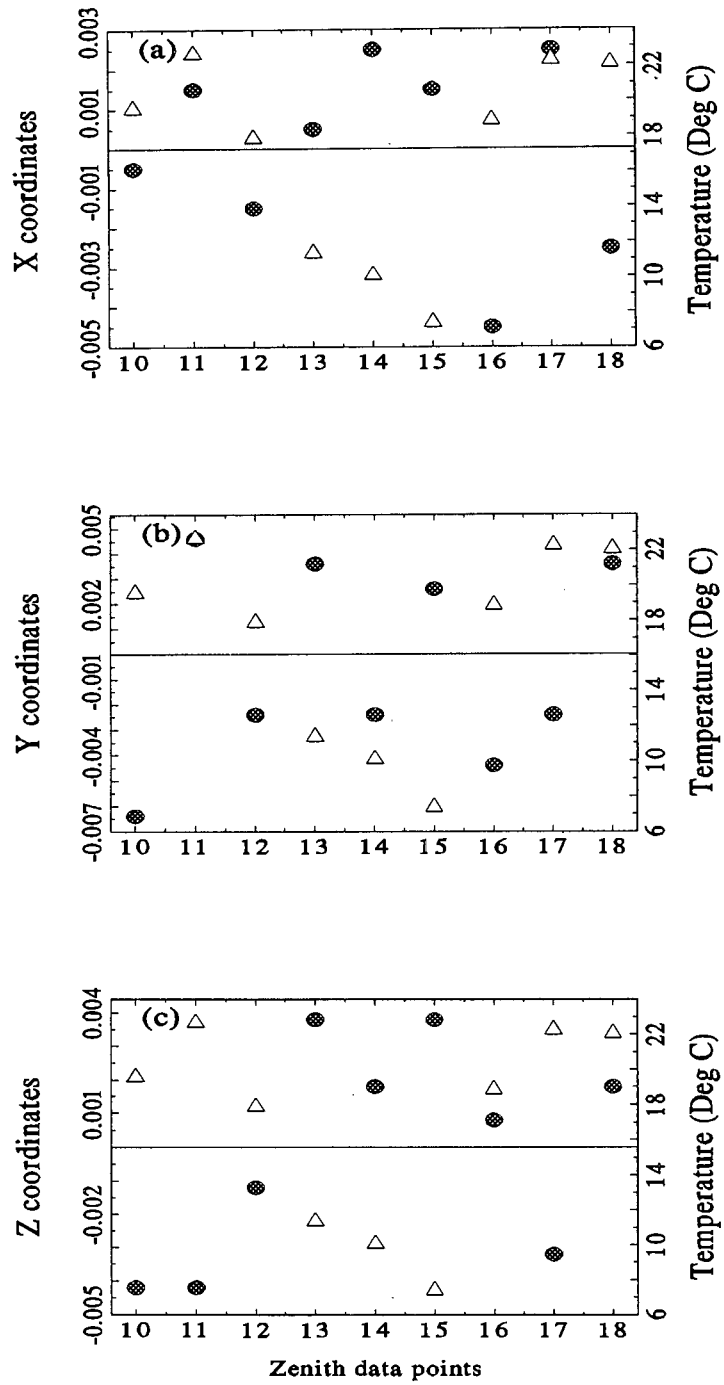

Figure 7.2: Coordinates and temperature as a function of zenith data points. The triangles denote temperature and the filled circles the coordinate. (a) X coordinate. (b) Y coordinate. (c) Z coordinate. Coordinates have been normalised to the mean value.

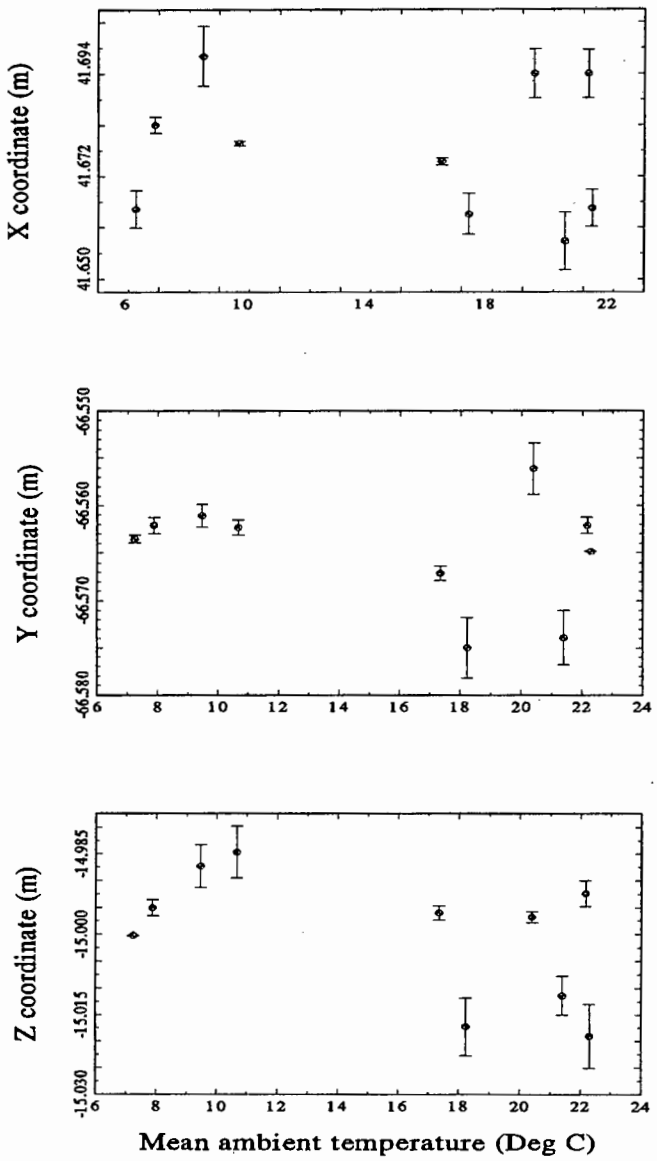

Figure 7.3: HA circle centre coordinates as a function of mean ambient temperature. (a) X coordinate. (b) Y coordinate. (c) Z coordinate. Coordinates are referenced to the SLR reference point.

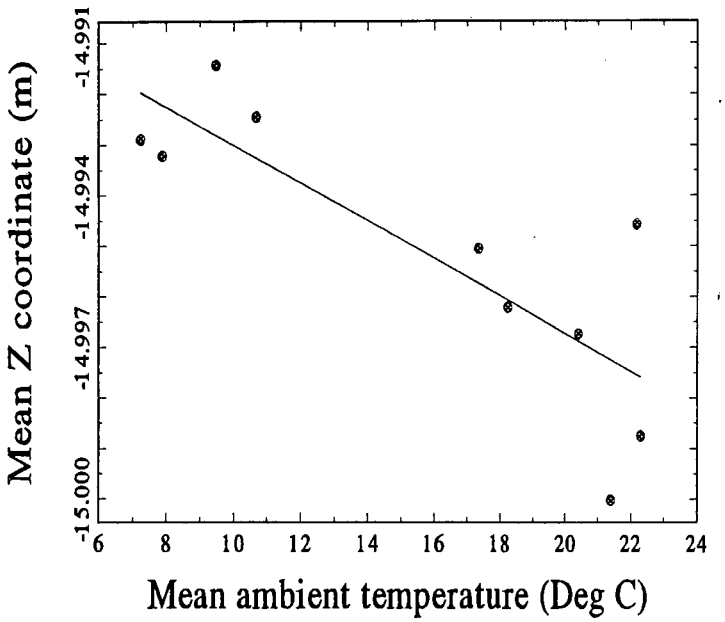

Figure 7.4: HA circle centre mean Z coordinate as a function of mean ambient temperature. Coordinates are referenced to the SLR reference point.

steel. Tests were run to see what the effect on the offset value would be if instead of the implicit thermal model, random solutions were used. A typical result shows an offset value of 6.6951 m with a standard deviation of 19.7 mm and standard error of the mean of ± 3.1 mm. These values are both poorer than when the implicit thermal model is used.

The coordinates of the DEC and HA circle centres as a function of mean ambient temperature was investigated. The mean temperatures for each intersection determination is the mean of the three temperature measurements sampled for each of the three points on the arc used for the particular intersection determination. Figure 7.3 depicts the HA circle centre coordinates as a function of mean ambient temperature. No trend is apparent in (a) or (b) where a reasonably linear relationship exists over the whole temperature range. However, in figure 7.3 (c) there appears to be some movement in the Z coordinate. This is made clearer by plotting the running mean of the centre Z coordinate as a function of mean temperature as in figure 7.4. Figure 7.5 depicts the DEC circle centre coordinates as a function of mean ambient temperat-

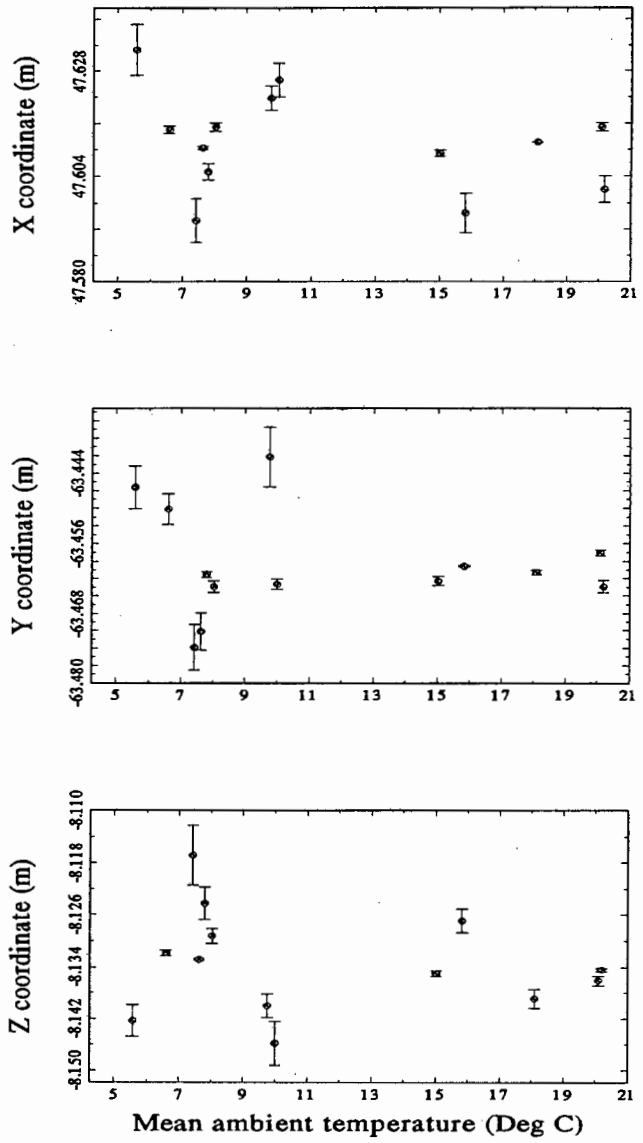

Figure 7.5: DEC circle centre coordinates as a function of mean ambient temperature. (a) X coordinate. (b) Y coordinate. (c) Z coordinate. Coordinates are referenced to the SLR reference point.

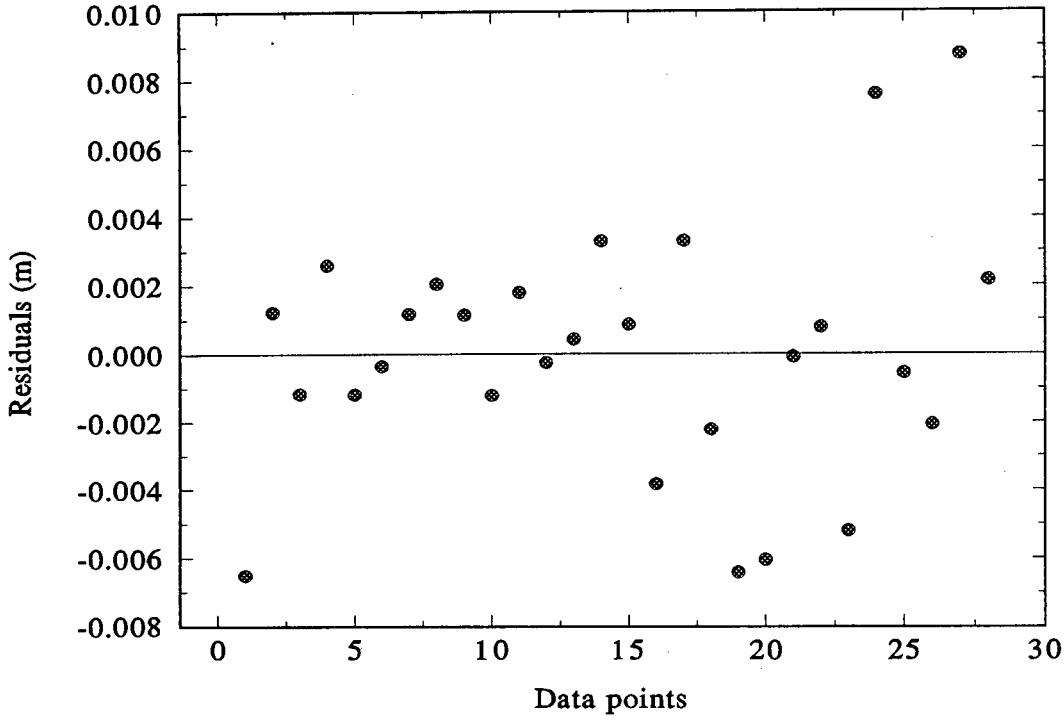

Figure 7.6: Residuals of HA circle least-squares fit as a function of data points. The residuals are deviations from a theoretical circle.

ure. A reasonably linear relationship exists over the whole temperature range but there is an indication of larger deviations from the mean at the lower end of the temperature range.

7.4.6 Least-Squares applied to Circle, Ellipse and Gravitational Modelling

Least-squares was used to determine fits of circles and ellipses with and without sine gravity terms. As previously discussed, least-squares is not a feasible method to determine circle parameters when using less than a semi-circle. Consequently, the circle centre for the HA circle was used as a pivot point to rotate the HA arcs and zenith data through 180 degrees to create an image of the data in the same plane,

which created a data distribution over more than a semicircle. This was done by using vector products to find a vector of rotation normal to the plane and through the circle centre (see Appendix A.8).

Deviations from a true circle Although these data did not allow a unique circle centre determination, it did provide some information on the residuals between a theoretical circle and the data using the circle centre coordinates determined using *Hart3D*. The residuals as a function of data points are plotted in figure 7.6. Maximum deviation was 8.8 mm with an average deviation of 2.6 mm. Standard error of the estimate was 3.9 mm. The values found for the circle centre coordinates were within a fraction of a millimetre of the values found by *Hart3D*.

Fitting an ellipse showed conclusively that the circle data in fact describes a circle as the a (major axis) and b (semi-major axis) parameters of the ellipse differed by only 0.5 mm.

Gravitational modelling using least-squares It was thought that using the HA circle data would indicate some structural sagging or deformation as the HA axis carries the largest weight of the two axes and is also subjected to the most leverage. If some bending took place a sine term would result, and the radius value should decrease. Adding sine gravity parameters to the circle and ellipse functions produced parameter values on the order of 10^{-7}. No conclusive evidence of gravitational deformation was found. If the telescope was pointing towards the horizon, the gravitational effect would be greater. As previously mentioned in section 4.4, the movement of the telescope was restricted to an elevation of about 45 degrees so points could not be measured that would enhance the gravity effect.

7.5 Comparison of Results from Different Methods

As mentioned in the introduction of this chapter, other independent methods have been used to determine the antenna axis offset, they are discussed below. The different values found are summarised at the end of this section. They are listed in chronological order.

Engineering Drawing The original engineering specification for the HartRAO antenna specifies an antenna axis offset value of 6.706 m. No errors are quoted. This value of the offset is 11 mm larger than the GPS determined value. Considering

the fact that the telescope was designed, manufactured and crated in the USA, then shipped to South Africa and assembled locally as a large do-it-yourself kit, the engineering drawing value is an indication of the precision engineering that went into these antennas.

VLBI solutions Referring to the summary below, the first two VLBI solutions by Marshall Eubanks (USNO) (personal communication) and Chopo Ma (NASA/GSFC) (personal communication) were found by adjusting HartRAO as well as the other fixed stations, in a VLBI solution along with geodetic, astrometric, station clock and atmosphere parameters. The last VLBI (1996) estimation by Chopo Ma shows a significant reduction in the size of the offset. The main difference between this and the 1995 solution is the estimation of atmosphere gradients. The gradients seem to improve geodetic consistency and are reasonable in terms of global atmospheric distribution.

Conventional Surveying Mark Newling of Surveys and Land Information (Department of Land Affairs) completed a determination of the axis offset in 1990 using conventional surveying methods. Reflective targets were fixed to the perimeters on both sides of the two gear wheels. The planes in which the targets lay and the circles were determined using leasts-squares (each gear describes a semicircle). It is worthwhile to compare the results found using this conventional method against the method using GPS. The errors for the radii of the HA and DEC gear wheels are $\pm$ 3 mm and $\pm$ 1 mm respectively. Using GPS, the standard error of the mean of the radii for the HA and DEC circles were $\pm$ 1.6 mm and $\pm$ 2.1 mm. Using the conventional surveying data the computed value for the axis offset was 6.695 $\pm$ 0.003 m. This compares very well with the GPS value of 6.6956 $\pm$ 0.0023 m.

Summary of offset values as determined from the different techniques

(1) Standard Value (JPL Progress Report 42-49) 6706 mm

(2) Conventional surveying 1993: Mark Newling 6695 $\pm$ 3mm

(3) VLBI 1995: Chopo Ma 6693.6 $\pm$ 2.5mm

(4) VLBI 1995: Marshall Eubanks 6692.5 $\pm$ 1.5 mm

(5) HartRAO GPS solution 1995: 6695.6 $\pm$ 2.3 mm

(6) VLBI 1996: Chopo Ma 6688.8 ± 1.8 mm

With the exception of the standard value and Chopo Ma's 1996 estimation, all other solutions are within the errors of the GPS solution. Using GPS, the data required for a solution can be sampled in three days. The VLBI data was collected over several years and involves many VLBI stations in cross-continental networks.

7.6 Summary

Preliminary DEC and HA circle parameters were found using data set 1. Only a subset consisting of the outermost points of the arcs were useful in the solutions. Using a tensioned cubic spline fit and Bézier curve a reasonable offset value was determined. The sigma and standard errors are however unreliable as the estimated points on the fitted curves are not independent.

Consequently the experiment was redesigned to yield data set 2, which gave reliable and accurate estimates of the antenna axis offset and VLBI reference point. The solutions using data set 2 included pointing corrections for the antenna. An implicit thermal model helped in reducing the errors. No evidence of structural sagging or deformation was found in the data. A final antenna axis offset of 6.6956 ± 0.0023 m was found which compares favourably with other independent determinations.

The relative distance between the VLBI and SLR pad reference points agree reasonably well between ITRF93 and the distance determined using GPS. It is suggested that this local tie be used as a constraint in the terrestrial reference frame.

Chapter 8

Conclusions

8.1 Introduction

In order to achieve millimetre precision in geodetic VLBI, parameters such as the axis offset must be known to a high degree of accuracy. It has a direct impact on the VLBI delay model by influencing the dry tropospheric and geometric delay. With GPS as a measurement tool, it was found to be a practical way to determine this offset in a reasonably short space of time, with the measurements having a fair degree of accuracy. In order to use the GPS data, the proper method for the determination of the circle centres and other parameters must be used. It has been demonstrated that GPS is a viable measurement tool even when a receiver(s) is used in close proximity to a large metal structure. This allows several other experiments to be considered.

8.2 GPS as a Measuring Method

The GPS system is suitable for a multitude of Earth science and other applications and highly accurate measurements can be made on scales ranging from very local to global using the carrier phase observable. Several errors are reduced and eliminated by the process of differencing and for the work presented here, single frequency (L1) carrier phase receivers are adequate.

The accuracy obtained by GPS using a standard commercial post-processing package was found to be adequate. Smaller deviations and standard errors of the mean might be achievable if the duration of receiver occupation at the points on the circle arcs were to be increased. An improvement will also follow if the density of the point distribution were accordingly increased. This will necessitate a considerable increase in the telescope time required. The time allocated to this project and the resultant data collected is probably the minimum practical to obtain reasonable

results.

The design and construction of a gimbal for the GPS antenna to keep it level and minimise antenna phase centre position variation is an absolute necessity. Without the gimbal, the errors would have been much larger due to phase centre variation and multipathing.

8.3 Offset Determination

Of the three approaches to find circle centres as discussed, i.e. analytical geometry, matrices and least-squares, the circle centre finding algorithm which proved to be the most suitable for this work was the spatial intersection of two co-planar lines as described in section 5.2. The data sampling and experimental method could be optimised for this method. This method requires only three data points for a single solution and is very robust. It is clear that least-squares is not a suitable method for determining the circle centre of data describing less than a semi-circle, but it can be used once the centre has been determined to calculate the residuals between a theoretical circle and the GPS data.

8.4 Software Development

The graphical interface of the software used for the solutions greatly enhanced the understanding and mental visualisation of the problems involved. It is not always easy to visualise problems in three dimensions, therefore having the ability to perform various transformations, scaling, translations and viewpoint (eye) operations on the data proved to be very useful.

8.5 Experimental Method

The use of a tensioned cubic spline fit and Bézier curve on data set 1 indicates some use for non-optimsed data as a reasonable offset value was determined. The sigma and standard errors are however unreliable as the estimated points on the fitted curves are not independent. The redesigned experiment resulting in data set 2, is the better approach and reliable estimates of the antenna axis offset and VLBI reference point were found. The inclusion of pointing corrections for the antenna and an implicit thermal model is necessary to reduce errors.

8.6 Impact of Results

This work demonstrates an independent method of determining the antenna axis offset and VLBI reference point. These values compare favourably with those found using other techniques as discussed. It thus enhances the credibility of the values used when solving for station position and baseline length. The method is not very time consuming, and the axis offset for any other telescope could be determined in a period of about three to four days. Radio telescopes which use either the VLBI determined offset, or the engineering specification, would be well advised to have an independent determination as verification, using GPS. This value should be used as a fixed parameter in the VLBI solutions.

This method does however have the distinct advantage that as in our case, having an SLR reference point available, which has been visited by both GPS and SLR, the three reference frames, VLBI, SLR and GPS can be tied to the same point.

8.7 Future Work

8.7.1 Polar Axis Alignment

The Polar axis can be measured by the same methods as described in this work. Several points of rotation in the axis can be found and when joined, will provide a description of the orientation and behaviour of the axis. Misalignment of the axis is present in all polar axes and GPS can be used to obtain another independent estimate of this value.

8.7.2 Sphere Mapping

Were a GPS receiver to be permanently installed on the telescope, plus one or two other receivers elsewhere on site, an accurate error map of the pointing behaviour of the telescope could be made. The data would eventually describe a spherical surface map resulting from the movement of the GPS antenna. This could be used to develop a dynamic pointing error map. It would also allow a very accurate determination of the behaviour of the structure due to thermal expansion. The errors in the determination of the axis offset and VLBI reference point would also be reduced due to the larger sample of points.

8.7.3 Maintenance of Reference Systems Tie

This measurement should be monitored on a regular basis to maintain the tie between the three reference frames. Verification of the offset values and implementation of possible improvements would be worthwhile.

8.8 Recommendations

Resulting from the final solutions The offset value of 6.6956 m should be used as a fixed parameter in the VLBI solutions. The ΔX, ΔY and ΔZ values which describe the relative distance between the VLBI and SLR reference point should be used as a constraint in the IERS solutions. The local tie can be done very accurately.

On equipment The lack of GPS equipment at HartRAO necessitated the use of borrowed equipment for this work. To operate fully as a national facility, with specific reference to its responsibility of providing a national reference point, it is necessary that HartRAO purchase at least one dual frequency GPS receiver, preferably three, in order to do its own local surveying and provide reference data to the IGS and local users.

Chapter 9

References

Anderson, D.A. 1981. The Circular Structural Model. *J.R. Statist. Soc.* B. **43**, 2, 131-141.

Ammeraal, L. 1988. *Interactive 3D Computer Graphics.* John Wiley & Sons. Chichester. UK.

Angel, I. and Barber, J. 1977. An Algorithm for Fitting Circles and Ellipses to Megalithic Stone Rings. *Science and Archaelogy*, **20**, 11-16.

Apostol, T.M. 1957. *Mathematical Analysis.* Addison-Wesley Publishing Company. USA.

ARINC Research Corporation, 1991. *GPS Navstar User's Overview.* Public Release Document YEE-82-009D, prepared for the Program Director, Navstar Global Positioning System, Joint Program Office, Los Angeles, California. USA.

Berman, M. and Culpin, D. 1986. The Statistical Behaviour of Some Least-Squares Estimators of the Centre and Radius of a Circle. *J.R. Statist. Soc. B.* **48**, 2, 183-196.

Bevington, P.R. 1969. *Data Reduction and Error Analysis for the Physical Sciences.* McGraw-Hill Book Company. New York. USA.

Bielig-Schulz, G. and Schulz, C. 1990. *3D Graphics in Pascal.* John Wiley & Sons, Inc. New York. USA.

Briggs, W and Bryan, G.H. 1910. *The Right Line & Circle (Coordinate Geometry).* 3rd edition. University Tutorial Press. London.

Blewitt, G. 1993. Advances in Global Positioning System technology for Geodynamics Investigation: 1978-1992, in *Contributions of Space Geodesy to Geodynamics.* eds. Smith, D.E and Turcotte, D. L. Geodynamics Series. Vol.25. American Geophysical Union. Washington, D.C. USA.

Blewitt, G. and Lichten, S.M. 1992. GPS Carrier Phase Ambiguity Resolution up to 12000 km: Results from the GIG'91 Experiment, in *Proceedings of the Sixth International Geodetic Symposium on Satellite Positioning*, Ohio State University, Columbus, Ohio, USA.

Blinchikoff, H.J. and Zverev, A.I. 1976. *Filtering in the Time and Frequency Domains.* John Wiley & Sons, Inc. New York. USA.

Blomenhofer, H., Hein, G.W. and Walsh, D. 1993. On-The-Fly Carrier Phase Ambiguity Resolution for Precise Aircraft landing, in *Proceedings of the Institute of Navigation GPS-93 Vol II*, Sixth International Technical Meeting of the Satellite Division of the Institute of Navigation, Salt Lake City, Utah.

Bosworth, J.M., Coates, R.J. and Fischetti, T.L. 1993. The Development of NASA's Crustal Dynamics Project, in *Contributions of Space Geodesy to Geodynamics.* eds. Smith, D.E and Turcotte, D. L. Geodynamics Series. Vol.25. American Geophysical Union. Washington, D.C. USA.

Boucher, C. and Altamimi, Z. 1993. Development of a Conventional Terrestrial Reference Frame, in *Contributions of Space Geodesy to Geodynamics.* eds. Smith, D.E and Turcotte, D. L. Geodynamics Series. Vol.24. American Geophysical Union. Washington, D.C. USA.

Bu-qing, S and Ding-yuan, L. 1989. *Computational Geometry. Curve and Surface Modelling.* Academic Press, inc. New York. USA.

Chan, N.G. 1965. On Circular Functional Relationships. *J.R. Statist.Soc.* B, **27**, 45-46.

Chen, D. 1993. Fast Ambiguity Search Filter (FASF): A Novel Concept for GPS Ambiguity Resolution, in *Proceedings of the Institute of Navigation GPS-93 Vol I*, Sixth International Technical Meeting of the Satellite Division of the Institute of Navigation, Salt Lake City, Utah.

Conte, S.D. and de Boor, C. 1972. *Elementary Numerical Analysis, an Algorithmic Approach.* McGraw-Hill Kogakusha, Ltd. Tokyo.

Corey, B.E. and Clark, T.A. 1991. The Rf Bandwidth Upgrade: Doubling the X-Band Spanned Bandwidth of Geodetic VLBI Receiving Systems, in *Proceedings of the AGU Chapman Conference on Geodetic VLBI:Monitoring Global Change.* NOAA Tech. Rep. NOS 137 NGS 49. U.S. Department of Commerce, Rockville, Maryland, USA.

Daly, P. 1993. Navstar GPS and GLONASS: Global Satellite Navigation Systems. *Electronics and Communication Engineering Journal.* December 1993. 349-357.

Dennis, J.E, Gay, D.M and Welsch, R.E. 1981. An Adaptive Nonlinear Least-Squares Algorithm. *ACM Transactions on Mathematical Software*, **7**, 3, 348-368.

Dennis, J.E, Gay, D.M and Welsch, R.E. 1981. Algorithm 573 NL2SOL - An Adaptive Nonlinear Least-Squares Algorithm [E4]. *ACM Transactions on Mathematical Software*, **7**, 3, 369-383.

Draper, N.R and Smith, H. 1966. *Applied Regression Analysis.* John Wiley & Sons. USA.

Edwards, J. 1903. *Differential Calculus for Beginners.* MacMillan & Co. London. UK.

Farin, G. 1988. *Curves and Surfaces for Computer Aided Geometric Design.* Academic Press, inc. New York. USA.

Felli, M. and Spencer, R.E. eds. 1989. *Very Long Baseline Interferometry. Techniques and Applications.* Kluwer Academic Publishers. Dordrecht. The Netherlands.

Fisher, N.I., Lewis, T. and Embleton, B.J.J. 1987. *Statistical Analysis of Spherical Data.* Cambridge University Press. Cambridge. UK.

Fu, X. 1992. Investigations of Multipath Carrier Phase Effects in GPS Hydrographic Applications, in *Proceedings of the Institute of Navigation GPS-92*, Fifth International Technical Meeting of the Satellite Division of the Institute of Navigation, Albuquerque, New Mexico.

Foley, J.D. and van Dam, A. 1984. *Fundamentals of Interactive Computer Graphics.* Addison-Wesley Publishing Company. USA.

Frodge, S.L., Shannon., Remondi, B.W., Lapucha, D. and Barker, R. 1993. Results of Real-Time tesing of GPS Carrier Phase Ambiguity resolution On-The-Fly, in *Proceedings of the Institue of Navigation GPS-93 Vol I*, Sixth International Technical Meeting of the Satellite Division of the Institute of Navigation, Salt Lake City, Utah.

Gasson, P.C. 1983. *Geometry of Spatial Forms.* John Wiley & Sons. U.S.A.

Gates, J. 1993. Testing for Circularity of Spatially Located Objects. *J. Appl.Stat.*, **20**, 1, 95-103.

Gates, J. 1994. Distance Mean and Variance Functions and Sphere Fitting. *Statistics*, **25**, 251-266.

Giloi, W. K. 1978. *Interactive Computer Graphics. Data Structures, Algorithms, Languages.* Prentice-Hall, Inc. New Jersey. USA.

Gold, T. 1967. Radio Method for the Precise Measurement of the Rotation of the Earth. *Science,* **157**, 302-304.

Gordon, D and Ryan, J. 1994. Calc 8.1 Release Document. Unpublished document released to the VLBI community.

Haines, E. 1989. Essential Ray Tracing Algorithms, in *An Introduction to Ray Tracing*, ed. A.S. Glassner. Academic Press. London. UK.

Herring, T., Clark, T. and Rogers, A. 1991. Very Long Baseline Interferometry (VLBI) in *Solid Earth Science in the 1990s.* Vol. 3-Measurement Techniques and Technology. NASA Tech. Memo. 4256, Vol. 3. NASA Office of Space Science and Applications. Washington, D.C. USA.

Hofmann-Wellenhof, B., Lichtenegger, H, and Collins, J. 1993. *Global Positioning System.* Theory and Practice. Springer-Verlag. Wien.

Kåsa, I. 1976. A Circle Fitting Procedure and its Error Analysis. *IEEE Trans. Instrumentation and Measurement*, **25**, 8-14.

Kolaczek, B. 1989. Earth Rotation Monitoring, in *Reference Frames in Astronomy and Geophysics.* (eds. Kovalesky, J., Mueller, I.I and Kolaczek, B.) Kluwer Academic Publishers. London.

Kreyszig, E. 1988. *Advanced Engineering Mathematics.* John Wiley & Sons, Inc. USA.

Lambeck, K. 1988. *Geophysical Geodesy. The Slow Deformations of the Earth.* Clarendon Press. Oxford. UK.

Leick, A. 1990. *GPS Satellite Surveying.* John Wiley & Sons. New York. USA.

Ma, C. 1978. Very Long baseline Interferometry Applied to Polar Motion, Relativity and Geodesy. *NASA Tech. Memo*, **79582**, Goddard Space Flight Center. USA.

Ma, C. 1989. Extragalactic Reference Frames, in *Reference Frames in Astronomy and Geophysics.* (eds. Kovalesky, J., Mueller, I.I and Kolaczek, B.) Kluwer Academic Publishers. London.

Ma, C., Ryan, J.W. and Caprette, D.S. 1992. Crustal Dynamics Project Data Analysis–1991. VLBI Geodetic Results. *NASA Tech. Memo*, **104552**, Goddard Space Flight Center. USA.

Ma, C., Ryan, J.W., Gordon, D., Caprette, D.S. and Himwich, W.E. 1993. Reference Frames from CDP VLBI Data, in *Contributions of Space Geodesy to Geodynamics.* eds. Smith, D.E and Turcotte, D. L. Geodynamics Series. Vol. 24. American Geophysical Union. Washington, D.C. USA.

Mardia, K.V. 1972. *Statistics of Directional Data.* Academic Press. London. UK.

Meyer, S. L. 1992. *Data Analysis for Scientists and Engineers.* John Wiley & Sons, Inc. USA.

Mc Carthy, D.D. 1993. The Use of Crustal Dynamics Project Data to Predict the Orientation of the Earth, in *Contributions of Space Geodesy to Geodynamics.* eds. Smith, D.E and Turcotte, D. L. Geodynamics Series. Vol. 24. American Geophysical Union. Washington, D.C. USA.

Mueller, I.I. 1989. Conventional Terrestrial Reference Frames, in *Reference Frames in Astronomy and Geophysics.* (eds. Kovalesky, J., Mueller, I.I and Kolaczek, B.) Kluwer Academic Publishers. London.

NASA Technical Paper 2147. 1983. *The NASA Geodynamics Program: An Overview.* Scientific and Technical Information Branch. Office of Space Science and Aplications. NASA. Washington. USA.

NATO 1991. *NAVSTAR GPS User Equipment.* Public release version of NATO Document ANP2. NAVSTAR-GPS Joint Program Office. Los Angeles Air Force Base, California. USA.

Nolan, J.M., Webster, I.R., Gourevitch, S.A. and Ladd, J.W. 1993. Rapid Static Surveying with an Operational GPS System, in *Proceedings of the Institute of Navigation GPS-93 Vol II*, Sixth International Technical Meeting of the Satellite Division of the Institute of Navigation, Salt Lake City, Utah.

Oren, S.S. 1973. Self-Scaling Variable Metric Algorithms without Line Search for Unconstrained Minimization. Math. Comput., 27, 873-885.

Parkinson, B.W. and Gilbert, S.W. 1983. NAVSTAR:Global Positioning System-Ten Years Later. *Proceedings of the IEEE*, **71**, 10, 1177-1186.

Pipes, L.A. 1946. *Applied Mathematics for Engineers and Physicists.* McGraw-Hill Book Company, Inc. new York. USA.

Press, W.H., Flannery, B.P., Teukolsky, S.A. and Vetterling, W.T. 1989. *Numerical Recipes in Pascal.* Cambridge University Press. Cambridge.

Raby, P and Daly, P. 1993. Using the GLONASS System for Geodetic Survey, in *Proceedings of the Institute of Navigation GPS-93 Vol II*, Sixth International Technical Meeting of the Satellite Division of the Institute of Navigation, Salt Lake City, Utah.

Ratkowsky, D.A. 1989. *Handbook of Nonlinear Regression Models.* Marcel Dekker, Inc. New York. U.S.A.

Reinhardt, V.S. and Rueger, L.J. 1980. The Performance of NASA Research Hydrogen Masers, in *Radio Interferometry Techniques for Geodesy.* NASA Conference Publication 2115. Scientific and Technical Information Office. NASA, USA.

Roy, A.E. 1982. *Orbital Motion.* Adam Hilger Ltd. Bristol, UK.

Rogers, A.E., Cappallo, R.J., Corey, B.E., Hinteregger, H.F. et al. 1993. Improvements in the Accuracy of Geodetic VLBI, in *Contributions of Space Geodesy to Geodynamics.* eds. Smith, D.E and Turcotte, D. L. Geodynamics Series. Vol.25. American Geophysical Union. Washington, D.C. USA.

Ryan, J.W., Clark, T.A., Ma.C., Gordon, D., Caprette, D.S., and Himwich, W.E. 1993. Global Scale Tectonic Plate Motions Measured with CDP VLBI Data, in *Contributions of Space Geodesy to Geodynamics.* eds. Smith, D.E and Turcotte, D. L. Geodynamics Series. Vol. 23. American Geophysical Union. Washington, D.C. USA.

Sherrod, P.H. 1991. NLREG version 3.0. *Nonlinear Regression Analysis Program.* Unpublished software documentation.

Sokolnikoff, I. S. 1939. *Advanced Calculus.* McGraw-Hill Book Company, Inc. New York and London.

STANAG 4294. 1990. NAVSTAR Global Positioning System (GPS) System Characteristics, Preliminary Draft. NATO Unclassified Document. Prepared by ARINC Research Corporation for the Joint Program Office, Headquarters Space System Division (AFSC), Los Angeles Air Force Base.

Sovers, O.J. and Jacobs, C.S. 1994. Observation Model and Parameter Partials for the JPL VLBI Parameter Estimation Software "MODEST"-1994. *JPL Publication 83-39,* Rev. 5. NASA. USA.

Stein, S. 1993. Space Geodesy and Plate Motions, in *Contributions of Space Geodesy to Geodynamics.* eds. Smith, D.E and Turcotte, D. L. Geodynamics Series. Vol.23. American Geophysical Union. Washington, D.C. USA.

Sydnor, R.L. 1983. Frequency Standards for VLBI, Present and Future, in *Very Long Baseline Interferometry Techniques.* Conference proceedings, Centre National d'Etudes Spatiales. Toulouse. France.

Vessot, R.F.C. 1980. Hydrogen MASER Frequency Standard, in *Radio Interferometry Techniques for Geodesy.* NASA Conference Publication 2115. Scientific and Technical Information Office. NASA, USA.

Thompson, A.R., Moran, J.M. and Swenson, G.W. 1986. *Interferometry and Synthesis in Radio Astronomy.* John Wiley. New York. USA.

Wade, C.M. 1970. Precise Positions of Radio Sources. *Astrophys. J.,* **162**, 381-390.

Walter, H.G. 1983. Very Long Baseline Interferometry Applied to Fundamental Astrometry, in *Very Long Baseline Interferometry Techniques.* Conference proceedings, Centre National d'Etudes Spatiales. Toulouse. France.

Whitney, A.R. 1988. The Mark IIIA Correlator System, in *The Impact of VLBI on Astrophysics and Geophysics.* IAU Symposium No. 129. eds. Reid, M.J. and Moran, J.M. Kluwer Academic Publishers. Dordrecht. The Netherlands.

Appendix A

Additional Clarification of Certain Concepts

Introduction This appendix has been included to allow additional clarification of certain concepts if required. It is structured to follow the reasoning in the main text from where reference to it is made and has not been structured to be read as a separate chapter. Each section therefore does not necessarily follow on from the previous. A list of the topics discussed is included in the contents (page viii).

A.1 Absolute position of a data point

An individual data point is referred to by the description $P_i(x, y, z)$ and the points $P_i(xy)$, $P_i(yz)$, $P_i(zx)$ are the orthogonal projections of the points on the xoy, yoz, zox reference planes.

A.2 Direction ratios of a line

Given two points on a straight line $P_1(x, y, z)$ and $P_2(x, y, z)$ then $(x_2 - x_1) : (y_2 - y_1) : (z_2 - z_1)$ are the direction ratios. The convention adopted therefore is $(x : y : z)$ for direction ratios and (x, y, z) for coordinates spaced by a colon and comma respectively. The inclination of a straight line is the same throughout its length and therefore the inclination can be defined by any two points on the line.

A.3 Direction cosines

Following Gasson 1983, if a point P with origin O creates a line OP and the true angle between the line OP and the axis ox is α, the true angles between the line OP and the axes oy and oz are β and γ respectively, then $\cos\alpha$, $\cos\beta$, $\cos\gamma$ are the direction cosines of the line OP. Common notation for direction cosines are l,m,n,

where

$$l = cos\alpha, m = cos\beta, n = cos\gamma.$$

If e is the length of the line OP and $(a : b : c)$ are the direction ratios then

$$l = \frac{a}{e}, m = \frac{b}{e}, n = \frac{c}{e}.$$

A convenient means of checking the validity of direction cosine data is by using the identity

$$l^2 + m^2 + n^2 = 1$$

which can be derived by squaring and adding the three direction cosines

$$\cos^2\alpha + \cos^2\beta + \cos^2\gamma = \frac{a^2 + b^2 + c^2}{e^2}$$

As

$$e^2 = a^2 + b^2 + c^2,$$

it follows that

$$\cos^2\alpha + \cos^2\beta + \cos^2\gamma = 1.$$

A.4 True angle between two intersecting straight lines

With reference to figure 5.1, and applying the cosine rule, we have

$$\cos\theta = \frac{d_3^2 + d_1^2 - d_2^2}{2d_3d_1}$$

Using the coordinates of the lines

$$d_1, d_2, d_3,$$

it follows that

$$\begin{aligned}\cos\theta \;=\; & \frac{1}{2d_3d_1}[(x_3 - x_1)^2 + (y_3 - y_1)^2 + (z_3 - z_1)^2 + (x_2 - x_1)^2 + (y_2 - y_1)^2 \\ & + (z_2 - z_1)^2 - (x_3 - x_2)^2 - (y_3 - y_2)^2 - (z_3 - z_1)^2].\end{aligned}$$

Expanding the above equation for $\cos\theta$ leads to

$$\cos\theta = \frac{1}{2d_3d_1}[2(x_1^2 - x_1x_3 - x_1x_2 + x_2x_3) + 2(y_1^2 - y_1y_3 - y_1y_2 + y_2y_3) + 2(z_1^2 - z_1z_3 - z_1z_2 + z_2z_3)]$$

and

$$\frac{(x_2 - x_1)}{d_1}\frac{(x_3 - x_1)}{d_3} + \frac{(y_2 - y_1)}{d_1}\frac{(y_3 - y_1)}{d_3} + \frac{(z_2 - z_1)}{d_1}\frac{(z_3 - z_1)}{d_3}.$$

Furthermore

$$\frac{(x_2 - x_1)}{d_1} = l_3, \frac{(y_2 - y_1)}{d_1} = m_3, \frac{(z_2 - z_1)}{d_1} = n_3,$$

and

$$\frac{(x_3 - x_1)}{d_3} = l_2, \frac{(y_3 - y_1)}{d_3} = m_2, \frac{(z_3 - z_1}{d_3)} = n_2,$$

therefore

$$\cos\theta = l_2 l_3 + m_2 m_3 + n_2 n_3.$$

If one defines the lines d_1 and d_3 in terms of the notation introduced in sections 2 and 3 of this appendix then line d_1 has direction ratios $(a_1 : b_1 : c_1)$ and line d_3 has direction ratios $(a_2 : b_2 : c_2)$. The true angle θ between two intersecting lines is then

$$\cos\theta = \frac{a_1 a_2 + b_1 b_2 + c_1 c_2}{(\sqrt{a_1^2 + b_1^2 + c_1^2})(\sqrt{a_2^2 + b_2^2 + c_2^2})}.$$

This is equivalent to equation (5.1).

A.5 Parametric representation of a line

The parametric representation of a line (Foley & van Dam 1984) for a line P_1 to P_2 can be written as:

$$\left.\begin{array}{rcl} x_v & = & (x_2 - x_1) \times kv + x_1, \\ y_v & = & (y_2 - y_1) \times kv + y_1, \\ z_v & = & (z_2 - z_1) \times kv + z_1. \end{array}\right\} 0 \leq kv \leq 1$$

The coordinates of the line at all points on the line is given by the three equations as kv is varied from 0 to 1.

A.6 Great and small circles

A plane passing through the centre of a sphere results in a great circle when it cuts the surface of the sphere. The intersection created when the plane does not pass through the centre of the sphere is a small circle (Roy 1982).

A.7 General form of plane equation

The general equation of a plane can be written as:

$$Ax + By + Cz + D = 0 \tag{9.1}$$

The planes which are perpendicular to the reference planes xoy, xoz, and yoz correspond to the three equations where C=0, B=0 and A=0 respectively.

$$Ax + By + D = 0 \perp xoy \tag{9.2}$$

$$Ax + Cz + D = 0 \perp xoz \tag{9.3}$$

$$By + Cz + D = 0 \perp yoz \tag{9.4}$$

A.8 Vector and inner product of two vectors

Assume that the vector from the circle centre P_9 to P_1 and the vector from the circle centre to P_3 (see figure 5.1 and figure 5.3) are vectors $\boldsymbol{a}$ and $\boldsymbol{b}$ respectively. In order to rotate the points P_1 and P_2 in the plane π_2 defined by P_9, P_1 and P_2, one requires a directed axis $\boldsymbol{v}$ which is perpendicular to plane π_2 and passing through P_9. This vector $\boldsymbol{v}$ is found using the vector product of the vectors $\boldsymbol{a}$ and $\boldsymbol{b}$:

$$\boldsymbol{v} = \boldsymbol{a} \times \boldsymbol{b} \tag{9.5}$$

The angle of intersection α of the two vectors $\boldsymbol{a}$ and $\boldsymbol{b}$ can be found from their inner product

$$\boldsymbol{a} \times \boldsymbol{b} = a \times b \times \cos\alpha \tag{9.6}$$

A.9 Propagation of errors

In the case of measurements in group 1 or group 2 of the HA circle zenith points, the errors are uncorrelated in each group. If for example x and y are independent variables and $z = f(x, y)$, the errors are independent and uncorrelated (Meyer 1992) so that ($S_{xy} = 0$) and

$$S_z = \sqrt{\left(\frac{\partial f}{\partial x}\right)^2 S_x^2 + \left(\frac{\partial f}{\partial y}\right)^2 S_y^2} \tag{9.7}$$

The absolute standard deviations of sums and differences is the sum in quadrature of the absolute standard deviations of the quantities that were measured

$$S_z = \sqrt{S_x^2 + S_y^2} \tag{9.8}$$

A.10 Taylor's expansion

Following discussions by Edwards (1903), Sokolnikoff (1939), Pipes (1946), Apostol (1957), Draper & Smith (1966), Bevington 1969, Kåsa (1976) and Kreyszig (1988), every analytic function $f(x)$ can be represented by power series, the Taylor series of $f(x)$. The power series

$$f(x) = \sum_{n=0}^{\infty} \frac{f^{(n)}(x_0)}{n!}(x - x_0)^n \tag{9.9}$$

where $f^{(n)}(x_0) = \frac{df}{dx}\,|_{x=x_0}$, as generated by f about x_0 is the Taylor's series if $f \epsilon C^{\infty}$, i.e. f has derivatives of every order. The series $\sum a_n(x - x_0)^n$ is a real power series where x, x_0 and a_n $(n = 0, 1, 2, \ldots)$ are real numbers. The *interval of convergence* is where the circle of convergence intersects the real axis. If a real-valued function f is defined in some neighbourhood of a point x_0 in the real line E_1, and f has derivatives of every order in this neighbourhood, the power series as given in equation (9.9) can be formed. To indicate that this series is generated by f, $f(x)$ can be written as

$$f(x) \sim \sum_{n=0}^{\infty} \frac{f^{(n)}(x_0)}{n!}(x - x_0)^n. \tag{9.10}$$

Taylor's theorem can be written as

$$f(x) = f(x_0) + \sum_{k=1}^{n-1} \frac{f^{(k)}(x_0)}{k!}(x - x_0)^k + \frac{f^{(n)}(x_1)}{n!}(x - x_0)^n. \tag{9.11}$$

where f is a function having a finite nth derivative f^n everywhere in the open interval (a, b) and it is assumed that $f^{(n-1)}$ is continuous on the closed interval $[a, b]$. It is further assumed that $x_0 \epsilon [a, b]$ and that for every x in $[a, b]$, $x \neq x_0$, there exists a point x_1 interior to the interval joining x and x_0. The last term is the remainder after n terms (Sokolnikoff 1939) and is an indication of the error in this approximation. The $\sim$ in equation (9.10) can be replaced by $=$, as according to the formula of Taylor, if $f \epsilon C^{\infty}$ on $[a, b]$ and if $x_0 \epsilon [a, b]$, then, for every n and for every x in $[a, b]$ it can be shown that

$$f(x) = \sum_{k=0}^{n-1} \frac{f^{(k)}(x_0)}{k!}(x - x_0)^k + \frac{f^{(n)}(x_1)}{n!}(x - x_0)^n. \tag{9.12}$$

For convergence for any other x besides $x = x_0$, as well as meeting the condition that the sum of the power series be equal to $f(x)$, a necessary condition for the Taylor's series to converge to $f(x)$ can thus be found using Taylor's Theorem. The point x_1 is somewhere between x and x_0 and depends on the last two variables and on n.

For convergence of the Taylor's series to $f(x)$ a necessary and sufficient condition (Apostol 1957) is that

$$f(x) = \lim_{n\to\infty} \frac{f^{(n)}(x_0)}{n!}(x - x_0)^n = 0. \tag{9.13}$$

Equation (9.13) wil hold if the sequence f^n is uniformly bounded on the interval $[a, b]$.

Using a simple composite function $f = f(x, y)$ as example, Taylor's theorem can be expanded to two or more dimensions.

$$f(x,y) = \sum_{k=0}^{n-1} \left(\frac{f^{(k)}(x_0)}{k!}(x - x_0)^k + \frac{f^{(k)}(y_0)}{k!}(y - y_0)^k \right) + \frac{f^{(n)}(x_1)}{n!}(x-x_0)^n + \frac{f^{(n)}(y_1)}{n!}(y-y_0)^n \tag{9.14}$$

where $f_x^n = \frac{\partial^n f}{\partial x^n} \mid_{x=x_0}$ and $f_y^n = \frac{\partial^n f}{\partial y^n} \mid_{y=y_0}$.

Linearising the Equation of a Sphere

Equation (5.36) can be written in its implicit form as

$$(x_i - x_c)^2 + (y_i - y_c)^2 + (z_i - z_c)^2 - s_r^2 = 0 \tag{9.15}$$

The surface of the sphere is expressed as an implicit equation (Haines 1989) and points on the sphere can be tested conditionally by the implicit equation to establish whether a point is on the surface. Equation (9.15) of the sphere can be written as an implicit function where

$$F(x_i, y_i, z_i, x_0, y_0, z_0, R) = 0. \tag{9.16}$$

Taking the above discussion on Taylor's expansion into account, the linearised form of equation (9.15) is then

$$F = F_0 + \frac{\partial F}{\partial x_0}\Delta x + \frac{\partial F}{\partial y_0}\Delta y + \frac{\partial F}{\partial z_0}\Delta z + \frac{\partial F}{\partial R}\Delta R + \frac{\partial F}{\partial x_i}e_{x_i} + \frac{\partial F}{\partial y_i}e_{y_i} + \frac{\partial F}{\partial z_i}e_{z_i} \tag{9.17}$$

where

$$\left.\begin{aligned}
\frac{\partial F}{\partial x_0} &= -2(x_i - x_0) \\
\frac{\partial F}{\partial y_0} &= -2(y_i - y_0) \\
\frac{\partial F}{\partial z_0} &= -2(z_i - z_0) \\
\frac{\partial F}{\partial x_i} &= 2(x_i - x_0) \\
\frac{\partial F}{\partial y_i} &= 2(y_i - y_0) \\
\frac{\partial F}{\partial z_i} &= 2(z_i - z_0) \\
\frac{\partial F}{\partial R} &= -2R
\end{aligned}\right\} \tag{9.18}$$

and e_i is the residual.

A.11 The von Mises Distribution

A circular random variable θ has a von Mises distribution if its p.d.f. is given by (Mardia 1972, Fisher et. al., 1987)

$$f(\theta) = C \exp[\kappa \cos(\theta - \alpha)], \quad 0 \leq \theta < 2\pi. \tag{9.19}$$

Where α is the mean direction, it serves as a location parameter, the distribution having a mode at α and symmetry about the direction α. The constant C equals $1/[2\pi I_0(\kappa)]$, where $I_0(\kappa)$ is the modified Bessel function of the first kind and order zero, so that

$$I_0(\kappa) = \sum_{r=0}^{\infty} \frac{1}{r!^2} (\frac{1}{2}\kappa)^{2r}. \tag{9.20}$$

The distribution around α increases with an increase in the concentration parameter κ.

A.12 Conventional Terrestrial Reference System (CTRS)

The terrestrial Cartesian coordinate system is "Earth-fixed" and thus has its origin at the centre of the Earth. The u axis is oriented towards the Greenwich Mean Astronomic Meridian of zero longitude, the w axis is oriented towards the Conventional Terrestrial Pole (CTP) and the v axis is perpendicular to both and forms a right-handed coordinate system (Mueller 1989). The theory of precession and nutation defines the motion of the true celestial pole, and this polar motion defines

the Celestial Ephemeris Pole (CEP). The CTP is usually selected to be near the average position of the CEP taken over a certain time interval. The high accuracy achieved by space geodetic techniques such as VLBI, has led to a CTRS definition in a relativistic framework (Boucher and Altamimi 1993).

A.13 Least-Squares and Circle Centre Determination

Although it might not be readily be apparent from the main text, considerable effort went into trying to make least-squares "work" in order to solve the circle centres and radii of the DEC and HA circles. This effort is not documented here, but it is felt that the reader should benefit from my and others attempts, lest he walks into this area with eyes closed. A short review of several contributions is made to indicate the different approaches and the type of problems encountered. Most contributions to the literature utilise either one of two basic models. The models and notation are described first to present a unified approach.

Notation The term M is assigned to indicate the value which is being minimised. The radius and centre of a circle is denoted by ρ and (ξ, η) respectively. The data points (x_i, y_i) range from $i = 1, \ldots, n$. When the radius is used in a minimising function or functional model the radius is denoted by r so that for the two-dimensional case $r_i = \sqrt{(x_i - \xi)^2 + (y_i - \eta)^2}$ and $\overline{r} = \sum r_i / n$. Assume that $\theta_1, \ldots, \theta_n$ is a sample of size n from a circular population. The angles $\theta_1, \ldots, \theta_n$ are measured from the x-axis in the anti-clockwise direction. The θ_i can be either fixed or random. If θ has a uniform distribution (no concentration about any particular direction) over the half-closed interval $(0, 2\pi]$ then the notation $\theta \sim Uniform(0, 2\pi]$ is used. The use of τ_i is basically analogous to θi, but denotes a direction and not an angle. T is sometimes used to denote the polar angle in radians. Model definitions follow those of Berman & Culpin (1986).

Radial Model This model is defined as

$$\left.\begin{aligned} x_i &= \xi + r_i \cos \tau_i, \\ y_i &= \eta + r_i \sin \tau_i, \end{aligned}\right\} \tag{9.21}$$

$i = 1, \ldots, n$ is a set of independent, identically distributed random variables, which are independent of $\tau_1, \ldots, \tau_n$. The r_i are independent, identically distributed random variables with mean $\overline{r}$, independent of all τ_i.

Cartesian Model This model is

$$\left.\begin{aligned} x_i &= \xi + \rho\cos\theta_i + \omega_i\cos\phi_i, \\ y_i &= \eta + \rho\sin\theta_i + \omega_i\sin\phi_i, \end{aligned}\right\} \tag{9.22}$$

where $\omega_1,\ldots,\omega_n$ and $\phi_1,\ldots,\phi_n$ are assumed to be mutually independent sets of identically distributed random variables, independent of $\theta_1,\ldots,\theta_n$. The direction $\phi_i \sim Uniform(0,2\pi)$. The disturbance on the data point is described by its size ω_i and direction ϕ_i. When the θ_i are fixed, but unknown angles, the model is the *Cartesian functional model.* If the θ_i are independent and identically distributed, the *Cartesian structural model* is implied. When ω_i^2/σ^2 has a chi-squared distribution with two degrees of freedom, the *(Cartesian) Gaussian model* results.

Chan (1965) Problems encountered in the consistency of the parameters of a circular functional relationship are discussed. The Cartesian functional model is examined. Minimisation with respect to (ξ,η) is reduced to

$$\sum(\rho_i - \overline{r})^2 = M. \tag{9.23}$$

A necessary and sufficient condition for the unique solution of $(\hat{\xi},\hat{\eta})$ to be consistent is that both $(1/n)\sum\cos\theta_i$ and $(1/n)\sum\sin\theta_i$ tend to zero as $n\to\infty$. This indicates that only observations which are distributed symmetrically on the circumference of the circle will lead to proper estimation of the centre.

Kåsa (1976) Using a modified least-square criterion

$$\sum_{i=1}^{n}(r_i^2 - r^2)^2 = M \tag{9.24}$$

which is easier to manage analytically than equation (9.23) an efficient circle fitting procedure was developed using the parameter linearisation (see Appendix A.10) method. Investigation of the data point distribution and a random-error analysis showed that the error decreased with an increase in the number of data points and increased when data points were crowded around two points instead of being placed over the interval $(0,2\pi]$.

Angel and Barber (1977) An algorithm for fitting circles and ellipses was developed which does not require an initial guess at the values of the parameters. They minimise the value of M, a measure of goodness of fit for a function $F(x,y)$ to a set of points where

$$M = \sum_{i=1}^{n} F^2(x_i,y_i) - \frac{1}{n}\left(\sum_{i=1}^{n} F(x_i,y_i)\right)^2. \tag{9.25}$$

If the data points (x_i, y_i) were to lie on the curve $F(x, y) = 0$ then the value of M would be zero. An important conclusion was made; circle fitting should never be used on any arc of a circle less than a semi-circle as the error factors will be of the same order of magnitude for a large range of radii values.

Anderson (1981) A Gausssian circular structural model is discussed and the difficulties of dealing with this model in practice is mentioned. A detailed analysis of maximum likelihood estimation of the parameters is given. If it is assumed that the τ_i's are independent and identically distributed random variables with their distribution function $G(\tau)$ being unknown, and $\Theta = (\xi, \eta, \rho, \sigma^2)$ is the vector of structural parameters for a circle where $T = (0, 2\pi]$, then for at least three data points, Θ and G can be uniquely found. This can be done either from the joint distribution of (x, y), or from their joint characteristic function.

Several problems are mentioned which might be encountered in the functional model. If the maximum likelihood estimator of Θ and G is to be found, most procedures require the maximisation of the likelihood over the function space which contains all possible G's. This is not feasible unless severe restriction is placed on the function space. Simulation studies show that when the support of τ_i are less than a semi-circle, i.e. $\tau_i < (0, \pi]$, the resultant estimators are unstable. This is especially true when the number of observations are small. The estimators seem to perform well only when τ_i are fairly evenly distributed over the complete circle circumference.

Berman & Culpin (1986) The statistical behaviour of some least-squares estimators for two models with theoretical emphasis on the asymptotic biases, variances and covariances is examined. Here $R_i(u, v)$ is the distance from the point (u, v) to the data point (x_i, y_i), so that

$$R_i(u, v) = \sqrt{(x_i - u)^2 + (y_i - v)^2}. \tag{9.26}$$

The sum of the squares of the distances as measured by a metric on the non-negative real line $\mu(s, t)$ with lower and upper bound s and t, from the data points to the circumference of the circle with radius r and centre (u, v) is defined as

$$S(u, v, r) = \sum_{i=1}^{n} [\mu\{R_i(u, v), r\}]^2. \tag{9.27}$$

A least-squares estimator is defined as $(\hat{\xi}, \hat{\eta}, \hat{\rho})$ of (ξ, η, ρ) to be that value of (u, v, r) which minimises $S(u, v, r)$, so that

$$S(\hat{\xi}, \hat{\eta}, \hat{\rho}) = \min S(u, v, r). \tag{9.28}$$

The estimators based on the metric of the form

$$\mu\{s, t\} = \mid s^m - t^m \mid \tag{9.29}$$

are denoted by $\hat{\xi}_m, \hat{\eta}_m$ and $\hat{\rho}_m$ and are called *LSm estimators*. These are obtained by minimising

$$S^*(u, v) = \sum_{i=1}^{n} \{R_i(u, v)^m - \overline{R^m}(u, v)\}^2 \tag{9.30}$$

with respect to (u, v) where $\overline{R^m}(u, v) = n^{-1} \sum R_i(u, v)^m$ and $\hat{\rho}_m = \{\overline{R^m}(\hat{\xi}_m, \hat{\eta}_m)\}^{1/m}$.

Several difficulties are found with $LS1$ estimation. For some data sets $S^*(u, v)$ has several local minima, while others have no minimum, but have a stationary point. However, a unique solution at the minimum of $S^*(u, v)$ was found using $LS1$ when the data were close to the circumference of the circle and sufficiently distributed around it. Their conclusion was that as there may be one or more zero derivatives of $S^*(u, v)$, which may not be at a minimum, $LS1$ estimation is not a trouble-free method for obtaining estimators. $LS1$ estimators do however have smaller biases than their $LS2$ counterparts in large samples when the errors are not too large. In the case of $LS2$ when equating the derivatives of $S^*(u, v)$ to zero, the minimum of $S^*(u, v)$ is found to be an unique explicit solution. $LS2$ estimators were found to have more stable numerical properties than $LS1$.

The asymptotic bias of $(\hat{\xi}_2, \hat{\eta}_2)$ and the mean of $\hat{\rho}_2$ were examined for special cases of the two models, where the angular distribution did not cover only the total circumference of the circle, but also less than $\tau \sim Uniform(0, 2\pi]$. The von Mises (see Appendix A.11) distribution is used to specify the distributions for the angles θ and τ. The Gaussian model has a von Mises distribution denoted by $VM(\theta_0, \kappa)$, where θ_0 is the mean direction and κ the concentration parameter. It is clearly shown that for the Cartesian model, the asymptotic bias of the $LS2$ estimator of (ξ, η) is an increasing function of κ, whereas the asymptotic mean of $\hat{\rho}_2$ is a decreasing function of κ.

Gates (1993) The Monte Carlo method is used to ascertain whether a sample of spatially located objects show evidence of being circularly arranged. The maximum likelihood approach is used to fit the circle and a log-likelihood ratio is used as a

test statistic and measure of circularity. The likelihood surface shows several local maxima in addition to saddle-points which create problems when fitting a circle. Fitting the centre in this case requires minimisation of

$$V(\xi,\eta) = \sum(d_i - \overline{d})^2. \tag{9.31}$$

where d_i is the distance from P_i to (ξ,η).

Gates (1994) Further to his 1993 publication it is shown again that least-squares may be an inconsistent method when used to estimate the centre of a circle. Two examples are described where the minimum of the variation function exhibit asymptotic bias.

A.14 NLREG

Using the same notation as Dennis et al (1981), the nonlinear least-squares problem can be written as a least-squares criterion function

$$minf(x) = \frac{1}{2}R(x)^T R(x) = \frac{1}{2}\sum_{i=1}^{n} r_i(x)^2 \tag{9.32}$$

where $R : \mathcal{R}^p \rightarrow \mathcal{R}^n$ is given, n represents the data and p the parameters. The gradient of f is

$$\nabla f(x) = J(x)^T R(x) \tag{9.33}$$

if $J(x) = R'(x) = (\partial_j r_i(x))$. The Hessian[1] of f is defined as

$$\nabla^2 f(x) = J(x)^T J(x) + \sum_{i=1}^{n} r_i(x)\nabla^2 r_i(x). \tag{9.34}$$

Dennis et al (1989) suggested a way to augment the Gauss-Newton model

$$q_k^G(x) = \frac{1}{2}R(x_k^T R(x_k) + (x-x_k)^T J(x_k^T R(x_k) + \frac{1}{2}(x-x_k)^T J(x_k)^T J(x_k)(x-x_k) \tag{9.35}$$

by the addition of an approximation to the difference of it and the quadratic Taylor expansion around x_k to obtain

$$q_k^S(x) = \frac{1}{2}R(x_k^T R(x_k) + (x-x_k)^T J(x_k^T R(x_k) + \frac{1}{2}(x-x_k)^T [J(x_k)^T(x_k) + S_k])(x-x_k) \tag{9.36}$$

[1]The Hessian is the second derivative matrix of the least-squares merit function or the inverse of the covariance matrix.

A sizing factor, which is a modification of the Oren-Luenburger (Oren 1973) self-scaling technique is used which made a significant improvement in the algorithm's performance. The augmented model is initially equal to the Gauss-Newton model but the algorithm uses a model/trust-region strategy to select the change Δx_k. The step is defined as

$$\Delta x_k = -(H_k + \lambda_k D_k^2)^{-1} \nabla f(x_k) \tag{9.37}$$

where the current Hessian approximation is denoted by H_k, D_k is a diagonal scaling matrix and $\lambda_k \leq 0$ is chosen by set criteria as defined by Dennis et al (1989).

There is a large variety of commercial software available which can or attempt to do nonlinear regression, most of these however linearise the function as discussed previously. A linear regression is thus performed on the transformed function, so that the parameter values are determined for the transformed, linearised function. Utilising the algorithm of Dennis et al (1981), NLREG minimises the squared residuals for the actual function, producing a better fit to the data. The software can also fit functions which are far from linear, and which due to their intrinsic nonlinearity can not be linearised.